Studies of tumor heterogeneity, tumor microenvironment, and radiotherapy: A mathematical and computational approach

by

Farinaz Forouzannia

A thesis
presented to the University of Waterloo
in fulfillment of the
thesis requirement for the degree of
Doctor of Philosophy
in
Applied Mathematics

Waterloo, Ontario, Canada, 2018

Examining Committee Membership

The following served on the Examining Committee for this thesis. The decision of the Examining Committee is by majority vote.

External Examiner: Philip Maini
Professor, Wolfson Centre for Mathematical Biology,
University of Oxford

Supervisor(s): Sivabal Sivaloganathan
Professor, Dept. of Applied Mathematics,
University of Waterloo

Mohammad Kohandel
Associate Professor, Dept. of Applied Mathematics,
University of Waterloo

Internal Member(s): Zoran Miskovic
Professor, Dept. of Applied Mathematics,
University of Waterloo

Sander Rhebergen

Assistant Professor, Dept. of Applied Mathematics,

University of Waterloo

Internal-External Member: Adil Al-Mayah

Assistant Professor, Dept. of Civil & Environmental Engineering,

University of Waterloo

I hereby declare that I am the sole author of this thesis. This is a true copy of the thesis, including any required final versions, as accepted by my examiners.

I understand that my thesis may be made electronically available to the public.

Abstract

Radiotherapy uses high doses of energy to eradicate cancer cells and thus destroy the bulk of tumors. Radiobiologists try to precisely deliver radiation to a targeted area in order to maximize the cancer cell kill rate while trying to minimize damage to normal cells. To achieve this goal, various treatment schedules have been developed, but there still remain significant obstacles to improving the effectiveness of these schedules. It has been observed that various factors play important roles in the effectiveness of treatment. One important factor is tumor heterogeneity, that is, the genetic and epigenetic variations in tumors. This cellular diversity can influence the efficacy of radiotherapy due to the different radiosensitivities among cancer cells. In addition, the interplay between this heterogeneous cellular population and the tumor microenvironment can negatively affect the treatment process. In this thesis, deterministic and stochastic mathematical models are developed to explore the role of heterogeneity and the impact of cellular repair on radiotherapy outcomes. The results suggest that shrinking a tumor is not sufficient to control the disease; the fraction of cells resistant to treatment must also be reduced. In addition, supposedly optimal treatment schedules can lead to markedly different results even in patients with the same type of cancer, due to cellular and microenvironmental differences among tumors. Therefore, based on these variations, it is important to design new therapeutic approaches for each cancer type and even each patient. The modified Gillespie algorithm for discontinuous time changing rates is applied to explore the impact of plasticity, as well as random demographic factors on the tumor control probability. The random modification of tumor microenvironment is shown to influence the efficiency of radiotherapy. Increasing the standard deviation

leads to an initial rise in the tumor control probability, which thereafter drops over time if a tumor is not eradicated entirely. The results also confirm that plasticity in a tumor reduces the tumor control probability, especially in highly resistant tumors. In addition, in the presence of plasticity, combining radiotherapy with a targeted therapy increasing the differentiation of CSCs does not increase the probability of CSC and tumor removal greatly. Finally, the impact of regulatory negative feedback on the sphere formation potential of a single CSC is explored. The sphere formation efficiency and average sphere size are shown to escalate when CSC division and dedifferentiation are subject to negative regulatory feedback.

Acknowledgements

First, I would like to express my deepest appreciation to my supervisors Professors Mohammad Kohandel and Sivabal Sivaloganathan for their support and guidance during my PhD program. Special thanks also to my committee members Professor Philip Maini, from the University of Oxford, and Professors Zoran Miskovic, Sander Rhebergen, and Adil Al-Mayah from the University of Waterloo for their comments and suggestions. My sincere thanks to my collaborators Professors Heiko Enderling and Vahid Shahrezaei for their useful discussions and comments. I am also grateful to the Applied Mathematics Department administrations for providing a respectful, warm, and friendly environment. I must also acknowledge and thank to the members of the Biomedical Research Group of the Department of Applied Mathematics at the University of Waterloo for interesting scientific discussions.

On a more personal level, I am profoundly thankful to my parents, Parvin and Gholamhossein, and my siblings Faranak and Fariborz, for their love and support. In particular, I would like to express my sincere gratitude to my father, whose inspiration and encouragement have been the light on my life path. Finally, Thank you Sina, for your love and patience. Your enthusiasm and encouragement continue to help me through my life and career.

Dedication

To My Father

Table of Contents

List of Tables

List of Figures

Chapter 1

Introduction

1.1 Overview

Cancer is a highly complex disease that involves uncontrolled growth of abnormal cells and often results in the death of the host. Although an incredible amount of effort has been expended in trying to understand the process of angiogenesis, as well as the initiation, progression and evolution of malignancies, our knowledge of the fundamental mechanisms still leaves much to be desired. The original cause of cancer is believed to be the molecular events that lead to the accumulation of genetic or epigenetic mutations in normal cells. The majority of these genetic instabilities correspond to the upregulation of oncogenes and inactivation of suppressor genes or gate keepers, which interrupt cellular functions and prompt tumorigenesis (Sjöblomet al., 2006). In addition, cancer cells are subject to ongoing evolution and mutation. In fact, tumors consist of genetically diverse cellular pop-

ulations, presenting different phenotypic features with differing cell surface receptors, and proliferative, angiogenic and metastatic strength. One suggested prospective on this diversity is given by the cancer stem cell (CSC) hypothesis, which explains the intratumoral heterogeneity arising from the symmetric and asymmetric division of CSCs, regenerating themselves and giving rise to their offspring. The interaction between heterogenous malignant cells, with their aberrant microenvironment, can increase aggressiveness and the emergence of treatment resistance in tumors. Although exposure to most available cell-kill agents results in tumor bulk shrinking, the resistant tumor cells remain unaffected. Therefore, it is important to study the role and impact of tumor heterogeneity and the microenvironment on therapeutic approaches.

In this thesis, a mathematical model is used to study the effect of tumor heterogeneity on radiotherapy outcomes. In addition, the impact of random microenvironments on tumor control is investigated using stochastic simulations. Chapter 2 presents a comprehensive literature review of mathematical models exploring the specific role of CSCs in treatment. Thus, this introduction is limited to a general overview of relevant biological information.

1.2 Tumor heterogeneity, CSCs, and microenvironments

The characteristics and features of tumors change based on their site and cell of origin. These variations also exist for the same cancer in an individual (Heppner, 1984). In general, the cellular population within tumors are both phenotypically and genotypically heteroge-

nous as a result of genetic and epigenetic changes. Clonal evolution theory posits that the accumulation of these modifications in a single cell can lead to malignancy, and over time, leads to heterogeneity within tumors. The more recent CSC hypothesis proposes a hierarchical model in which CSCs sit at the apex, and have a tumorigenic ability to reproduce themselves and their progeny (Meacham & Morrison, 2013; Shackleton et al., 2009). Recently, it has also been observed that there is a degree of bidirectionality, as a result of plasticity among cancer cells. This suggests that non CSCs have the capacity to display cancer-stem cell like behavior and posses higher tumorigenic potential (Marjanovic et al., 2013b). Experimental observations have been able to identify CSCs in different types of cancers ranging from leukemia, breast, colon, CNS, to head and neck cancers (Schatton et al., 2009, and references therein). However, it is difficult to determine the fraction of CSCs in a tumor due to the lack of perfect biomarkers for CSCs and due to the phenomena of plasticity.

CSCs and cellular heterogeneity are linked with tumor progression, treatment resistance, and metastasis. On the other hand, the tumor microenvironment also has a significant impact on the initiation and propagation of tumors, in addition it can trigger cellular diversity among cancer cells (Rich et al., 2016). The tumor microenvironment is a highly variable and complex structure that regulates the connection among cancer cells, normal cells, abnormal vascular system and signaling pathways. The formation of irregular vascular networks, which occurs through angiogenesis, leads to the aberrant of erratic transport of oxygen and nutrition to the tumor cells. This variable blood flow results in metabolic changes, high interstitial fluid pressure, hypoxia, and acidosis, all of which contribute to treatment resistance and metastatic potential (Trédan et al., 2007). For example, there

is a decrease in the proliferation of cancer cells under conditions of nutrition shortage. The cells move into a quiescent state (cell cycle arrest) and become resistant to therapeutic approaches. In addition, hypoxia is believed to be correlated with the induction of angiogenesis and cell survival, as well as with changing biochemical pathways, leading to treatment resistance (Trédan et al., 2007). Therefore, a better understanding of the impact of tumor heterogeneity and the tumor microenvironment on cancer evolution is necessary in order to develop appropriate treatment strategies. In this frame work, it is highly desirable to investigate the role and impact of intatumoral variation and arbitrary microenvironments on treatment efficiency.

1.3 Radiotherapy

Radiotherapy is one type of cancer treatment that can be prescribed as a single agent or in combination with other therapeutic strategies (such as chemotherapy, surgery, and immunotherapy). Originally, the treatment was delivered as a large single dose, which caused many complications and toxicities. Later, smaller fractions of radiation were administered over a period of several weeks, (a process called fractionated radiotherapy), to reduce radiotherapy-induced complications (Mitchell, 2013; Pajonk et al., 2010). To understand the idea behind fractionated radiotherapy, it is important to study cellular death due to radiation.

In general, radiation damages critical targets such as the DNA of cells, resulting in mutation or cellular death through apoptosis and necrosis if cells fail to repair the damage. The biological effects of radiation on DNA can be both direct or indirect. In the former,

radiation interacts with DNA directly; indirect effects are due to the ionization of water and other molecules in the cells, which generate free radicals that are able to diffuse and alter DNA (Cox & Ang, 2009; Hall & Giaccia, 2006). The radiation-induced damage leads to a number of DNA lesions, resulting in single strand breaks that usually arise from exposure to smaller doses of radiation, and double strand breaks that are mostly responsible for cellular death and chromosomal aberrations.

The outcome of fractionated radiotherapy depends on the DNA repair mechanism, redistribution of cancer cells in the cell cycle, and repopulation and reoxygenation of cells between fractions (Pajonk et al., 2010). The main cause of radiation induced cell death is the production of lethal damage such as double strand breaks in the DNA, which mainly occurs at higher doses of radiation. Yet, the majority of damage to the DNA is sublethal and can be repaired at lower doses. However, exposure to fractions of lower doses of radiation can lead to the accretion of sublethal lesions contributing to destruction but with lower toxicity to normal tissues (Mitchell, 2013).

The response of cells to radiotherapy depends on their stage in the cell cycle. The cell cycle is a sequence of events leading to cellular division. It consists of four major phases G_1, S, G_2, and M. In this process, cells expand in size and DNA control mechanisms monitor and initiate any repairs needed during DNA synthesis (G_1). Replication of DNA (S) follows with further DNA check points and repair as required (G_2). Finally, cellular growth stops and cellular division is complete (M). Commonly, cells in the late synthesis phase (S) are more radioresistant, and cells in late G_2 or mitosis (M) are more readiosensitive (Otani et al., 2016). Fractionation prepares surviving cells to move forward in the cell cycle into more radiosensitive stages, where they can be targeted in the next fraction of treatment.

Both normal and cancer cells show an increase in cellular proliferation after exposure to radiation. This can be a potential benefit of fractionated radiotherapy, since quick cellular proliferation can raise the number of damaged cells in the mitosis phase and so increase radiosensitivity and cellular death. However, for prolonged radiation protocols, the efficiency of downstream doses of fractions might diminish due to accelerated cellular division. In addition, applying larger doses of radiation can increase toxicity and necessitate stopping the treatment process for (Mitchell, 2013).

Hypoxic tumors are more radioresistant, and lack of oxygen has been shown to be linked to better repair rates. In fact, the presence of oxygen can generate permanent damage (through oxygen fixation), increasing cellular kill (Cox & Ang, 2009). The oxygen level changes continuously in tumor microenvironments, and the hypoxic regions can be categorized into two different groups, chronic and acute. Chronic hypoxia occurs in regions beyond the limit of oxygen diffusion from the vascular system, but acute hypoxia occurs in regions where there is temporary disruption of oxygen diffusion (Bayer & Vaupel, 2012). The gap between radiation fractions is assumed to allow reoxygenation among cancer cells, which increase radiosensitivity to the radiotherapy.

Radiotherapy protocols have improved with advancing technologies. Today's better-designed regimens allow tumors to be targeted with precision and reduce the risk of normal tissue complications. For example, in addition to conventional schedules, which deliver a fraction of the total radiation daily, hyperfractionated and hypofractionated protocols have been suggested to enhance outcomes. The hyperfractionated strategy consists of two or three fractions per day with small doses of radiation, decreasing late regime toxicity and increasing total administered doses. In contrast, Hypofractionation shortens treatment

durations by applying fewer number of fractions but higher doses of radiation per fraction.

Despite recent progresses, however, available therapeutic approaches have not been successful in most cases. Although the underlying mechanisms are truly complicated and not well understood, one important reason is the radiation refractoriness of CSCs to radiation. As a result, radiation is more prone to kill differentiated cells than the CSCs, responsible for driving tumor growth. Basically, CSCs benefit from superior DNA repair mechanisms with enhanced checkpoint activation that can exacerbate cellular resistance to radiotherapy (Bao et al., 2006; Wang, 2015). It is also assumed that CSCs are generally in the quiescent state G_0, in which cells stop dividing. This slow cycling subpopulation of cells displays higher proliferation potency after exposure to fractions of radiation, which explains the enhanced regeneration of cancer cells after treatment. In addition, stochastic effects in tumor microenvironments also prompt CSC proliferation. In particular, CSCs possess greater tumorigenicity in hypoxic conditions (Pajonk et al., 2010; Vlashi et al., 2009). Therefore, targeting CSCs can be beneficial in developing more efficient radiotherapy schedules. Moreover, there has been significant effort in treatment planning strategies to take into consideration personalized therapeutic approaches that account for differences in genetic backgrounds between individuals, and the heterogeneity and aggressiveness of their specific tumors.

The effect of fractionated radiotherapy on tumor heterogeneity and the impact of randomness in the microenvironment on tumor control are discussed in Chapters 3 and 4 respectively.

1.4 Sphere forming assay

A Sphere forming assay is a cell culture technique that hinges on the ability of a single cell to proliferate and form a sphere (Johnson et al., 2013; Pastrana et al., 2011). This in vitro technique was initially used to study normal neural stem cells; later, it has since also been applied to identify the subset of cancer cells that are capable of clonogenic growth (Stamatakos et al., 2006). One variation known as the mammosphere, has been widely used for mammary gland cells to investigate mammosphere formation efficiency (MFE), and to study the effect of radiotherapy and chemotherapy as well as the microenvironment on MFE (Lagadec et al., 2010; Lonardo et al., 2013).

The first intention of a sphere formation assay is to measure the activity of stem cells or early progenitor cells. It is usually assumed that each plated cell has the ability to form a sphere (Turner, 2009a). However, the former assumption has been questioned by Stamatakos et al. (2006), who showed the existence of migration and fusion between neurospheres.

Sphere forming assay protocols are usually designed guided by the underlying purpose of the study, the type of cell line, and the questions that need to be answered by the experiment. Nonetheless, almost all these procedures have common steps in which spheres are harvested from single cells appropriately dispersed in a well. Cells are allowed to grow for a number of days, which is determined based on the cell line and experimental conditions. Finally, cultures of cells are deemed to be sphere when they exceed a certain size threshold. Sphere formation efficiency is calculated as below:

$$\frac{\text{number of spheres per well}}{\text{number of cells seeded per well}} \times 100. \tag{1.1}$$

In this thesis, the mammosphere formation data for a breast cancer cell line is used for parameter estimation in Chapter 3.

1.5 Thesis objectives

This thesis consists of the following four main chapters that cover the impact of heterogeneity and the microenvironment on radiotherapy efficiency. Chapters 2 and 3 are based on peer-reviewed journal papers published from this thesis work.

1.5.1 Cancer stem cells, the tipping point: Minority rules?

Chapter 2, is a review of mathematical models, studying the impact of CSCs on therapeutic outcomes and efficiencies. Consequently, the chapter splits into three sections. The first section addresses the effect of CSCs on chemotherapy and radiotherapy resistance, the second focuses on the developing of new strategies to raise CSC kill rates, and the final section discusses the design of optimum treatment regimens based on the CSC hypothesis.

1.5.2 Mathematical modeling of the effects of tumor heterogeneity on the efficiency of radiation treatment schedule

In Chapter 3, a minimal mathematical model is proposed to investigate the impact of tumor heterogeneity and cell cycle arrest on the outcome of various radiotherapy regimens. The model parameter values are determined using stochastic and deterministic simulations applying mammosphere formation efficiency and the fraction of CSCs data on the breast cancer cell line. The following questions are answered:

- How do different radiotherapy schedules affect the phenotypic heterogeneity of cancer cell populations, in particular CSCs?
- Is tumor reduction after radiotherapy sufficient to control the disease?

1.5.3 The impact of random tumor microenvironment on tumor control probability

Chapter 4 analyzes a stochastic framework for studying the impact of random fluctuations on TCP, which is defined as the probability of cancer cell extinction. The derivation of the analytical solution is not feasible in all cases, for example, when cellular birth and death rates change arbitrarily over time. Therefore, a modified Gillespie algorithm is applied to determine the TCP in the presence of random discontinuous alterations in demographic rates. We investigate the following questions.

- What is the impact of random fluctuations on TCP?

- How does TCP change as randomness increases?
- What is the effect of randomness on extinction time distribution?

1.5.4 The impact of plasticity on tumor control probability

In Chapter 5, a stochastic model is developed based on the CSC hypothesis, to study the impact of plasticity on TCP. The model considers the time evolution of CSC and progenitors in the presence of plasticity. Therefore, TCP_S and TCP_{S+P} are defined as the probability of CSC and tumor removal, respectively. Consequently, a modified Gillespie algorithm is used to evaluate TCP_S and TCP_{S+P}, because the derivation of an analytical solution is not possible when plasticity comes into play. The following questions are studied.

- What is the effect of cellular plasticity on CSC and tumor removal?
- What is the effect of combination therapy, including radiotherapy and targeted therapy designed to increase CSC differentiation, on CSC and tumor removal?

1.5.5 The impact of plasticity and negative feedback regulations on sphere formation capacity

Chapter 6 explores the impact of negative feedback on CSC division and dedifferentiation on the sphere formation potential of a CSC. For this purpose, a two compartment model consisting of a population of CSCs and progenitors is considered, in which the stochastic

behavior of cellular divisions is studied. Applying a Gillespie algorithm, the sphere formation efficiency and the average sphere size of a single CSC is measured in the presence of plasticity. Thus, the following questions are addressed in this chapter.

- How does regulatory negative feedback affect the sphere formation ability of a single CSC?
- What is the impact of plasticity and negative feedback on sphere formation efficiency? (i.e. does a decrease in the plasticity rate have a direct impact on sphere formation efficiency?)

Chapter 7 concludes this thesis, and suggests possible future work.

Chapter 2

Cancer stem cells, the tipping point: Minority rules?

Putative studies continue to support the assertion of the cancer stem cell (CSC) hypothesis, namely that a very small subgroup of a malignant tumor population initiates and drives tumor growth. These cells are purported to possess similar biological properties to their normal adult stem cell counterparts. The CSC hypothesis arises from the observation that tumors like normal tissues have their origin in cells that display potential for self-renewal as well as the ability to generate differentiated cells of various lineages. In addition, CSCs have developed basic characteristics that enable them to evade the effects of standard therapies and these may in fact underly the mechanisms leading to chemo-resistance and tumor relapse.

In recent years, mathematical and computational modeling have emerged as powerful

tools in biomedical research that can be used to study biological systems at multiple scales ranging from molecular processes to cell-cell interactions and how these interactions lead to changes at tissue and organ levels. In addition to accelerating biomedical research through computational simulation of physical experiments, modeling can also be used to guide experimentalists by identifying possible factors and mechanisms underlying the particular problem being studied; this in turn, may suggest physical experiments that eventually lead to the resolution of this very problem.

In this chapter, we review mathematical models that explore the role of CSCs in treatment response, in developing chemo and radio resistance, as well as those that suggest new treatment strategies. In addition, mathematical models that focus on optimal therapeutic protocols will be discussed. The work presented here has been published in the peer reviewed journal of Current Stem Cell Reports:

Forouzannia, Farinaz, and Sivabal Sivaloganathan. Cancer Stem Cells, the Tipping Point: Minority Rules? Current Stem Cell Reports. 2017;3(3):240-247.

2.1 Introduction

Cancer is a group of diseases that involves abnormal cell proliferation in which the interaction of cellular mechanisms and the tumor microenvironment imbue some tumor cells with metastatic potential resulting in the dissemination of malignant cells to other parts of the body. Tumor heterogeneity is one of the important features that has been observed in different types of cancers and this has a significant impact on tumor development and response to treatment. Both the clonal and CSC hypothesis go some way to explaining the genesis and evolution of this heterogeneity (Marjanovic et al., 2013a; Shackleton et al., 2009). Cancer clonal evolutionary theory suggests that tumor initiation relies on multiple mutations occurring in an arbitrary single cell (Nowell , 1976). However, the cancer stem cell hypothesis proposes that a small sub-population of cells, known as cancer stem cells (CSCs), are endowed with tumor initiation and propagation potential (Figure 2.1). These CSCs are able to perpetuate themselves through selfrenewal and to generate non-CSC progenies through symmetrical and asymmetrical divisions, respectively. Recent evidence suggests that the transition from CSCs to normal cancer cells is not unidirectional, and that there is a degree of plasticity between non-CSC and CSC states (Gupta et al., 2011; Marjanovic et al., 2013b). Such interconversion can arise as a result of genetic modifications to cancer cells, random mutations or microenviromental effects.

The therapies that patients receive are usually proposed based on the type, the stage and location of a particular cancerous malignancy, and on the overall health of the individuals. The most common types of therapeutic interventions are surgery, chemotherapy and radiotherapy and in practice, a combination of more than one treatment is applied.

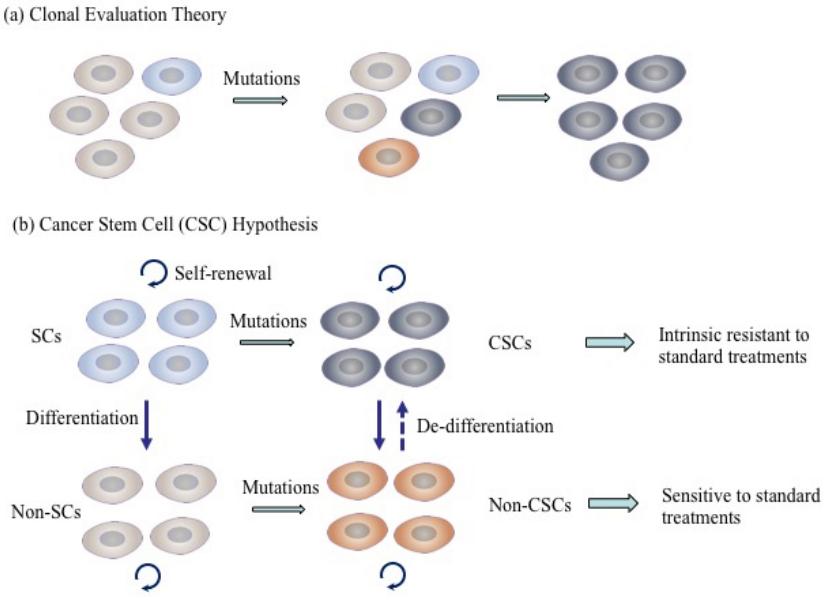

Figure 2.1: *Schematic diagram of CSC hypothesis and clonal evolution theory. In cancer evolution theory, the acquisition of mutations occurs, followed by expansion of the dominant clone (a). But, the CSC hypothesis suggests that CSCs share similar properties to normal stem cells (SCs) and are responsible for cancer initiation as well as the generation of non-CSCs (b).*

Chemotherapy drugs can target tumor cells in different ways. Generally, these drugs prevent cancer cells from growing and reproducing rapidly through DNA damage; however, in the process this often results in damage to normal cells, as well. Chemotherapy can be given before, during and after radiotherapy (referred to as neoadjuvant, concurrent, and adjuvant respectively). Current conventional radiotherapies also deliver high-energy beams to tumor tissues, which induce various types of DNA damage and genomic instability. Some of the resulting types of lesions, such as double strand breaks, are severe

enough to cause cell apoptosis. However, the majority of treatment failures for different types of cancers are a direct result of the emergent resistance of cancer cells to conventional therapies, which leaves patients with limited treatment options (Eyler & Rich., 2008; Mathews et al., 2013). CSCs show higher resistance to available therapies due to upregulated DNA repair mechanisms. The ability of non-CSCs to reenter the CSC state can also contribute to poor clinical results. Furthermore, most available treatment strategies also target cells that are actively dividing, which is not the most efficient way to destroy CSCs since they are relatively quiescent. In addition, dysregulated signaling pathways that control CSC self-renewals, including Notch, PTEN, BMI-1, and WNT, are usually not targeted by current conventional therapies (Boman et al., 2008). Thus, understanding the tumorigenic potentials and the effective mechanisms that CSCs develop to enhance their aggressive phenotype, is essential for the development of more efficient and effective treatment strategies.

Along with the concerted effort that is underway in different branches of science to combat cancer, mathematical models have also been effectively utilized to probe the underlying mechanisms driving tumor growth and make predictions that can be validated experimentally (Anderson & Quaranta, 2008; Altrock et al., 2015; Byrne , 2010; Enderling, 2015). For example, mathematical modeling that is grounded in experimental data can be used to predict therapeutic outcomes and improve clinical results (Altrock et al., 2015; Dionysiou et al., 2004; Dhawan et al., 2014; Enderling et al., 2009b; Stamatakos et al., 2006). Mathematical modeling has been extensively used to try and understand cancer on different scales, but in this chapter particularly we focus on models that try to simulate and predict the effects of treatment. Hence, a brief review of these types of models will be

given next.

Earlier seminal work of Norton & Simon (1977, 1986), utilized mathematical modeling to integrate biological growth information in to treatment scheduling. This led to perhaps the greatest clinical trial innovation in half a century, and the wide spread acceptance of the "Norton-Simon" hypothesis in clinical circles. Norton and Simon proposed that tumor growth dynamics follows a sigmoidal function during chemotherapy and suggested that a dense dose protocol would have better outcomes than standard schedules, which has been clinically verified, for example in (Citron et al., 2003) amongst numerous others. In addition, a number of mathematical models discussed tissue response to fractionated radiotherapy treatments with either acute or protracted doses (Dale, 1985; Oliver, 1964; Roesch, 1978). One of the early models in this area was developed by Thames et al. (1984); Thames (1985) who used it to investigate the dynamics of radiation damage repair. The approach used a linear quadratic model to describe cell survival, modified to account for incomplete repairs between fractions (for fractionated acute continuous exposure) and the repair during the administration of the fractions (for low dose rate continuous exposure). The linear quadratic model and its modifications have been considered extensively in the literature, to simulate the response to radiation exposure. The evolution of resistance before and during treatment is also one of the first problems that was addressed in the mathematical modeling of treatment responses (Coldman & Goldie, 1986; Goldie & Coldman, 1983; Panetta, 1996; Swan, 2013). Coldman & Goldie (1986), and Goldie & Coldman (1983) proposed a stochastic model to explore the risk of developing resistance during treatment. The model assumed that sensitive cells can be eliminated upon receiving treatment and that resistant mutations can occur with a certain given probability. The results imply

that the probability of resistance (when treatment includes two drugs given sequentially) depends on the total number of cells and their mutation rates. The authors suggested that to improve success rates, drugs should be administered as soon as possible after diagnosis. They proposed that drugs should be given in an alternating fashion rather than sequentially to have a significant impact on the heterogenous cell populations; nevertheless, this suggestion could not be confirmed clinically (Bonadonna et al., 2004).

In medicine, to proceed from bench to bedside, numerous clinical trials are needed to determine the best treatment procedure and protocol. In this context, mathematical modeling can play an important and critical role in the prediction of the most efficient treatment strategies, thus avoiding unnecessary and often excessive clinical trials. Several mathematical models have been developed in the literature to establish the most practical treatment protocols (Foo & Michor, 2009; Martin et al., 1994; Michor et al., 2005). Many models try to rapidly minimize the total tumor size; however, successfully controlling tumor growth depends critically on reducing effectively both drug sensitive and drug resistant cells. Some of the early work by Costa et al. (1992) describes the dynamics of a tumor that includes drug resistant cells. The model aims to efficiently find the optimal treatment schedule by minimizing the total tumor size. The development of better-designed treatment regimens is still a field of significant research activity; nevertheless, the attainable benefits from treatment must still be evaluated and quantified to be of any clinically relevant significance. The tumor control probability (TCP) is a measure that attempts to quantify the probability of destroying or removing malignant cells using a variety of radiation therapy schedules. In order to establish a better formalism for TCP, different models have been introduced in the literature such as that of Kendal (1998); Munro &

Gilbert (1961); Tucker et al. (1990); Yakovlev (1993); Zaider & Minerbo (2000). For example, one model frequently discussed in the radiation therapy literature is the so-called Poisson model of TCP (Munro & Gilbert, 1961; Zaider & Minerbo, 2000). This model assumes that the number of cells that survive radiation has a binomial distribution; and if the survival probability is small enough, the probability of no malignant cells remaining follows a Poisson distribution after treatment. However, the model neither captures the proliferation of cells during treatment nor the stochastic effects. Later, Zaider & Minerbo (2000) acknowledged the impact of stochastic effects on radiation-induced cell death and suggested a model based on a simple stochastic birth/death process.

Generally, most of the primary mathematical models are established based on the clonal evolution theory, where all cells are capable of giving rise to mutants that lead ultimately to the formation of tumors. However, the emerging CSC hypothesis has become the subject of theoretical analysis to explore the role of CSCs in tumor response to treatment and the acquisition of resistance. The main scope of this chapter is to highlight various mathematical models that incorporate the CSC hypothesis as well as some of the fundamental traits of CSCs. These will be discussed in more detail in Sections 2.2, 2.3 and 2.4.

2.2 The roles of CSCs in evolving resistance and tumor response

Despite much improvement in the design of practical cancer therapies, the majority of patients often develop tumors resistant to standard therapies (Bao et al., 2006; Chen et

al., 2016; Dean et al., 2005; Pajonk et al., 2010). It may be that conventional cancer treatments act more efficiently on highly proliferating cells, and thus leave the quiescent CSCs relatively unscathed . For example, resistance to Imatinib is one of the complications that can arise for patients treated for chronic myelogenous leukemias (CML), which can cause initial refractoriness of the disease and relapse. The evolution of resistance from an exponentially growing cell population was studied using a continuous time branching process by Iwasa et al. in (Iwasa et al., 2006). The model starts with a single sensitive cell that can undergo mutations and become resistant to Imatinib. Finally, the probability of resistance at the time of diagnosis was calculated and it was concluded that a higher number of cell devisions increases the occurrence of resistant cells. The quiescence of cancer stem cells is also a critical characteristic that safeguards them from Imatinib. Hence, a mathematical model has been developed to explore the impact of cellular quiescence on the dynamics of drug resistance (Komarova & Wodarz, 2007). For a single drug, if the resistant cells exist before treatment, the quiescent cells do not modify the chance of resistance, although they can increase the probability of developing resistant mutants when patients receive a combination of more than one drug with various targets. In fact, the therapy phase is not important for emergence of mutants since they existed before the diagnosis, but the dormant cells may delay the time that is required for the therapy to eliminate the tumor burden. The authors ultimately suggested that reducing the number of quiescent stem cells during therapy is not beneficial for reduction of resistance risk, since plasticity is another key factor that contributes to resistance and invasion. Poleszczuk et al. (2016) used a mathematical model to simulate and investigate the effects of different rates of transitions (from non-CSCs to CSCs) on tumor growth and treatment response. The results show

that tumors with low rates of plasticity can regrow after radiotherapy. Nevertheless, for tumors with high plasticity rates, post therapy cancerous cells undergo remission after regrowth, because radiotherapy appears to increase CSC depletion. Although the results seem interesting, more experimental investigation is required, to ensure this is not an experimental or computational artifact.

Gupta et al. (2011) combines both biological experiments and mathematical simulations to examine the sensitivity of distinct phenotypic states (Stem like, basal, luminal) to treatment. For this purpose, breast cancer cell lines (SUM159 and SUM149) have been treated with two conventional chemotherapy drugs: paclitaxel and 5-fluorouracil (5-FU), which resulted in increasing the portion of cancer stem like cells for both cell lines. To gain a comprehensive understanding of these results, a Markov model has been established to examine the dynamics of breast cancer cell populations and transition between different states. The results indicate that basal cells are more sensitive to paclitaxel in comparison to the other two states for the SUM159 line. Moreover, the proportion of both stem like cells and basel cells show approximately a 5 fold increase after receiving paclitaxel, but the growth in basal cells is due to the resistance of stem like cells to the treatment, which can reproduce basal cells afterwards. In addition, Gao et al. (2013) demonstrate that resistance to radiotherapy is not the only critical factor responsible for CSC enrichment in gliomas and that repeated exposure to radiotherapy can create a microenvironment that tilts the proliferation in favor of symmetric divisions.

Cell surface protein expression profiles are the main tool used to isolate cancer stem cells in different tissues. For example, CD34highCD38low, CD133+, and CD44highCD24low are common biomarkers used for leukaemia and brain and breast tumors, respectively, see

(Singh et al., 2004) and references there in. However, clearly not all cells that have the same protein expression are necessarily cancer stem cells, and it appears that both cancer stem cells and early generations of progenitors often express the same protein markers (Charafe-Jauffret et al., 2009). These findings have been taken into consideration in developing a hierarchical model that includes stem cells, the N^{th} generation of progenitor cells, and mature cells. Dhawan et al. (2014) have employed a fully stochastic model for a hierarchy of heterogenous cell populations and used numerical simulations to obtain the tumor control probability (TCP). The TCP is defined as the probability of eradicating all cancerous cells in a particular tissue and is used as a measure of radiotherapy efficacy. Based on the CSC hypothesis, removing CSCs is essential to achieve a cure. Therefore, the probability of controlling cancer stem cells only (TCP_S) was also determined. Furthermore, because of imperfect biomarkers for CSCs, the probability of eliminating biomarker positive cells (TCP_{CD^+}) was calculated. Finally, it is suggested that TCP_{CD^+} can be a potentially better clinical alternative for TCP_S.

2.3 New therapeutic strategies targeting CSCs

CSCs are generally not targeted by commonly used treatment strategies, so designing therapies that are able to specifically target CSCs is of paramount importance (Koury et al., 2017; Maugeri-Sacc et al., 2011; Ogawa et al., 2013). For example, it has been shown that the fraction of CSCs is enriched after radiotherapy due to the highly efficient DNA damage response in gliomas (Bao et al., 2006). Thus, developing effective treatment strategies that target and eradicate CSCs is crucial to improving clinical results and minimizing recur-

rence. Consequently, designing therapies that include both standard anticancer treatments and CSC-targeting agents may be an effective double pronged attack to eliminate various types of cancer cells. For instance, Goldman et al. (2015) used both mathematical modeling and experimental studies to investigate the mechanisms behind adaptive resistance in breast cancer patients treated with a high concentration of taxanes. The results indicate that treatment with taxane leads to a phenotypic cell state transition to the CSC population, which can contribute to tumor resistance. Moreover, it is demonstrated that applying inhibitors that can control the SFK/HcK pathways in a proper temporal schedule (after exposure to taxanes) increases the sensitivity to chemotherapy treatment and thus increases cell death. Furthermore, a simple mathematical model has been presented (Dingli & Michor, 2006) to illustrate the importance of eradicating CSCs. The model includes two layers of differential equations to account for the hierarchy of stem cells and differentiated cells for both normal and tumor cells. Analysis of different therapeutic possibilities implies that increasing apoptosis or decreasing the generation of malignant mature cells are not useful approaches to controlling and removing the disease due to plasticity and replenishment of CSCs. However, the therapeutic protocols that prevent CSCs from reproduction have the potential to eradicate the disease if CSCs are subjected to such a therapy for an extended period of time. Furthermore, it is predicted that agents that either decrease the division rate or increase the death rate of CSCs can improve the results, however the eradication of cancerous mature cells is needed to minimize the risk of failure and eliminate the potential impact of plasticity. Additionally, a mathematical model has been developed based on the work of Youssefpour et al. (2012) to explore the advantage of "differentiated" therapies and radiotherapy combinations, which push CSCs to differentiate into descendants that

are more sensitive to radiotherapy (Bachman et al., 2013). Consequently, applying "differentiated" therapies along with radiotherapy appears to improve treatment success and decrease side effects for head and neck, brain and breast cancers.

Piccirillo et al. (2006) have reported that exposure to bone morphogenetic proteins (BMPs) decreases proliferation and increases the expression of non cancer initiating cells in glioblastomas (GBMs). This study demonstrated that brain tumor stem cells (BTSCs), identified by biomarker $CD133^{+}$, are induced by BMPs to differentiate into $CD133^{-}$ cells, which are not tumorigenic and are more responsive to conventional cancer therapies. These findings suggest that adding proteins like BMPs to the currently available radiotherapy protocols might significantly improve outcomes; nevertheless, more investigation is required due to other possible interactions in the complicated underlying mechanisms driving tumor growth. From this perspective, Turner et al. (2009b) have proposed a mathematical model that represents the effect of BMPs on radiotherapy results for glioblastoma based on the cancer stem cell hypothesis. The model describes the stochastic effects of the small number of cells for different types of BTSC divisions, symmetric self-renewal $S \to S+S$, asymmetric self-renewal $S \to S + P$ and symmetric proliferation $S \to P + P$. These two subgroups of cells can also undergo apoptosis and be discarded. On a larger scale, however, the model considers the corresponding average equation to study the role of BMPs and the cell kill response of radiotherapy on tumor dynamics. The model is mathematically given by:

$$\begin{aligned} \frac{dS(t)}{dt} &= \tilde{\rho}_s(S,P) r S - \Gamma_s S - \alpha_s S \sum_j d_j f\left(\frac{t-t_j}{\tau_s}\right) \\ \frac{dP(t)}{dt} &= \tilde{\rho}_s(S,P)(1-r) S - \Gamma_p P - \alpha_p P \sum_j d_j f\left(\frac{t-t_j}{\tau_p}\right), \end{aligned} \tag{2.1}$$

where $\tilde{\rho}_s(S,P) = \rho_s(1 - S/S_{lim} - P/P_{lim})$, which employs logistic growth dynamics to capture the competition between species for limited nutrition. Here, S_{lim} and P_{lim} stand for the maximum population of BTSCs and progenitors, respectively. Additionally, ρ_s denotes a rate of proliferation for stem cells that can occur with probability $r = r_1 - r_3$, where r_1 and r_3 are the probability that BTSCs go through symmetric self-renewal and symmetric proliferation, accordingly. These two types of cells can undergo apoptosis with probability Γ_i ($i \in \{S,P\}$). In addition to apoptosis, cells can also be removed with radiation dose d_j given at time t_j on j^{th} fraction of treatment. Here, the function f is assumed to be negative exponential for $x \geq 0$ and 0 otherwise. The clearance times for dead BTSCs and progenitors after radiation are given by τ_s and τ_p, respectively. Further, α_i for $i \in \{S,P\}$ represents the radiobiological parameters for BTSCs and progenitors. Experimental results demonstrate that BTSCs are more resistant to radiation than $CD133^-$ cells (Bao et al., 2006). Therefore, the radiosensitivity parameter for $CD133^-$ cells is chosen to be 3 fold more than the radiosensitivity parameter for $CD133^+$ cells ($\alpha_s < \alpha_p$).

The effect of BMPs is mathematically captured by reducing the probability r together with fixing r_2, which is the probability of BTSCs going through asymmetric self-renewal. Following Piccirillo et al. (2006), it is assumed that $r = r_1 - r_3$ is changed from the pretreatment value 0.1 to a negative value -0.1 after receiving BMPs. Modifying r to a negative value implies an increase in symmetric differentiation divisions and a decrease in symmetric self-renewing divisions. The effect of radiation kill is also examined for different treatment schedules. Since the model assumes a higher radiosensitivity for $CD133^-$ cells, the fraction of BTSCs is elevated. In addition, eradicating $CD133^-$ cells raises the number of $CD133^+$ due to the logistic growth impact on cell proliferation that necessitates a small

increase in the number of BTSCs after radiotherapy (in comparison with the control group). But, BMP therapy-only lowers the number of BTSCs at the expense of a slight increase in the number of $CD133^-$ cells. Regardless, the results have shown that adding BMPs or probably any other CSC targeting agents in addition to radiation therapy effectively shrinks the tumor along with an associate decrease in $CD133^+$ cells.

2.4 Finding the optimum treatment schedule under the CSC hypothesis

Cancer treatments have evolved over time with the purpose of enhancing life expectancy for cancer patients. In the last two decades, mathematical modeling has started to play an important and pivotal role in developing optimal treatment strategies and protocols as well as providing a new experimental tool for investigating the impact of a new proposed therapy on tumor cells, in silico (Badri & Leder, 2016; Kohandel et al., 2006; Leder et al., 2014; Powathil et al., 2007). For instance, the analysis and simulation of Powathil et al. (2007) makes it clear that the combination of neo-adjuvent chemotherapy followed by radiotherapy might be a better treatment strategy than adjuvant chemotherapy for gliomas. Understanding the importance of targeting CSCs and their distinct properties may lead to the development of new therapeutic protocols, which might achieve better tumor control. As an example, Enderling et al. (2009b) presented a mathematical model that studies the effect of CSCs and quiescent cells on treatment outcomes. The CSC fraction size and the stem cell proliferation rates have been reported as critical factors determining

treatment response. Assuming less radiosensitivity for quiescent cells, which are mainly located in the core of a solid tumor, it has been suggested that applying hypofractionated radiation protocols can control the disease if the CSC pool size is small and as long as the CSC repopulation does not interfere with the higher capacity of radiation kill. Moreover, heterogeneity and instability among various lineages of cancer cells can reduce the potency of available treatment options. Hence, a mathematical model and an experimental study were designed to predict an efficient radiotherapy regimen for Glioblastoma (Leder et al., 2014). The model considers plasticity between CSCs and differentiated cells and assumes that CSCs are more radioresistant. Furthermore, surviving cells lapse into a quiescent state after radiotherapy, but can repopulate again, after exiting quiescence. Consequently, two radiotherapy protocols, which deliver larger fractions at the beginning and end of radiotherapy treatment, have been recommended claiming to lead to better outcomes than conventional therapies. These predicted regimens have been tested experimentally and demonstrated to lead to greater survival in mice. The model was later extended to predict a radiotherapy regimen maximizing survival and minimizing toxicity in the corresponding tissues arising from exposure to larger doses of radiation at the beginning and end of the therapy (Badri et al., 2016). The problem is reduced to two optimization problems: the first deals with optimization of the total dose and dose per fraction, and the second handles optimization of time intervals for each fraction. The results obtained imply that the best arrangement for the time intervals corresponds to the dose distribution that maximizes the return to the stem like state. However, these approaches may lead to a growth in CSC population, which can contribute to therapy resistance and recurrence.

2.5 Conclusions

The emergence of resistance to conventional therapies has been long recognized as one of the major causes of tumor relapse and recurrence. CSCs, also known as cancer initiating cells, develop superior mechanisms such as activated DNA damage repair, upregulated drug transporters, and maintenance of cellular pathways which allows them to survive standard therapeutic protocols and triggers relapse in many cases. Therefore, identifying and understanding the role of CSCs in therapeutic resistance can improve the overall efficacy of available treatments and assist in the development of new treatment strategies targeting CSCs. Here, mathematical modeling following experimental validation is useful to understand the underlying mechanisms and design new treatment approaches.

Here, we have presented an idiosyncratic survey of mathematical models that investigate the impact of different characteristics of CSCs such as differentiation, quiescence, and plasticity, on treatment response and emergent tumor resistance. However, CSCs employ other complex mechanisms such as upregulated drug transporters, which play critical roles in the development of tumor resistance. Mathematical oncology is a nascent field of research with the potential for significant clinical impact, but this requires much more theoretical investigation using mathematical and computational modeling validated through experimental results. Moreover, studying the impact of microenvironmental effects (e.g. hypoxia) on the proliferation and control of CSCs may lead to significant advances in clinical oncology.

Furthermore, in this chapter we have also reviewed mathematical models that provide experimental predictions in the quest to develop new therapeutic strategies targeting CSCs.

The main purpose of these new treatment strategies is to increase the sensitivity of CSCs to chemotherapy and radiotherapy. This includes a combination of conventional therapies with molecular inhibitors controlling CSC pathways, which enhance CSC death. Selfrenewal is considered to be the main reason for radioresistance in CSCs, but understanding other pathways such as those contributing to apoptosis is also of clinical interest (Ogawa et al., 2013). Here, Mathematical modeling can be applied to predict other critical pathways and possible clinical outcomes, which can be validated experimentally. In addition, using chemotherapeutic agents together with radiotherapy to increase the effect of radiation on CSCs have been shown to improve results. However, it is important that these agents inflict minimal damage on normal stem cells since they share many of the same features as CSCs (Eyler & Rich., 2008; Ogawa et al., 2013).

Current radiotherapy and chemotherapy schedules have been improved in an attempt to optimize treatment outcomes and minimize toxicity. Mathematical models actively play a crucial role in attempts to design better treatment strategies. Nevertheless, most current clinical protocols still focus on reducing the tumor burden, and normally disregard CSCs. This can lead to the emergence of resistant CSCs which in turn leads to relapse and aggressive metastatic invasion. Thus, developing mathematical models suggesting new therapeutic schedules that at the same time reduce the fraction of CSCs or include recent molecularly targeted approaches can be helpful. Moreover, clinical and experimental research to improve clinical outcomes are fields that have seen rapid growth in recent years. For example Klement et al. (2000) suggested a combination therapy comprised of continuous low dose chemotherapy regimen and a VEGF receptor-2 antibody, to increase the antivascular effects of the treatment in order to shrink the tumor and reduce the

evolution of drug resistance. Mathematical and computational approaches herald a new era in clinical oncology with the potential to address questions arising from experimental studies and vice-versa to guide experimental studies to resolve many of the puzzles and paradoxes that are part and parcel of cancer biology. Indeed, we are optimistic that these approaches will not only accelerate clinical developments, but elucidate and reveal some of the basic mechanisms driving tumor growth.

(SS) is grateful for financial support provided by the Natural Science and Engineering Research Council of Canada (NSERC) through a Discovery grant.

Chapter 3

Mathematical modeling of the effects of tumor heterogeneity on the efficiency of radiation treatment schedule

Radiation therapy uses high doses of ionizing radiation to eradicate cancer cells and control tumors. Various treatment schedules have been developed and tested in clinical trials, yet there are still significant obstacles and there remains much room for improvement in radiotherapy fractionation. Cellular diversity within tumors can lead to different radiosensitivity among cancer cells that can affect radiation treatment outcomes. In this chapter, we propose a minimal mathematical model to study the effects of tumor heterogeneity and

repair under different radiation treatment schedules. We perform stochastic and deterministic simulations to estimate model parameters using available experimental data. Our results suggest that gross tumor volume reduction is not sufficient to control the disease if a fraction of radioresistant cells survives therapy. If a cure cannot be achieved, protocols should balance volume reduction with minimal selection for radioresistant cells. We show that the most efficient treatment schedule is dependent on the biology and model parameter values and, therefore, emphasize the need for careful tumor-specific model calibration before clinically actionable conclusions can be drawn. The model is also applied to the fractionated radiotherapy protocols discussed in the UK standardisation of breast radiotherapy (START) trials. The work reported here has been published in the peer reviewed journal of Bulletin of Mathematical Biology:

Forouzannia, Farinaz, Heiko Enderling, and Mohammad Kohandel. Mathematical Modeling of the Effects of Tumor Heterogeneity on the Efficiency of Radiation Treatment Schedule. Bulletin of mathematical biology. 2017: 1-11.

3.1 Introduction

Radiation is a commonly used modality in cancer treatment, either as monotherapy or as combination therapy together with surgery and/or chemotherapy. Radiation is a DNA damaging agent; and radiation as cancer therapy is predicated on cancer cells being less efficient in repairing radiation-induced damage than normal cells. The total radiation dose is divided into small fractions and administered in a regular periodic fashion to provide temporal windows for normal tissue recovery. Treatment schedules (fractionation) are predominantly based on evolving empirical knowledge and wisdom, but greatly constrained by logistical considerations. Recent developments include hypo- and hyperfractionation for various cancer types, that is delivery of either larger doses temporally further separated or smaller doses more frequently.

Despite many technical improvements in the efficiency of radiotherapy, many tumors become refractory to irradiation. Various clinical and biological factors explain such complications, including DNA damage repair (Hall & Giaccia, 2006; Mathews et al., 2013), prevalence of hypoxia, and tumor heterogeneity and plasticity. Recently, the presence of cancer stem cells and a tumor hierarchy has been discussed as a source of intratumoral heterogeneity and poor therapy response (Marjanovic et al., 2013a; Shackleton et al., 2009). The cancer stem cell hypothesis proposes that a small sub-population of so-called cancer stem cells (CSCs) is critically important for the initiation and maintenance of a tumor. These CSCs are able to self-renew indefinitely, and undergo symmetric and asymmetric divisions to retrospectively increase the CSC population and produce progenitor cells that will make up the bulk of the tumor (Reya et al., 2001). Recent evidence suggests plasticity

between non-CSC and CSC states (Gupta et al., 2011), due to genetic or microenvironmental perturbations. CSCs have been shown to utilize superior radiation-induced DNA damage repair mechanisms to prevent cell death (Bao et al., 2006). After radiation exposure, cells with damaged DNA attempt different pathways of repair, and the repair time is likely dependent on the delivered radiation dose (Lagadec et al., 2010; Sarcar et al., 2011).

The conventional radiotherapy protocol for most tumors delivers a total dose of $50-70$ Gy in 2 Gy fractions on each weekday, with no treatment given on weekends. To reduce toxicity and increase efficacy, alternative treatments have been considered, including a hyper-fractionated protocol with 1 Gy per fraction twice a day; an accelerated regimen of 1.2 Gy per fraction twice daily; and hypo-fractionation with 5 Gy twice-a-week fractions. Here, we develop a minimal mathematical model to study the effect of tumor heterogeneity and repair in tumors exposed to theses different radiation treatment schedules.

Several mathematical models have been developed to simulate the effects of radiotherapy. Most models utilize the so-called linear quadratic (LQ) model and its various extensions (Hall & Giaccia, 2006). In the original LQ model, cell survival probability S after acute doses of radiation d can be estimated as

$$S(d) = \exp(-\alpha d - \beta d^2), \tag{3.1}$$

where α (Gy^{-1}) and β (Gy^{-2}) are tissue-specific radiosensitivity parameters that are usually derived from fitting the LQ model to clonogenic survival data (Hall & Giaccia, 2006). More recently, mathematical frameworks have been combined with experimental data to investigate the different responses to clinically available radiation protocols (Dhawan et al.,

2014; Dionysiou et al., 2004; Enderling et al., 2009b; Stamatakos et al., 2006). Recently, Leder et al. (2014) proposed an optimized radiation dosing schedule for PDGF-driven glioblastoma. The model, however, is dependent on a large number of parameters and, with limited biological data, some parameters are far from biological realism. In particular, tissue-specific radiosenstivity parameters α and β are derived such that the derived ratio of $\alpha/\beta = 865,789$ Gy is five orders of magnitude larger than frequently derived $\alpha/\beta = 3 - 10$ Gy (Leder et al., 2014). Nevertheless, the model-predicted optimal dose fractionation showed prolonged survival in subsequent mouse experiments, emphasizing that the currently applied standard-of-care radiation fractionation may not yield optimal outcomes. Mathematical models may help decipher the complex biology underlying cancer cell response to irradiation, with the ultimate aim of improving clinical applications of radiotherapy.

Herein we propose a simple mathematical model of breast cancer cell dynamics under fractionated radiation exposure. The model includes phenotypic cell heterogeneity and plasticity, as well as radiation-induced cell cycle arrest, which may play a pivotal role in analyzing radiation protocols with multiple doses per day. The effect of different model parameters and repair mechanisms on heterogeneity are studied for different clinically feasible radiotherapy treatments. Finally, the model is applied to fractionated radiation protocols obtained from UK standardization of breast radiotherapy (START) trials. The START trials (START A and START B) were two experiments applied randomly to a group of women who received radiation as part of their treatment for breast cancer in the UK between 1999 and 2002 (Haviland et al., 2013).

3.2 Method

We developed a two-compartment mathematical model to analyze the effect of radiation therapy on the two phenotypically distinct sub-populations of radioresistant and radiosensitive cancer cells. In breast cancer, these populations have been identified by respectively CD44highCD24low (CD^+; biomarker positive) and CD44lowCD24high (CD^-; biomarker negative), which are also markers of cancer stemness (Al-Hajj et al., 2003; Fillmore & Kuperwasser., 2008). Both sub-populations are capable of self-renewal, albeit with lower rates for biomarker negative CD^- cells that also feature higher death rates. We discuss the balance of self renewal and cell death as the net population growth rate, which does not affect the behavior of the system. As a visualization of phenotypic plasticity, cells can switch from one phenotype to the other (Marjanovic et al., 2013a). After exposure to radiation, cells in each compartment are forced into cell cycle arrest to attempt repair from radiation-induced DNA damage. Biomarker positive cells have been shown to have better repair mechanisms (Bao et al., 2006; Boman et al., 2008) and, thus, a larger fraction of growth-arrested biomarker positive CD^+ (calculated by the LQ model with phenotype-specific α_S and β_S parameters) returns into the viable population after successful repair. Figure 3.1 shows a schematic diagram of the proposed model, and model parameters are summarized in Table 3.1.

We denote by N_S, N_{RS}, N_P and N_{RP} the population of resistant cells, resistant repairing cells, sensitive cells, and sensitive repairing cells, respectively. The model can be mathematically represented by the following system of equations

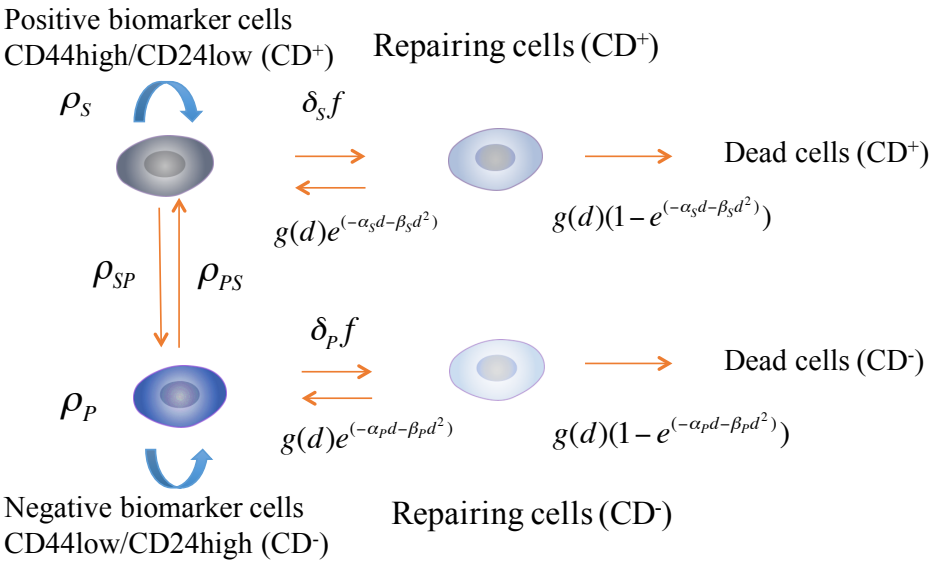

Figure 3.1: *Schematic diagram of the model.*

$$
\begin{aligned}
\frac{dN_S}{dt} &= \rho_S N_S + \rho_{PS} N_P + g(d) e^{(-\alpha_S d - \beta_S d^2)} N_{RS} - \rho_{SP} N_S - \delta_S f N_S, \\
\frac{dN_{RS}}{dt} &= \delta_S f N_S - g(d) N_{RS}, \\
\frac{dN_P}{dt} &= \rho_P N_P + \rho_{SP} N_S + g(d) e^{(-\alpha_P d - \beta_P d^2)} N_{RP} - \rho_{PS} N_P - \delta_P f N_P, \\
\frac{dN_{RP}}{dt} &= \delta_P f N_P - g(d) N_{RP}.
\end{aligned}
\tag{3.2}
$$

Cells acquire on average one DNA double strand break after exposure to 1 Gy of radiation. Therefore we assume that each cell will enter cell cycle arrest and attempt repair after each radiation fraction, but no new damage arises in the interval between radiation treatments. Hence, $f = 1$ at discrete times when radiation is given, and $f = 0$ otherwise. Dependent on radiosensitivity parameters α_i and β_i with $i \in \{S, P\}$, cells will either die due to radiation induced DNA damage with probability $1 - S_i(d)$ or return to the viable non-repairing

Table 3.1: *Description of the model parameters.*

Parameters	Description
ρ_S	Net proliferation rate of CD^+ cells.
ρ_{SP}	Rate of switching of CD^+ cells to CD^- cells.
ρ_P	Net proliferation rate of CD^- cells.
ρ_{PS}	Rate of switching of CD^- cells to CD^+ cells.
$\delta_S f$	Rate at which CD^+ cells go for repair.
$\delta_P f$	Rate at which CD^- cells go for repair.
$g(d)(1-e^{(-\alpha_S d-\beta_S d^2)})$	Rate at which CD^+ cells that are in repair die.
$g(d)(1-e^{(-\alpha_P d-\beta_P d^2)})$	Rate at which CD^- cells that are in repair die.
$g(d)e^{(-\alpha_S d-\beta_S d^2)}$	Rate at which CD^+ cells that are in repair become active again.
$g(d)e^{(-\alpha_P d-\beta_P d^2)}$	Rate at which CD^- cells that are in repair become active again.

population S or P with probability $S_i(d)$ at dose-dependent rate $g(d)$. We assume the function $g(d)$ to be of the order of the inverse square of the dose (Lagadec et al., 2010; Sarcar et al., 2011), such that cells irradiated with a dose of 1 Gy spend on average 1 hour attempting repair, and 4 hours after exposure to 2 Gy.

3.2.1 Parameter estimation

Stochastic and deterministic simulations have been compared to two sets of experimental data to derive suitable values for model parameters. The experimental study on breast cancer initiating cells (i.e. CSCs) and mammosphere formation assay (MFA) data calibrates the fraction of biomarker positive CSCs (Lagadec et al., 2010). In this study, the breast cancer cell line is irradiated with a single dose or daily doses of 2 Gy. After 48 hours, single cells are seeded to form spheres for 20 days. The fraction of CSCs and mammosphere

formation capacity are reported in Table 3.2 (Lagadec et al., 2010).

Table 3.2: *The fractionated irradition effect on CSC population and mammosphere formation capacity (Lagadec et al., 2010).*

	$CD24^{low/-}/CD44^{high}$	
Dose	% of CSCs	Sphere forming capacity
2	6.54 (+/- 1.95)	13.49 (+/- 1.32)
2-2	8.04 (+/- 1.47)	10.76 (+/- 0.96)
2-2-2-2	8.56 (+/- 1.21)	11.85 (+/- 1.81)
Overall average	7.71	12.03

As the MFA experiment was initiated from a single cell (Lagadec et al., 2010), stochastic effects are important. We apply the Gillespie algorithm to compare model sphere forming capacity predictions with the experimental data in Table 3.2. Since running the Gillespie algorithm is computationally expensive, it is only used to fit the parameters of the model when $\delta s = \delta_p = g = 0$. We vary model parameters without repair to obtain the best fit to the experimental data. At the same time, we use the deterministic equations 3.2 to compare the theoretical results of average CSC fraction to experimental data. The estimated model parameters are summarized in Table 3.3, alongside the fraction of CSCs and sphere forming capacity using those values, which show good agreement with the experimental results in Table 3.2. Of note is that the reported parameter value combinations are not unique and, thus, we will perform a sensitivity analysis to investigate the impact of each parameter on model outcome.

Herein, resistant and sensitive tumor cells are considered to have different radio-sensitivities. Thus, the total population of cells at time t is given by $N(t) = N_S(t) + N_P(t)$ (Hereafter,

Table 3.3: *Estimated model parameters when $\delta_S = \delta_P = g = 0$. The values of fraction of CSCs and sphere forming capacity that are evaluated based on the estimated parameters values are also reported. The unit of all parameters is $1/day$.*

Parameters	ρ_S	ρ_{SP}	ρ_P	ρ_{PS}	% of CSCs	Sphere forming capacity
Values	0.2	0.7	0.1	0.05	7.6	12.7

$N_S \equiv N_S + N_{RS}$ and $N_P \equiv N_P + N_{RP}$ unless stated otherwise); the population of cells after exposure to treatment for the period of time τ can be calculated as

$$\frac{N(t+\tau)}{N(t)} = \frac{N_S(t)}{N(t)} e^{(-\alpha_S d - \beta_S d^2)} + \frac{N_P(t)}{N(t)} e^{(-\alpha_P d - \beta_P d^2)}. \tag{3.3}$$

Assuming that the fraction of CSCs is at its steady state value before the radiation, and using the experimental data of (Lagadec et al., 2010), we set $\frac{N_S(t)}{N(t)} = 0.076$ (and $\frac{N_P(t)}{N(t)} = 0.924$). Then, the modified linear quadratic model (Equation 3.3) is used to fit model results to the experimental data of (Piccirillo et al., 2006), which yields $\alpha_S = 0.14$ Gy^{-1}, $\beta_S = 0.048$ Gy^{-2} (α_S/β_S=2.9 Gy), $\alpha_P = 0.41$ Gy^{-1} and $\beta_P = 0.17$ Gy^{-2} (α_S/β_S=2.4 Gy) (Figure 3.2). Since at each radiation fraction the majority of damaged cells undergo repair mechanisms, we assume that 90% of cells will be arrested (Withers, 1992). However, sensitivity analysis shows that reducing this fraction to as low as 40% does not qualitatively change the results (see Figure A.1 and Figure A.6 in supplementary materials). The list of all model parameters and their estimated values are reported in Table 3.4.

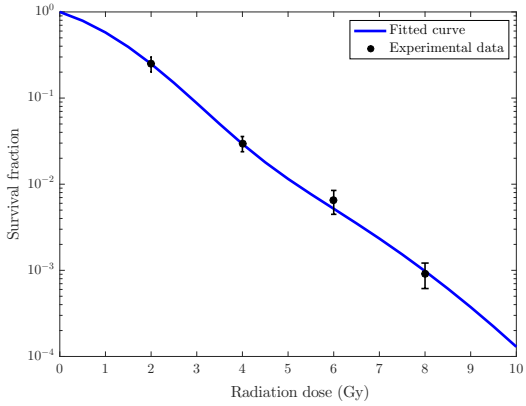

Figure 3.2: *Fitting the modified linear quadratic model to the experimental data of (Piccirillo et al., 2006). The black points are the extracted experimental data. The solid curve is the model result using the estimated radio-sensitivity parameters* $\alpha_S = 0.14\ Gy^{-1}$, $\beta_S = 0.048\ Gy^{-2}$, $\alpha_P = 0.41\ Gy^{-1}$ *and* $\beta_P = 0.17\ Gy^{-2}$.

3.3 Results

We consider different clinical radiotherapy treatment protocols for one week including standard of care (SoC; daily doses of 2 Gy), hyperfractionated (HR; two daily doses of 1 Gy), accelerated hyperfractionation (AC; two daily doses of 1.2 Gy), and hypofractionated (HO; twice a week doses of 5 Gy). Additionally we simulate the recently suggested optimal protocol for PDGF-driven glioblastoma by Leder (Leder et al., 2014) (Optimum-1, OP; see Table 3.5). All protocols deliver a total dose of $D = 10$ Gy per week, except accelerated hyperfractionated with a total dose of $D = 12$ Gy. However, the accelerated hyperfractionated protocol has the same biologically effective dose (BED) as SoC (see Table 3.6). BED is used to describe the biological effect of dose fractionation, and is defined as

Table 3.4: *Model parameter values.*

Parameters	Value (unit)	Reference
ρ_S	0.2 (day^{-1})	Using experimental data (Lagadec et al., 2010)
ρ_{SP}	0.7 (day^{-1})	Using experimental data (Lagadec et al., 2010)
ρ_P	0.1 (day^{-1})	Using experimental data (Lagadec et al., 2010)
ρ_{PS}	0.05 (day^{-1})	Using experimental data (Lagadec et al., 2010)
$\delta_S = \delta_P$	310 (day^{-1})	Assuming 90% of cancer cells undergo repair
α_S	0.14 (Gy^{-1})	Using experimental data (Piccirillo et al., 2006)
α_P	0.41 (Gy^{-1})	Using experimental data(Piccirillo et al., 2006)
β_S	0.048 (Gy^{-2})	Using experimental data (Piccirillo et al., 2006)
β_P	0.17 (Gy^{-2})	Using experimental data (Piccirillo et al., 2006)
f	1 or 0	1: radiation, 0: no radiation

$$\text{BED} = \frac{-\ln(SF(d))}{\alpha} = D(1 + \frac{d}{\alpha/\beta}), \tag{3.4}$$

where $SF(d)$ is the LQ Model derived single dose d dependent survival fraction with radiobiological parameters α and β (compare Equation 3.1). Due to the linear quadratic relationship of dose and survival, total dose can be increased when smaller doses are given in each fraction (Fowler, 1989). The model introduced in Section 3.2 considered two subgroups of cancer cells (resistant cells and sensitive cells) with different radiosensitivities. Thus, following the survival fraction of cancer cells in equation 3.3, the BED is given by

$$\text{BED} = \frac{-\ln(mSF_S + (1-m)SF_P)}{m\alpha_S + (1-m)\alpha_P}, \tag{3.5}$$

where SF_S and SF_P are survival fractions for resistant cells and sensitive cells respectively. The constant m represents the proportion of resistant cells in the tumor prior to irradiation.

Table 3.6 shows the BED for the standard of care (SoC), hyperfractionated (HR), and accelerated hyperfractionated (AC) protocols with different initial fractions of resistant cells: Tumors containing only resistant cells ($m = 1$), tumors containing only sensitive cells ($m = 0$), and heterogeneous tumors with a small subpopulation of resistant cells ($m = 0.076$) as estimated. The BED is almost identical for standard of care and accelerated hyperfractionation, but significantly smaller for hyperfractionation.

Table 3.5: *Radiotherapy schedules for one week of treatment. Different colors are used for corresponding colors in the figures.*

Schedule	Day 1	Day 2	Day 3	Day 4	Day 5
Standard of Care (SoC)	2	2	2	2	2
Hyperfractionated (HR)	2×1	2×1	2×1	2×1	2×1
Optimum-1 (OP)	3×1	1	2×1	1	3×1
Hypofractionated (HO)	5	-	-	-	5
Accelerated hyperfractionated (AC)	2×1.2	2×1.2	2×1.2	2×1.2	2×1.2

Table 3.6: *The Biological effective dose for Hyperfractionation, Standard of Care, and Accelerated Hyperfractionated protocols.*

	Schedules		
BED	HR (d=1, n=10)	SoC (d=2, n=5)	AC (d=1.2 n=10)
BED_S (m=1)	13.5	17.1	17.1
BED_P (m=0)	14.1	18.3	17.9
BED_{SP} (m=0.076)	11.1	12.7	12.7

Figure 3.3 shows the number of cancer cells $N_S + N_P$ and fraction of resistant cells $N_S/(N_S + N_P)$ for all considered radiation schedules (compare Table 3.5). Simulations

show that protocols with larger number of fractions leads to more cell kill, with accelerated hyperfractionation yielding the smallest number of cells after one week of therapy. However, the fraction of stem cells is largest compared to the other radiotherapy protocols. Hypofractionation with smallest overall cell kill leads also to least competitive release of the most resistant stem cell subpopulation (Enderling et al., 2009a).

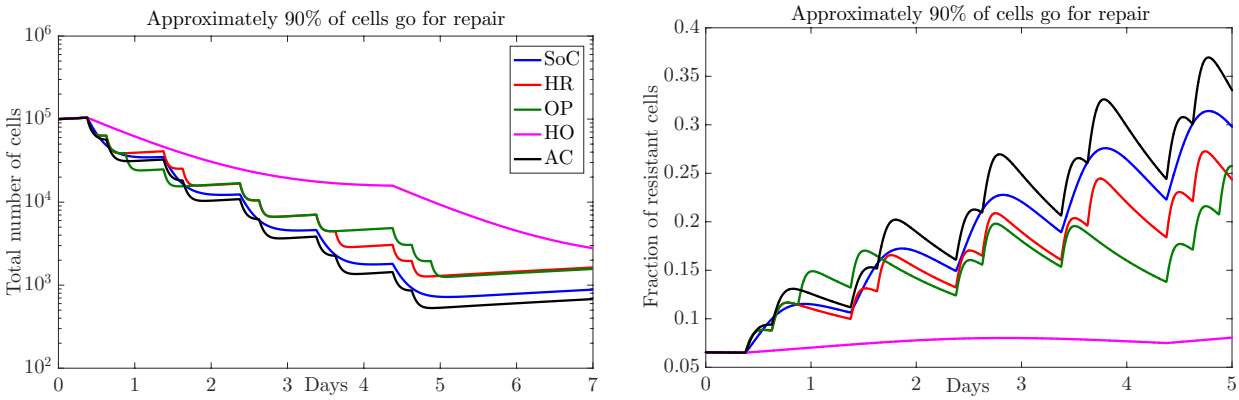

Figure 3.3: *The number of cancer cells N_S+N_P and the fraction of resistant cells $N_S/(N_S+N_P)$ for radiotherapy protocols reported in Table 3.5.*

For the chosen parameter combinations (Table 3.4), accelerated hyperfractionation and SoC schedules yield the lowest number of cancer cells after one week of treatment (Figure 3.3). Sensitivity analysis showed that the results are robust to changes in the parameter values (Table 3.7), with the exception that decreasing α_P and β_P by 50% produces hypofractionated and accelerated hyperfractionated as best protocols (Figure 3.4).

Heretofore we assumed that 90% of cells undergo arrest to attempt repair, and the parameter values for δ_S and δ_P were chosen large enough to satisfy this assumption. However, decreasing the values for these parameters so that less than 40% of cells attempt repair

suggests accelerated hyperfractionated as the best schedule (see Figure A.1 and Figure A.6 in Appendix A). Furthermore, the model considers that cells leave arrest with rate $g(d)$, which is assumed to be on the order of $1/\text{dose}^2$. If $g(d)$ was proportional to $1/\text{dose}$ the number of cancer cells at the end of the course of radiation therapy decreases significantly; however, the accelerated hyperfractionated schedule remains the best treatment protocol followed by SoC. Moreover, if $g(d) = 1$, the order of the best treatment regimens remains (see Figure A.3, Figure A.4, and Figure A.5 in Appendix A).

Table 3.7: *Sensitivity analysis for different parameters of the model.*

Parameters	α_S, β_S	α_P, β_P	ρ_S	ρ_P	ρ_{PS}	ρ_{SP}	1st best	2st best
Default	0.14, 0.05	0.41, 0.17	0.2	0.1	0.044	0.73	AC	SoC
α_S, β_S (+50%)	0.21, 0.07	0.41, 0.17	0.2	0.1	0.044	0.73	AC	SoC
α_S, β_S (-50%)	0.07, 0.04	0.41, 0.17	0.2	0.1	0.044	0.73	AC	SoC
α_P, β_P (+50%)	0.14, 0.05	0.61, 0.25	0.2	0.1	0.044	0.73	AC	SoC
α_P, β_P (-50%)	0.14, 0.05	0.21, 0.08	0.2	0.1	0.044	0.73	HO	AC
ρ_S (+50%)	0.14, 0.05	0.41, 0.17	0.3	0.1	0.044	0.73	AC	SoC
ρ_S (-50%)	0.14, 0.05	0.41, 0.17	0.1	0.1	0.044	0.73	AC	SoC
ρ_P (+50%)	0.14, 0.05	0.41, 0.17	0.2	0.15	0.044	0.73	AC	SoC
ρ_P (-50%)	0.14, 0.05	0.41, 0.17	0.2	0.05	0.044	0.73	AC	SoC
ρ_{PS} (+50%)	0.14, 0.05	0.41, 0.17	0.2	0.1	0.066	0.73	AC	SoC
ρ_{PS} (-50%)	0.14, 0.05	0.41, 0.17	0.2	0.1	0.022	0.73	AC	SoC
ρ_{SP} (+50%)	0.14, 0.05	0.41, 0.17	0.2	0.1	0.044	1.09	AC	SoC
ρ_{SP} (-50%)	0.14, 0.05	0.41, 0.17	0.2	0.1	0.044	0.36	AC	SoC

The UK standardisation of breast radiotherapy (START) trials constituted a study conducted to reduce late normal tissue complications and local tumour control in women with breast cancer exposed to radiotherapy after tumor removal (The START Trialists' Group, 2008). The study consisted of two parallel trials, START A and START B, which con-

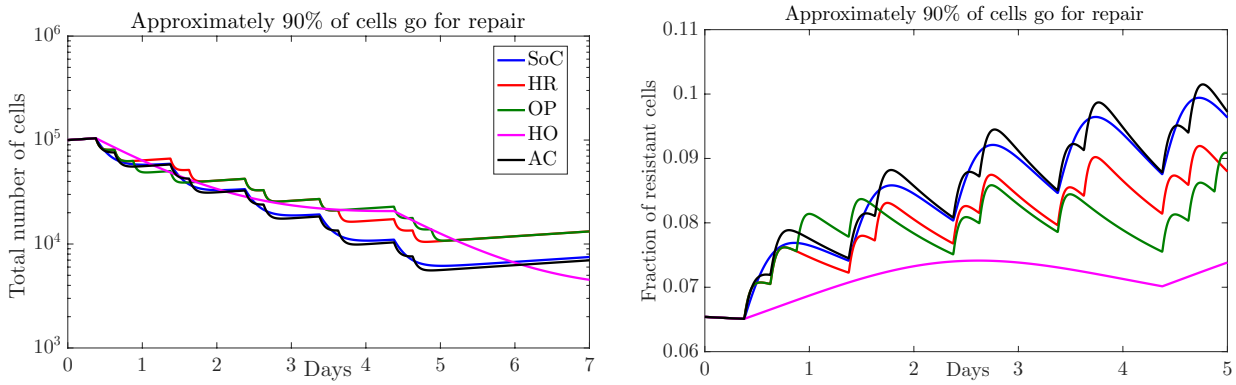

Figure 3.4: *The number of cancer cells N_S+N_P and the fraction of resistant cells $N_S/(N_S+N_P)$ when α_P and β_P are changed to $\alpha_P-0.5\alpha_P$ and $\beta_P-0.5\beta_P$ for radiotherapy protocols reported in Table 3.7 .*

sidered the standard radiotherapy protocol, including 50 Gy in 25 fractions delivered in 5 weeks, one highly-prescribed protocol. To reduce tumour relapse and normal tissue damage, the schedule was improved based on normal and cancerous cells radiosensitivities and their response to fractionated doses. Therefore, the conventional protocol was modified to deliver higher amounts of radiation at each fraction with acceptable reduction in the total dose. In the START A trial, patients were arbitrarily exposed to five weeks of treatment with either 50 Gy in 25 fractions, 41.6 Gy in 13 fractions, or 39 Gy in 13 fractions. In the START B study, patients were randomly assigned to either 50 Gy in 25 fractions over 5 weeks or 40 Gy in 15 fractions for three weeks (Haviland et al., 2013). The model proposed in this current chapter uses the treatment schedules discussed in the START trials to explore tumour diversity after each course of radiation. In addition, sensitivity analysis has been carried out to explore the effects of model parameters on the radiotherapy schedules used in the START trials.

The number of cancer cells and fraction of resistant cells for the treatment protocols reported in the START trails are presented in Figure 3.5. The conventional regimen treatment with total dose 50 Gy has the smallest number of cancer cells and a relatively high fraction of resistant cells. Thus, this Conventional treatment schedule can be effective to kill cancer cells, but the probability of relapse is fairly high. In addition, the treatment schedule with total dose 40 Gy, represents the highest number of cancer cells and highest fraction of resistant cells, which imply that this hypofractionated regimen is not efficient in curing the disease and it can also cause late side effects and relapse. On the contrary, the study conducted in the START trials reports that hypofractioned schedules are as safe and effective as standard control protocols. The sensitivity of the results to the parameters of the model was investigated. The outcome concluded that α_P and β_P were the most important parameters. The number of cancer cells and fraction of resistant cells when α_P and β_P are changed to $\alpha_P - 0.5\alpha_P$ and $\beta_P - 0.5\beta_P$ are sketched in Figure 3.6. As seen, the hypofractionated regimen with total dose 41.6 Gy behaves similarly to the standard control schedule with a lower fraction of resistant cells. Thus, the impact of the radiotherapy with respect to the treatment for these two protocols are comparable, however the hypofractionated schedule results in a smaller probability of relapse.

As previously stated, due to the fatal effects of 1 Gy of radiation, δ_S and δ_P are selected adequately large such that 90% of cells undergo DNA repair pathways. The reduction in the values of these parameters, so that less than 40% of cells go through repair stage, can change the behavior of the hypofractionated regimen (with total dose of 40 Gy) significantly. This hypofractionated protocol is improved to the second order in terms of the number of cancer cells. Furthermore, the fraction of resistant cells is comparatively similar to the fraction

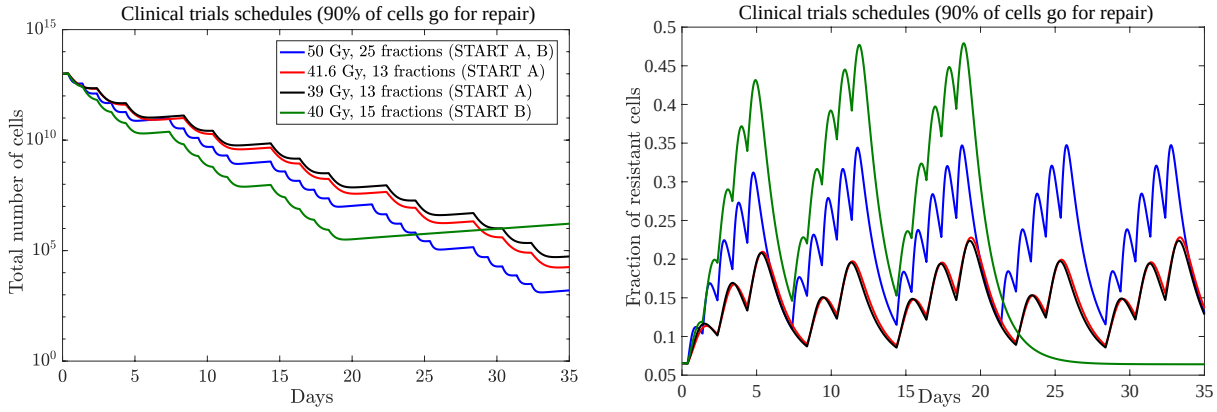

Figure 3.5: *The number of cancer cells N_S+N_P and the fraction of resistant cells $N_S/(N_S+N_P)$ for the radiotherapy schedules reported in START trials.*

of resistant cells for the Control conventional treatment strategy, but still worse than the other hypofractionated schedules. Thus, the hypofractioned protocol with total dose 40 Gy is at least as efficient as the conventional regimen (see Figure A.6 in Appendix A). The sensitivity of the outcomes to the assumption of the function $g(d)$ is also studied. Two sets of assumptions have been considered for the function $g(d)$ in this study: the inverse of the dose delivered at each fraction of treatment and the constant value 1. For the former assumption, the number of cancer cells decreases and the order of the schedules has not been changed. For the latter, the number of cancer cells also decreases and the treatment protocols show no qualitative differences (see Figure A.7 and Figure A.8 in Appendix A). Furthermore, the hypofractionated schedule (with a total dose of 40 Gy) drops quickly in comparison with the other three regimens when the function $g(d)$ is changed from being proportional to the inverse square of dose to the inverse of dose (see Figure A.9 in Appendix A).

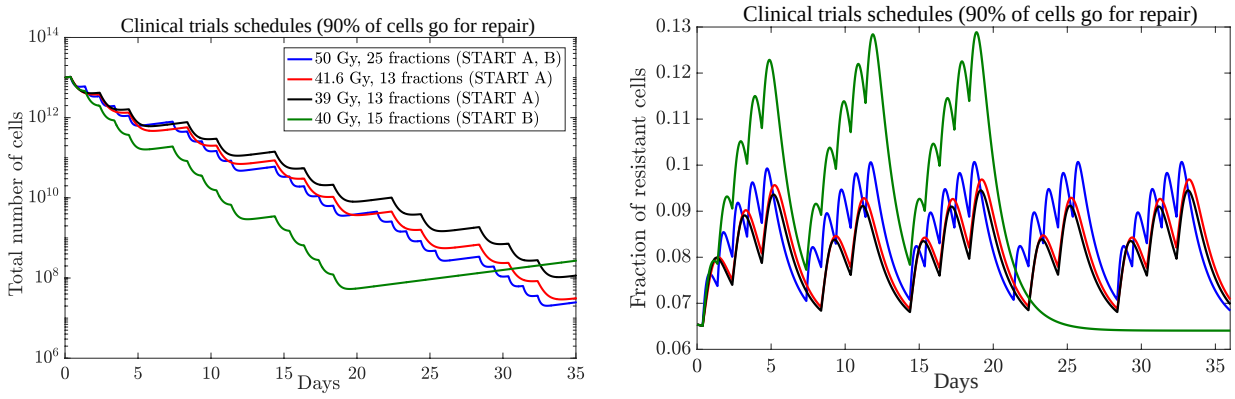

Figure 3.6: *The number of cancer cells N_S+N_P and the fraction of resistant cells $N_S/(N_S+N_P)$ for the radiotherapy schedules reported in START trials when α_P and β_P are changed to $\alpha_P - 0.5\alpha_P$ and $\beta_P - 0.5\beta_P$.*

3.4 Conclusion

In this chapter, a two-compartment mathematical model has been developed to assess the effects of tumor heterogeneity and radiotherapy fractionation on treatment response. Model simulations suggest that radiotherapy can alter tumor heterogeneity, and elevate the fraction of resistant cells. In future studies, we propose to further increase biological complexity by considering increased self-renewal of the resistant population in response to radiation (Gao et al., 2013). If the total radiation dose is insufficient to eradicate the tumor, enrichment in cancer stem cells may lead to tumor relapse and recurrence. Therefore, if total tumor control cannot be achieved, optimal therapies should balance decreases in tumor burden and prevention of outgrowth of the most resistant subpopulation. Interestingly, none of our simulations suggested the standard of care fractionation as the best therapeutic approach, further emphasizing the need to prospectively evaluate alternative

fractionation protocols in the clinic. Furthermore, our model calibrated for breast cancer was unable to confirm the optimum treatment schedule for PDGF-driven glioblastoma (as in Leder et al., 2014). This suggests that treatment optimization may be highly dependent on the tumor biology, the mathematical model, and model parameter dependent, and the utmost attention must be paid to identifying the underlying biological mechanisms. Hence, a general optimal radiation schedule as suggested in (Conforti et al., 2008; Leder et al., 2014; Wein et al., 2000) may not be feasible, and designing different efficient protocols may be required for each type of cancer, and even each individual patient.

The model has also been applied to the START trials to investigate the effect of the proposed protocols on tumor heterogeneity. In START trials, radiotherapy is administered after surgery and chemotherapy. Many different features such as demographic factors, and the stage and type of the disease can influence the results. Thus, our aim in this chapter was not to compare the model predictions with START trials outcomes, but rather to consider the impact of the radiotherapy schedules on tumor diversity. In general, the results suggest that the number of cells is minimal after the standard regimen, but the fraction of resistant cells is relatively high. In addition, the other three hypofractionated protocols, with larger doses of fractions and lower total dose, have different effects on cancer cell dynamics. For example, both the number of cancer cells and the fraction of resistant cells are large after exposure to the schedule with a total dose of 40 Gy. The regimens with total doses of 41.6 Gy and 39 Gy reduce the fraction of resistant cells to the minimum in comparison with other schedules, but the number of cells is still bigger than that after standard schedules.

At the moment, the study is hypothesis generating, and we sincerely hope that the presented results stimulate and encourage experimentalists and clinicians to test the presented

model predictions.

Financial support by the Natural Sciences and Engineering Research Council of Canada (NSERC) (MK) is gratefully acknowledged.

Chapter 4

The impact of random microenvironmental fluctuations on tumor control probability

The tumor control probability (TCP) is a metric used to calculate the probability of controlling or eradicating tumors through radiotherapy. Cancer cells vary in their response to radiation, and although many factors are involved, the tumor microenvironment is a crucial one that determines radiation efficacy. The tumor microenvironment plays a significant role in cancer initiation and propagation, as well as in treatment outcome. We have developed stochastic formulations to study the impact of arbitrary microenvironmental fluctuations on TCP. Since the derivation of analytical solutions may not be possible for complicated cases, we employ a modified Gillespie algorithm to analyze TCP, and take into

consideration the random variations in cellular proliferation and death rates. Our results show that increasing the standard deviation in demographic factors initially enhances the probability of tumor eradication. However, if the TCP does not reach a probability of 1, the increase in the standard deviation subsequently has a negative impact on treatment effectiveness, decreasing the TCP over time. The greatest effect on TCP has been observed when both birth and death rates are being randomly modified and are anticorrelated.

4.1 Introduction

Radiotherapy delivers high doses of energy to disrupt cancer cell proliferation and destroy tumor cells with the ultimate goal of maximizing tumor control and minimizing normal tissue complication. Radiotherapy efficiency and tumor response depend on many different factors, such as the degree of tumor heterogeneity, plasticity, hypoxia, the tumor microenvironment, and cell cycle regulation. The tumor microenvironment, which also creates substantial barriers to the delivery and effectiveness of anticancer treatments, consists of different cellular types such as vascular networks, immune system cells, fibroblasts, and inflammatory cells. The complex interaction between the tumor microenvironment and a heterogenous cancer cell population influences tumorigenesis, metastasis, and therapeutic outcomes. For example, the irregular signaling pathways regulating malignant cells simulate the activation of fibroblasts and other molecular mechanisms that impact cell proliferation (Wang et al., 2017). Moreover, the active process of angiogenesis generates abnormal vascular structures, which increase leakiness and elevate interstitial fluid pressure in the tumor, and interrupting the regular blood flow in the tissue (Fukumura & Jain, 2007; Hanahan & Weinberg, 2011). Consequently, these random and complicated interactions create regions of hypoxia and acidosis, leading to more aggressive and resistant tumor cells that prevent effective therapeutic interventions. The impact of such irregular fluctuations in natural selection and the fitness of emerging mutants have been discussed for a heterogenous population (Mahdipour et al., 2017; Nowak et al., 2003), but the effect of random environmental variations on tumor response to therapeutic protocols is not yet well understood.

The efficiency of radiotherapy and potential benefits of various treatment schedules are commonly evaluated using a range of treatment-planning tools and approaches. For example, the tumor control probability (TCP) qualitatively calculates the capability of administered doses and radiotherapy regimens to eliminate a tumor. Several mathematical models of TCP have been discussed in the literature (Kendal, 1998; Munro & Gilbert, 1961; Tucker et al., 1990; Yakovlev, 1993; Zaider & Minerbo, 2000). One of the preliminary models proposed that the probability of eradicating cancer cells approximates a Poisson distribution, if the number of surviving cells follows a binomial distribution (Zaider & Minerbo, 2000). However, the Poisson model of TCP does not consider cell proliferation during treatment and might underestimate the exact TCP (Tucker et al., 1990; Yakovlev, 1993). Zaider & Minerbo (2000) developed another well known TCP model to incorporate stochastic effects on cell proliferation and cell kill. This model was suggested based on a simple birth/death process and can be applied to any treatment protocol. The extension of these models and other approaches such as Monte Carlo simulations have been employed to take cell cycles and quiescent effects into consideration (Dawson & Hillen, 2006; Gong, 2011).

In this chapter, a stochastic model is developed to investigate the role of tumor microenvironmental fluctuations on tumor control probability. The arbitrary fluctuations in cell birth and death rates are modelled using a dichotomous Markov noise, which describes either birth and/or death rates as correlated noise with random discontinuous jumps. The derivation of the analytical solution is complicated when demographic rates change randomly. Therefore, a modified Gillespie algorithm for time changing discontinuous transition rates is applied to study the TCP. The results suggest that if either birth or death rates

change randomly, the probability of tumor eradication initially improves, however, random changes negatively impact TCP over time. Moreover, changing both birth and death rates such that cells with higher proliferation rates die with lower death rates has the highest impact on TCP. In this case, TCP is improved if birth and death rates are autocorrelated, and the best outcome is when cells with higher birth rates die with higher death rates.

4.2 Method

We assume that cancer cells can reproduce by splitting into two at a rate of $\rho(t)$ and can die autonomously at a rate of $\Gamma(t)$. In order to determine the stochastic dynamic of the model, we first define the probability distribution function for the system. Suppose that at an initial time, t_0, the number of cancer cells is denoted by n_0. The probability distribution of having a population of n_c cancer cells at time t is denoted by $p_{n_c}(t)$ with the following master equation

$$\frac{dp_{n_c}(t)}{dt} = \rho(t)p_{n_c-1}(n_c-1) - (\rho(t)+\Gamma(t))p_{n_c}n_c + \Gamma(t)p_{n_c+1}(n_c+1), \tag{4.1}$$

where $\rho(t)$ and $\Gamma(t)$ are the corresponding birth rate and death rate for cancer cells, respectively. Here, the initial condition is given by $p_{n_c}(t_0) = \delta_{n_c n_0}$ (with $\delta_{i,j}$ being the Kronecker delta function). Considering the probability generating function $U(z,t) = \sum_{i=0}^{\infty} p_i(t)z^i$ and substituting (4.1) into $\dfrac{\partial U(z,t)}{\partial t}$, we get

$$\frac{\partial U(z,t)}{\partial t} = (z-1)(\rho(t)z - \Gamma(t))\frac{\partial U(z,t)}{\partial z}, \tag{4.2}$$

with initial condition $U(z,0) = z^{n_0}$.

Partial differential equation 4.2 can be solved using the method of characteristics. Let $C : [z(\tau), t(\tau)]$ be a curve in the (z,t) plane. Hence,

$$\frac{dU}{d\tau} = \frac{dU}{dz}\frac{dz}{d\tau} + \frac{dU}{dt}\frac{dt}{d\tau}. \tag{4.3}$$

Assuming that $U(z(\tau), t(\tau))$ is constant along this characteristic curve, we get $\frac{dU}{d\tau} = 0$. Comparing 4.2 and 4.3 results in

$$\frac{dz}{d\tau} = -(z-1)(\rho(\tau)z - \Gamma(\tau)), \tag{4.4}$$

relabelling τ as t gives

$$\frac{dz}{dt} = -(z-1)(\rho(t)z - \Gamma(t)), \tag{4.5}$$

which can be written as

$$\frac{dz}{dt} = -(z-1)(\beta(t) - (1-z)\rho(t)), \tag{4.6}$$

where $\beta(t) = \rho(t) - \Gamma(t)$. It can be verified that multiplying $\lambda(t) = \exp(-\int_0^t \beta(t')dt')$ and adding $\frac{dz}{dt}(z-1)\phi(t)$ to both side of equation 4.6, where $\phi(t) = \int_0^t \rho(t')\lambda(t')dt'$ yields

$$\frac{d}{dt}\left(\frac{(1-z)}{\lambda(t) + (1-z)\phi(t)}\right) = 0, \tag{4.7}$$

which is valid when $\beta(t)$ is a continuous function. Consequently, $\left(\frac{(1-z)}{\lambda(t)+(1-z)\phi(t)}\right)$ is equal to a constant, and since $U(z,t)$ is constant along the characteristic curve, we get

$$U(z,t) = f\left(\frac{(1-z)}{\lambda(t)+(1-z)\phi(t)}\right). \tag{4.8}$$

Applying the initial condition $U(z,0) = z^{n_0}$ in 4.8 implies that $f(z) = (1-z)^{n_0}$. Thus,

$$U(z,t) = \left[1 - \frac{1}{\left(\frac{\lambda(t)}{1-z} + \int_0^t \rho(t')\lambda(t')dt'\right)}\right]^{n_0}, \tag{4.9}$$

and TCP can be defined as the probability of eradicating all cancer cells, given as below

$$TCP(t) = U(0,t) = \left[1 - \frac{1}{\left(\lambda(t) + \int_0^t \rho(t')\lambda(t')dt'\right)}\right]^{n_0}. \tag{4.10}$$

Evaluating equation 4.10 is trivial for the simple functional forms of $\rho(t)$ and $\lambda(t)$. However, the analytical computation can be difficult for more complicated functions $\rho(t)$ and $\lambda(t)$. In this latter case, numerical methods are beneficial. One possible approach is to solve differential equation 4.5 numerically (Appendix B). Alternatively, the master equation, 4.1, can be solved using the Gillespie algorithm. These three approaches are compared below to show that the Gillespie algorithm is a suitable method when the rates are either constant or vary over time (for simplicity we assume that $\rho(t)$ is constant). Reducing a partial differential equation to a related ordinary differential equation and deriving the analytical solution may not always be possible. However, the Gillespie algorithm is a useful approach for solving complicated systems.

Constant $\Gamma(t)$

Here, the mortality rate is assumed to be uniform over time (i.e. $\Gamma(t)$ is constant). The results show that there is good agreement among the analytical solution, the numerical method, and the Gillespie algorithm, assuming death rates are constant (Figure 4.1).

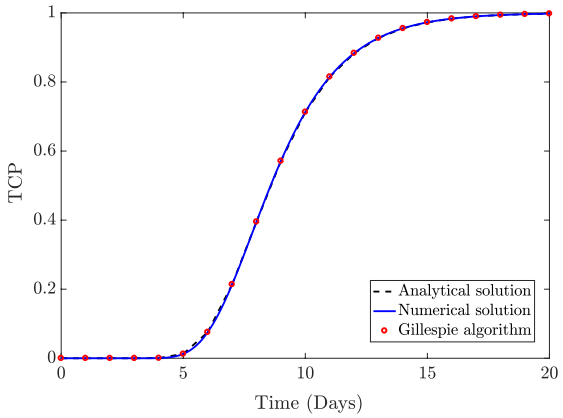

Figure 4.1: *Comparison of the analytical solution, the numerical method, and the Gillespie algorithm, when* $n_0 = 100$, $\rho = 0.5$ *and* $\Gamma = 1$.

$\Gamma(t)$ changes over time

In practice, it is not realistic to assume that the death rate is constant over time. For instance, when fractionated radiotherapy is given, the total administered dose is broken down into smaller fractions of doses, decreasing toxicity and damage to normal cells as well as increasing efficiency. Therefore, based on the prescribed protocol, each fraction is given for 15-30 minutes once or twice a day. The cell kill effect can be described as a step function in which there is a higher cell death rate in the presence of radiotherapy and a lower death rate when there is no radiation. Hence, $\Gamma(t)$ is assumed to be a piecewise

function given as below when $k_1 > k_2$.

$$\Gamma(t) = \begin{cases} k_1 & \text{radiation induced cell death,} \\ k_2 & \text{radiation independent cell death.} \end{cases} \tag{4.11}$$

As described above, for an analytical solution, $\rho(t)$ and $\Gamma(t)$ must be continuous functions. In this direction, in equation 4.10, $\Gamma(t)$ can be defined using a hyperbolic tangent function $H_\delta(t) = \frac{1}{2}(1 + tanh(\frac{x}{\delta}))$ to smooth out the approximation to the discontinuous Heaviside function $H(x)$, where δ determines the width of the smooth transition. Figure 4.2 compares the analytical, numerical, and Gillespie solutions for the two different cell-kill functions. The last uses a modified Gillespie algorithm for rates that change discontinuously over time (see Appendix C). The results show good agreement between the analytical solution and the Gillespie algorithm. However, the numerical solution displays an error, which is probably due to the instability of finite difference methods in the presence of sharp changes. Although, the error is negligible for linear differential equations, it can be large for nonlinear ones. Using the numerical method given in Appendix (B), TCP(t) equals the n_0-th power of the solution for the differential equation 4.5, and the relative error for TCP(t) approximately equals $n_0\delta z$, where δz is a relative error in z. Resolving this issue is not within the scope of this work, which focuses on applying the modified Gillespie algorithm (Shahrezaei et al., 2008) for solving problems with rates that are changing discontinuously over time.

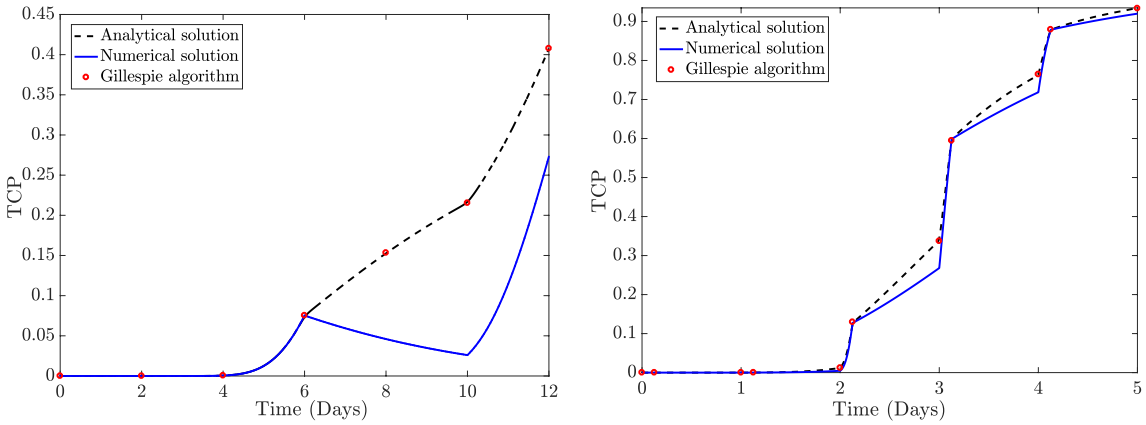

Figure 4.2: *Comparison of the analytical solution, the numerical method, and the Gillespie algorithm, when* $n_0 = 100$ *and* $\rho = 0.5$*, for two different cell kill rates: (a)* $\Gamma = 0.4$ *for* $6 < t \leq 10$ *and* $\Gamma = 1$ *otherwise. (b)* $\Gamma = 8$ *(every day for* 3 *hours) and* $\Gamma = 1$ *otherwise.*

The role of arbitrary fluctuations on TCP

Cancer cells live in a complex and ever-changing microenvironment that has a performed impact on their behavior and fate. For example, inflammation, hypoxia, and acidosis in and around a tumor can contribute to treatment resistance, reducing treatment induced cell kill effects. In this direction, we investigate TCP for a cancer cell population that is subject to microenvironmental randomness. Therefore, the simple birth/ death model discussed above is considered. To incorporate microenvironmental-induced fluctuations in the model, the proliferation and death rates are assumed to exchange stochastically between two values, k_1 and k_2, with an average $\overline{k} = (k_1 + k_2)/2$. This stochastic fluctuation occurs continuously based on dichotomous Markov noise $\xi(t) \in \{-1, +1\}$ with zero mean and autocorrelation $\langle \xi(t)\xi(t') \rangle = \exp(-2\nu|t - t'|)$, where ν is the rate of random changes and

$1/(2\nu)$ is the finite correlation time. Thus, proliferation and death rates are given by

$$\frac{1}{2}[\ (k_1 + k_2) + \xi(t)(k_1 - k_2)]\ . \tag{4.12}$$

The addition of this noise to the system describes birth and death rates as random step functions, changing over time. Consequently, we calculate TCP using a modified Gillespie algorithm for different switching rates, ν.

4.3 Results

4.3.1 Random birth rate

In this section, we consider $\Gamma(t) = \Gamma$ to be constant, and $\rho(t) = \frac{1}{2}[\ (k_1+k_2)+\xi(t)(k_1-k_2)]$, which alters stochastically, following the dichotomous Markov noise explained above. Here, TCP is measured for different random change rates ν. In addition, it is assumed that $\rho(t)$ alters randomly over time between two values k_1 and k_2 that are equidistant from the average $(\overline{k})$. Thus, $k_1 = \overline{k} + \sigma$ and $k_2 = \overline{k} - \sigma$, where σ is a standard deviation. The results show that tumor control probability approaches TCP, corresponding to a constant proliferation rate, as the random change rate (ν) increases or the finite correlation time $(1/(2\nu))$ decreases (Figure 4.3). Furthermore, as Figure 4.4 demonstrates, as the standard deviation (σ) increases, the probability of eradicating cancer cells initially increases, and thereafter decrease.

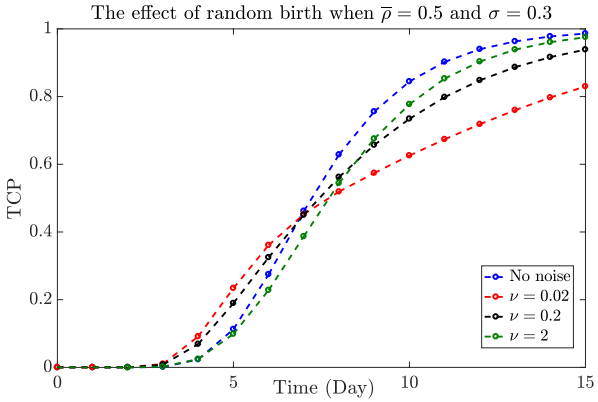

Figure 4.3: Tumor control probability when proliferation rate switches randomly, with an average $\overline{\rho} = 0.5$, standard deviation $\sigma = 0.3$, $n_0 = 50$, and $\Gamma = 1$ for the different switching rates.

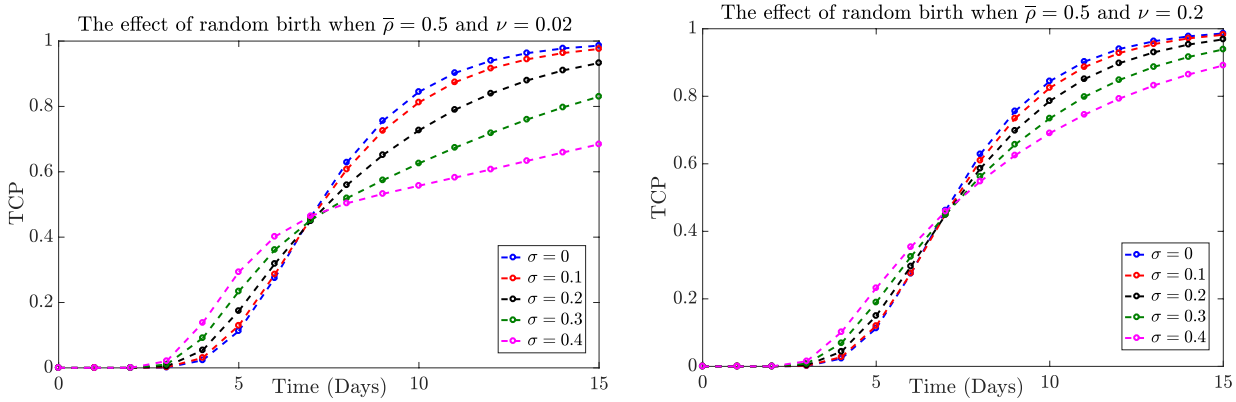

Figure 4.4: Tumor control probability when division rate is switching randomly with $\overline{\rho} = 0.5$, $n_0 = 50$, $\Gamma = 1$, and different standard deviations for switching rates $\nu = 0.02$ and $\nu = 0.2$.

Moreover, as σ increases, extinction time distribution is skewed to the right, and the average extinction time decreases (Figure 4.5). Therefore, Figures 4.4 and 4.5 confirm that higher variation (σ) is initially beneficial for tumor removal, but reduces the probability of tumor eradication over time. Increasing σ also modifies the dynamics of cell numbers,

enhancing their average and variance (Figure 4.6).

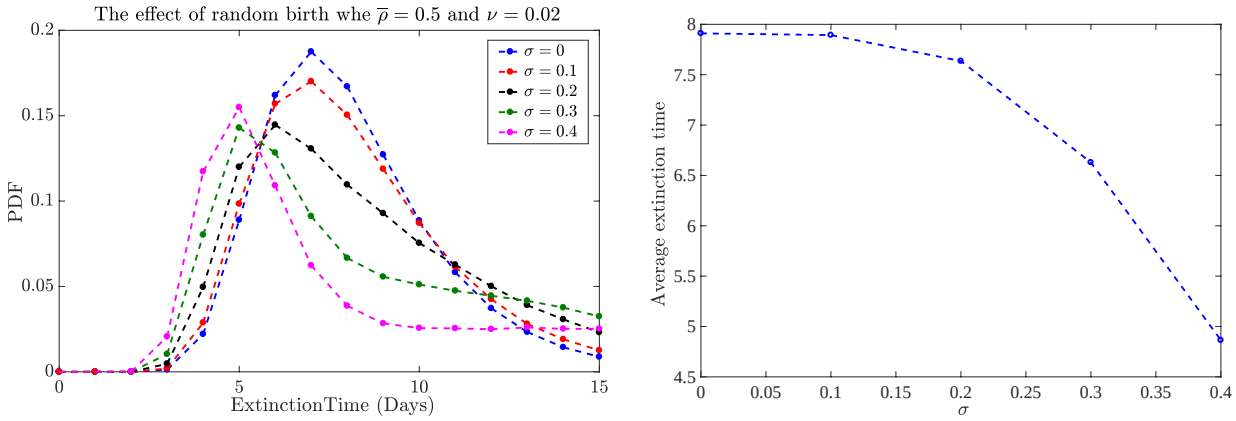

Figure 4.5: The average extinction time and extinction time distribution when $\overline{\rho} = 0.5$, $n_0 = 50$, $\Gamma = 1$, and different standard deviations for switching rate $\nu = 0.02$.

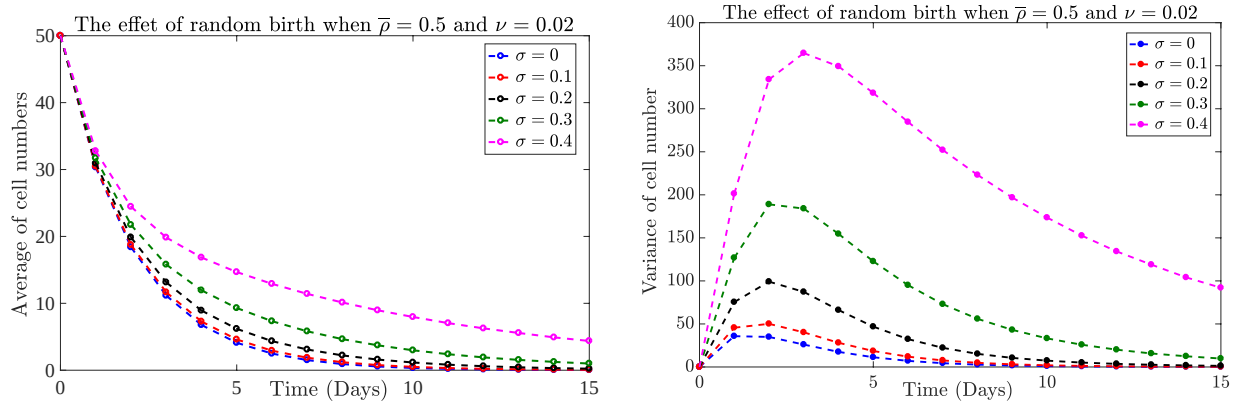

Figure 4.6: The average and variance of cell numbers with $n_0 = 50$, $\overline{\rho} = 0.5$, $\Gamma = 1$, and different standard deviations for switching rate $\nu = 0.02$.

It is important to understand why increasing the standard deviation primarily enhances TCP, but then reduces the efficiency of treatment over time. Consequently, TCP is calculated when the rate of random fluctuations, ν, is sufficiently small, or when the finite correlation time, $1/(2\nu)$, approaches infinity. Therefore, the proliferation rate is either

$\overline{\rho}+\sigma$ or $\overline{\rho}-\sigma$ at each realization, and so can be used in cases when a patient's randomly assigned cell division rate is one of these two values. Assuming these two specific cases, TCP can be measured using the analytical solution (equation 4.10), because both birth and death rates are constant. Figure 4.7 graphs TCP for proliferation rates corresponding to $\overline{\rho}$, $\overline{\rho}+\sigma$, and $\overline{\rho}-\sigma$, respectively. This figure also displays the average tumor control probability of $\text{TCP}_{\overline{\rho}+\sigma}$ and $\text{TCP}_{\overline{\rho}-\sigma}$. The lower birth rate $\overline{\rho}-\sigma$ results in a greater TCP value, which eventually saturates to the probability 1 over time. At the same time, the higher birth rate $\overline{\rho}+\sigma$ leads to a lower probability of tumor removal. Therefore, on average, TCP is controlled by $\text{TCP}_{\overline{\rho}-\sigma}$ before it approaches 1, and thereafter, TCP is determined by $\text{TCP}_{\overline{\rho}+\sigma}$. As a result, taking randomness into consideration, TCP can reduce to, at most, a probability of 0.5, which is the average of the highest and lowest possible probabilities for division rates $\overline{\rho}-\sigma$ and $\overline{\rho}+\sigma$, respectively, for enough large time t.

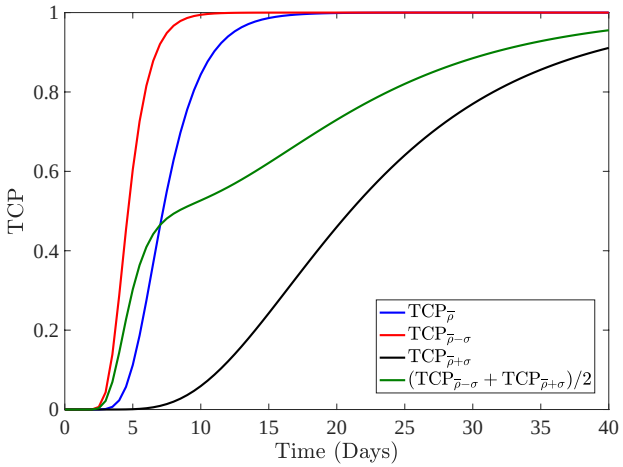

Figure 4.7: Tumor control probability obtained from analytical solution with $\overline{\rho}=0.5$, $\Gamma=1$, $\sigma=0.4$, and $n_0=50$.

In addition, Figure 4.8 shows $(\mathrm{TCP}_{\overline{\rho}-\sigma} + \mathrm{TCP}_{\overline{\rho}+\sigma})/2$ evaluated using an analytical solution for different standard deviations, confirming the same qualitative behavior as reported when the proliferation rate is changing randomly over time (ν is not small).

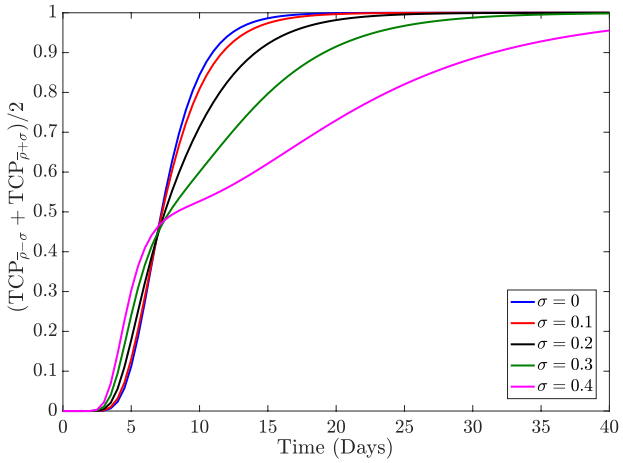

Figure 4.8: Tumor control probability obtained from analytical solution with $\overline{\rho} = 0.5$, $\Gamma = 1$, $n_0 = 50$, and different standard deviations.

4.3.2 Random death rate

We apply dichotomous Markov noise to describe the death rate $\Gamma(t) = \frac{1}{2}[\ (k_1 + k_2) + \xi(t)(k_1 - k_2)]$ and we consider a constant birth rate $\rho(t) = \rho$. The results for random death are similar to those explained above for the random birth case (see Figures D.1, D.2, D.3, D.4, and D.5 in Appendix D). The results indicate that, although higher death rate controls TCP at first, lower death rate basically governs the probability of tumor removal later in time.

4.3.3 Random birth and death rates

Figure 4.9 suggests that randomness in the death rate has more-negative impact on TCP than randomness in the birth rate. In addition, there is a minimum tumor control probability, when both proliferation and death rates are changing arbitrarily and they are anticorrelated (cells with smaller division rates die with higher death rates; conversely, cells with higher division rates die with lower death rates). TCP improves for cases where random birth and death rates are autocorrelated; finally, it approaches the TCP with constant birth and death rates when they are correlated (cells with smaller proliferation rates die with smaller death rates; in contrast, cells with higher proliferation rates die with higher death rates)

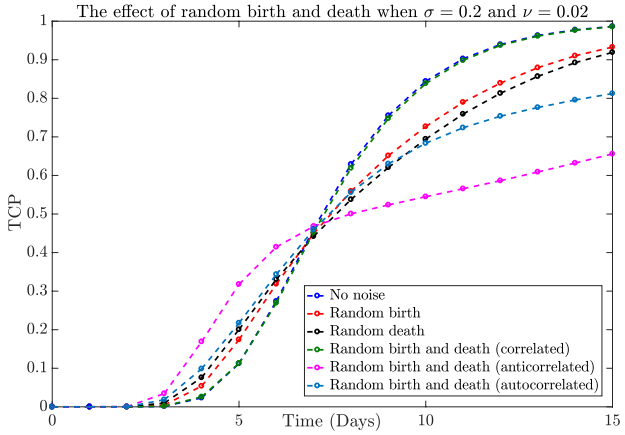

Figure 4.9: Tumor control probability when division and death rates are switching randomly, with $\overline{\rho} = 0.5$, $n_0 = 50$, and $\overline{\Gamma} = 1$ for standard deviations $\sigma = 0.2$ and switching rate $\nu = 0.02$.

4.3.4 The effect of randomness on TCP for a radiotherapy schedule

Studying the affect of random fluctuations on the performance of the potential clinical radiotherapy schedules is of practical interest. Fractionated radiotherapy usually splits the total administered dose into a smaller number of fractions that are given over the period of several weeks to reduce possible side effects. For instance, the standard regimen is given once each weekday, with the rest over the weekend. Here, the impact of random proliferation rate on the effectiveness of the standard schedule is investigated.

The proliferation rate $\rho(t)$ is assumed to switch randomly using the dichotomous Markov noise. It is also considered that cells can die during the radiation time interval and that the radiation induced cell kill rate follows a linear quadratic model in which the fraction of cells surviving a dose d is estimated by $\exp(-\alpha \mathrm{d} - \beta \mathrm{d}^2)$ (Hall & Giaccia, 2006). In this formulation, α and β are radiobiological parameters indicating the sensitivity of cells to the radiation. Thus, the hazard function for a single dose d during a treatment period ΔT is defined as

$$f(t, \mathrm{d}) = \alpha \frac{\mathrm{d}}{\Delta \mathrm{T}} + \beta \frac{\mathrm{d}^2}{\Delta \mathrm{T}}, \tag{4.13}$$

Consequently, the cellular kill rate is explained using a following step function

$$\Gamma(t) = \begin{cases} \alpha \frac{\mathrm{d}_j}{\Delta \mathrm{T}} + \beta \frac{\mathrm{d}_j^2}{\Delta \mathrm{T}} & t \in [t_j, t_j + \Delta T], \\ \gamma & \text{otherwise}, \end{cases} \tag{4.14}$$

where d_j is the dose administered at the j^{th} fraction of radiation. Here, ΔT is taken to be 15 minutes, and the chosen radiobiological parameters are $\alpha = 0.41$ and $\beta = 0.17$ (Forouzannia et al., 2018).

The graphs in Figures 4.10 and 4.11 demonstrate the probability of tumor extinction versus, respectively, the time and dose for different standard deviations (σ) and rates of random changes (ν). The results show similar behaviors, as reported in subsection 4.3.1, when the birth rate is changing stochastically and the death rate is constant over time ($\Gamma(t) = \Gamma$). The results confirm that when the standard deviation (σ) of the proliferation rate increases, the stochastic changes in the birth rate initially improve the efficiency of the standard schedule, but ultimately have a negative effect on treatment schedule efficacy over time and for larger doses. In addition, when the rate of random change, ν, grows, the TCP comes close to the tumor extinction probability found in the case where the proliferation rate is constant over time (see Figure 4.10 and Figure D.6 in Appendix D). The same results are also expected if the cellular death rate between radiotherapy fractionation alters randomly.

4.3.5 Special cases

TCP quantitatively measures the effectiveness of radiotherapy protocols that result in a cell kill rate which is higher than the cell proliferation rate, and this has been fully discussed above. Here, another topic of interest is explored: the impact of random cell birth and death rates on the extinction probability (EP) for two different cases. In the first, the average birth rate equals the average death rate, and in the second, the average birth rate

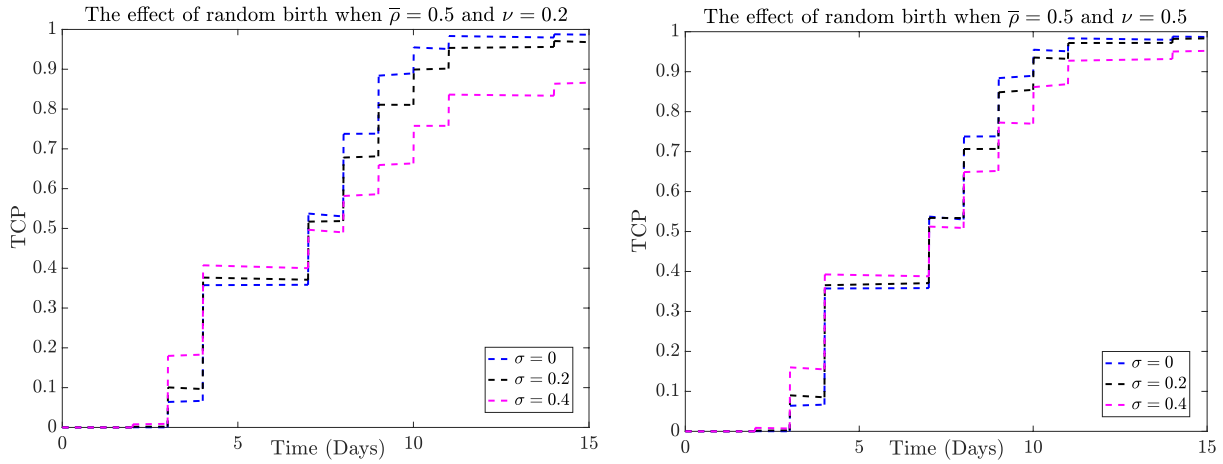

Figure 4.10: Tumor control probability for standard radiotherapy schedule with respect to time when proliferation rate switches randomly, with an average $\overline{\rho} = 0.5$, $\gamma = 0$, $n_0 = 300$, and different standard deviations for (a) $\nu = 0.2$ and (b) $\nu = 0.5$.

is greater than the average death rate.

To study the first case, we take an approach similar to that taken in the previous section, the extinction probability is studied when the proliferation rate $\rho(t)$ (defined based on dichotomous Markov noise) changes randomly between two values with an average $\overline{\rho} = \Gamma$. For the case when there is no noise in the system ($\rho = \Gamma$), the analytical solution (4.10) is reduced to $p_0(t) = (\frac{\rho t}{1+\rho t})^{n_0}$, which approaches 1 when t goes to infinity. The modified Gillespie algorithm is applied to evaluate the extinction probability when $\rho(t)$ changes randomly. The results are similar to those studied in the previous section that explored the extinction probability when the death rate is greater than the birth rate (Figures D.7, D.8, D.9, D.10 in Appendix D). As σ increases, the extinction probability initially rises. However, if the population does not become extinct, the probability of extinction decreases

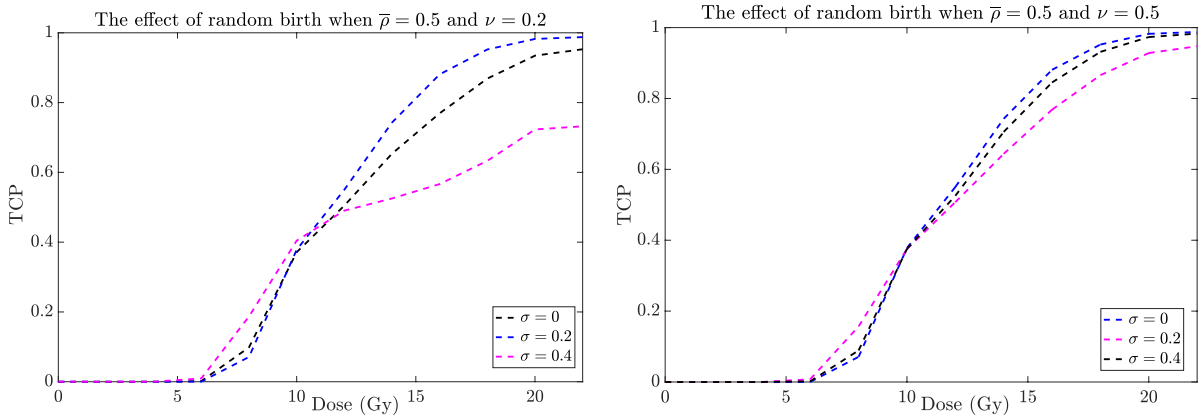

Figure 4.11: Tumor control probability for standard radiotherapy schedule with respect to dose when proliferation rate switches randomly, with an average $\overline{\rho} = 0.5$, $\gamma = 0$, $n_0 = 300$, and different standard deviations for (a) $\nu = 0.2$ and (b) $\nu = 0.5$.

thereafter over time as σ gets larger. To better clarify the results, the extinction probability is evaluated when the random fluctuation rate, ν, is small enough. Therefore, $\text{EP}_{\overline{\rho}+\sigma}$ and $\text{EP}_{\overline{\rho}-\sigma}$ are calculated for two constant proliferation rates, $\rho + \sigma$ and $\rho - \sigma$, respectively. The extinction probability is larger for the lower division rate $\overline{\rho} - \sigma$ and approaches a probability of 1 over time. However, the higher proliferation rate $\overline{\rho} + \sigma$ corresponds to the lower extinction probability, which reaches $(\frac{\Gamma}{\overline{\rho}+\sigma})^{n0}$ for sufficiently large time t, since $\overline{\rho}+\sigma > \Gamma$. Thus, the average probability of extinction is initially governed by $\text{EP}_{\overline{\rho}-\sigma}$, which goes to 1 over time. Thereafter, on average, the probability of extinction is controlled by $\text{EP}_{\overline{\rho}+\sigma}$ (Figure D.10 in Appendix D). In addition, both the average and variance of cell numbers is enhanced as σ escalates. Further, the extinction probability, when $\Gamma(t)$ is modified randomly between two numbers with an average $\overline{\Gamma} = \rho$ following a dichotomous Markov noise, displays the same behavior as that for random birth.

The impact of random fluctuations on the proliferation rate $\rho(t)$ is also investigated for the second case, in which the average birth rate is greater than the average death rate. The extinction time distribution is skewed to the right, and the average extinction time reduces as randomness increases. The results indicate that the extinction probability increases as σ increases. For further investigation, the extinction probability has been studied when the finite correlation time $(\frac{1}{\nu})$ is large. Consequently, the extinction probability corresponding to the proliferation rates $\overline{\rho} + \sigma$ and $\overline{\rho} - \sigma$ is evaluated. $\mathrm{EP}_{\overline{\rho}+\sigma}$ approaches $(\frac{\Gamma}{\overline{\rho}+\sigma})^{n0}$ as t gets large since $\overline{\rho} + \sigma$ is greater than Γ. Furthermore, $\mathrm{EP}_{\overline{\rho}-\sigma}$ reaches $(\frac{\Gamma}{\overline{\rho}-\sigma})^{n0}$ for large time t if $\overline{\rho} - \sigma > \Gamma$, but approaches 1 otherwise. As a result, the average of $\mathrm{EP}_{\overline{\rho}+\sigma}$ and $\mathrm{EP}_{\overline{\rho}-\sigma}$ is mainly influenced by $\mathrm{EP}_{\overline{\rho}-\sigma}$. Thus, increasing randomness increases the extinction probability, but the population does not become extinct (Figure D.11 in Appendix D). The study of random fluctuations in random death also leads to the same results.

4.4 Conclusion and Discussion

In this chapter, a stochastic formulation has been developed to study the impact of random demographic parameters on tumor control probability (TCP). In this direction, we have analyzed a simple birth-death model, when birth and death rates are changing randomly in response to dichotomous Markov noise. Therefore, these rates are defined using random step functions. Consequently, when calculating TCP, a novel computational approach, a modified Gillespie algorithm, has been employed to incorporate the effect of radiation-induced cell kill and arbitrary fluctuations through discontinuous step functions. The results confirm that higher randomness increases TCP, but thereafter, TCP decreases as

time passes if the tumor has not been removed completely. Therefore, a higher standard deviation corresponds to a greater TCP at the beginning and a lower probability of removal later on. In addition, TCP has been measured when both birth and death rates were being arbitrarily altered at the same time, lessening the effectiveness of radiotherapy when the rates are anticorrelated. In general, tumor microenvironmental changes can negatively influence the performance of radiotherapy protocols. Therefore, therapeutic approaches should consider these variations and place more emphasis on personalized treatment, since there is tumor diversity among patients, even with the same cancer types.

Considering a two compartment model consisting of a subpopulation of resistant and sensitive cells, the stochastic dynamics of the resistant subpopulation is independent of sensitive cells and can be explained using a simple birth/death model in the absence of plastic transitions from sensitive cells to resistant cells. The results of this work can be used to explain the impact of random changes in the birth and death rates of resistant cells on the probability of a resistant cell's eradication.

The existence of fluctuation and noise in biological systems has been observed at various levels from the molecular, to the sub-cellular and organism level, and even at the population level. Although the effects of noise in biological processes can differ, it has been suggested that random fluctuations and noise can result in the variation of properties among identical populations of cells (Schmidt et al., 2012; Tsimring, 2014). For example, experimental results have shown that environmental noise can induce the production of different levels of a specific protein in two genetically identical cells (Pilpel, 2011). In addition, although noise can be beneficial, it may lead to more unfavorable conditions in a biological context. In particular, bacteria use different strategies that help them to survive under stress conditions

such as starvation, heat, and antibiotic. For instance, dormant cells can resist antibiotics and maintain the population growth of bacterias (Schmidt et al., 2012; Tsimring, 2014). The mathematical model and computational approach explored in this chapter can be used to study the impact of noise in the response of bacteria and biofilms to antibiotics.

Chapter 5

The impact of plasticity on tumor control probability

The most efficacious administration of radiotherapy must be determined in order to deliver the most potent dose of radiation to the bulk of a tumor while minimizing radiation to the normal surrounding tissue and so reduce possible side effects. The tumor control probability (TCP) is a treatment planning tool that evaluates the probability of tumor eradication and helps in the assessment of the relative efficiency of different radiotherapy regimens. The response of tumors to radiation differs greatly even in patients with same types of cancers. Tumor heterogeneity or cellular diversity among cancer cells has a pronounced impact on the success of the administered radiotherapy protocols. Tumor heterogeneity can be explained using the (Cancer stem cells) CSC hypothesis, which posits that CSCs are responsible for tumor initiation and propagation. CSCs are believed to be the main cause of therapeutic resistance and metastasis, leading to treatment failure. Moreover, the

existence of plasticity or bidirectional transition between CSCs and non-CSCs indicates that, sometimes, non-CSCs appear to mimic CSC phenotypes, resulting in an increase in resistance. We have developed a stochastic model to investigate the impact of plasticity on the efficacy of radiotherapy. The effect of plasticity on TCP is explored by applying the model on standard, hyperfractionated, and accelerated hyperfractionated radiotherapy schedules. Results confirm that tumor control becomes more difficult in the presence of plasticity. It is also observed that the impact of plasticity on accelerated hyperfractionated schedules is marginal, although the efficiency of this radiotherapy protocol drops considerably with highly resistant tumors. In addition, the combination of radiotherapy and targeted therapy increasing CSC differentiation, improves both the probability of CSC and tumor removal in the absence of plasticity. However, in the presence of plasticity, the effect of the combination therapy is not significant.

5.1 Introduction

Tumor heterogeneity, which arises due to genetic and phenotypic diversity as well as environmental differences among cancer cells, has a fundamental impact on treatment outcomes. In particular, the resistance of CSCs to radiotherapy can lead to treatment failure and tumor recurrence (Forouzannia & Sivaloganathan, 2017; Hanahan & Weinberg, 2011). This cellular diversity has been observed between different patients and within a single tumor. The cancer stem cell (CSC) hypothesis proposes that tumor growth is governed by a scarce subpopulation of cancer cells (CSCs) undergoing symmetric and asymmetric proliferation to regenerate themselves and produce other lineages of cancer cells, thus, con-

tributing to intra-tumor heterogeneity. Furthermore, biological observations indicate that sometimes non-CSCs display CSC properties, suggesting some degree of plasticity between CSCs and non-CSCs (Marjanovic et al., 2013a,b). Several mathematical models have been developed to incorporate the effect of plasticity in cancer cell dynamics and mammosphere formation assays (Forouzannia et al., 2018; Gupta et al., 2011; Tonekaboni et al., 2017; Turner & Kohandel, 2010; Zapperi & La Porta, 2012). However, the impact of plasticity on the effectiveness of radiotherapy protocols has not been investigated, and this is the direction we study in this chapter.

A large proportion of patients who are suffering from cancer receive radiation therapy as part of their treatment. The aim of radiotherapy is to achieve a high probability of local tumor control at a low risk of associated side effects. TCP is a measurement that is defined as the probability of tumor-cell extinction by the end of the treatment. Consequently, TCP can be used to evaluate the performance of potential radiotherapy protocols and suggest the one with an optimum outcome. Several mathematical and computational approaches have been developed in the literature to study TCP (Dawson & Hillen, 2006; Gong, 2011; Kendal, 1998; Tucker et al., 1990; Yakovlev, 1993; Zaider & Hanin, 2011; Zaider & Minerbo, 2000). Stochastic models based on Poisson statistics have been used to investigate the probability of tumor control. One important model considers a simple birth/death master equation that includes the stochastic effect of cell kill due to radiation. Thus, TCP is defined as the probability of no cells remaining at the end of treatment (Zaider & Minerbo, 2000). The model is based on clonal evolution theory, which claims that carcinogenesis arises due to random mutations that occur in a single cell. But, based on the CSC hypothesis, the elimination of CSCs is essential to achieve a cure, since the CSCs

are capable of initiating and reestablishing tumor growth. Thus, Dhawan et al. (2014) developed a unidirectional hierarchical model (based on the CSC hypothesis) to determine the probability of eliminating CSCs from a heterogeneous cell population. However, the model does not consider the plasticity between non-CSCs and CSCs.

Here, we develop a stochastic model based on the CSC hypothesis to study the impact of plasticity on tumor control probability. The radiation induced cell kill rate is assumed to be different between CSCs and non-CSCs, to account for the various radiosensitivities among cancer cells. The cancer kill rate is also considered to be a step function such that the kill rate is high during radiation and lower otherwise. Moreover, calculating the analytical solution is not feasible in the presence of plasticity. Thus, a modified Gillespie algorithm for the reactions with rates changing discontinuously is used to solve the time evolution of the stochastic model and calculate the TCP. Consequently, the probability of CSC removal (TCP_S) and the probability of tumor eradication (TC_{S+P}) are evaluated for three different radiotherapy schedules: standard, hyperfractionated, and accelerated hypefractionated. In addition, TCP_S and TC_{S+P} are calculated for a therapy that combines radiotherapy and the targeted therapy in the presence and absence of plasticity. The results indicate that the accelerated hypefractionated schedule obtains the best probability of CSC and tumor removal. Yet, both TCP_S and TC_{S+P} noticeably decrease for the most resistant tumors. Furthermore, applying combination therapy does not substantially improve the control of either the CSC population or tumor in the presence of plasticity.

5.2 Method

This Chapter investigates how plasticity between progenitors and CSCs affects TCP. For this purpose, a two compartment model is designed by splitting the total population of cells into sub-populations of stem cells (S) and progenitor cells (P). Stem cells have the potential to go through numerous cell divisions to replicate themselves and to replace progenitors. Furthermore, it is assumed that there is a degree of plasticity in the system and that progenitors can revert to stem cells. In addition, cells can die independently of each other at a rate of Γ_i, for $i = S, P$, (stem cell, progenitor). Therefore, we can consider the following division pathways.

$$\begin{aligned} S &\to S + S : \rho_S, \\ S &\to P : \rho_{SP}, \\ P &\to P + P : \rho_P, \\ P &\to S : \rho_{PS}, \\ S &\to 0 : \Gamma_S(t), \\ P &\to 0 : \Gamma_P(t), \end{aligned} \tag{5.1}$$

where ρ_S and ρ_P are, respectively, the rates of self renewal for stem cells and proliferation for progenitors. In addition, stem cells can replace progenitors at rate ρ_{SP}, and progenitors can replace stem cells at rate ρ_{PS}. Cells can die at rate $\Gamma_i(t)$, for $i = S, P$, (stem cell, progenitor).

CSCs are capable of unlimited proliferation to maintain a tumor. Furthermore, they dis-

play resistance to radiotherapy through unregulated radiation-induced DNA repair mechanisms after exposure to treatment. Thus, the elimination of CSCs is essential to control a tumor. Consequently, the probability of eradicating CSCs is a key element in measuring the effectiveness of any particular treatment. In this context, the elimination of CSCs when no plasticity exists in the tumor (i.e. $\rho_{PS} = 0$) can lead to tumor control. The study of the probability of CSC removal in model 5.1 with $\rho_{PS} = 0$ is equivalent to analyzing the extinction probability in a simple birth/death process, and is independent of the dynamics of progenitors (as seen in Dhawan et al., 2014) and briefly explained in Appendix E. In the presence of plasticity, however, the removal of CSCs may not result in tumor control.

The stochastic dynamic of model 5.1 is described using the following probability distribution function for a population of n_S stem cells and n_P progenitors at time t with the initial condition $\mathrm{p}_{n_S,n_P}(t_0) = \delta_{n_S n_{S0}} \delta_{n_P n_{P0}}$. Here, n_{S0} and n_{P0} denote the number of stem cells and progenitors at time t_0.

$$\begin{aligned}\frac{dp_{n_S,n_P}(t)}{dt} &= \rho_S p_{n_S-1,n_P}(t)(n_S-1) + \rho_{SP}(n_S+1)p_{n_S+1,n_P-1}(t) + \rho_P(n_P-1)p_{n_S,n_P-1}(t) \\ &+ \rho_{PS}(n_P+1)p_{n_S-1,n_P+1}(t) + \Gamma_S(n_S+1)p_{n_S+1,n_P}(t) + \Gamma_P(n_S+1)p_{n_S,n_P+1}(t) \\ &- (\rho_S + \rho_{SP} + \Gamma_S)n_S p_{n_S,n_P}(t) - (\rho_P + \rho_{PS} + \Gamma_P)n_P p_{n_S,n_P}(t).\end{aligned} \tag{5.2}$$

Using the probability generating function $U(S,P,t) = \sum_{j=0}^{\infty}\sum_{i=0}^{\infty} p_{i,j}(t)S^i P^j$, we obtain

$$\begin{aligned}\frac{\partial U(S,P,t)}{\partial t} &= [(S-1)(\rho_S S - \Gamma_S(t)) + (P-S)\rho_{SP}]\frac{\partial U(S,P,t)}{\partial S} \\ &+ [(P-1)(\rho_P P - \Gamma_P(t)) + (S-P)\rho_{PS}]\frac{\partial U(S,P,t)}{\partial P},\end{aligned} \tag{5.3}$$

with initial condition $U(S,P,0) = S^{n_S^0} P^{n_P^0}$.

The derivation of an analytical solution for equation 5.3 is not possible. In addition, the cancer cell death rates are defined as step functions in which the radiotherapy-induced cancer kill rate is higher in each exposure duration and lower otherwise. Thus, the modified Gillespie algorithm (Shahrezaei et al., 2008) is employed to evaluate TCP in the presence of discontinuous death rates changes.

The radiation induced cell kill is assumed to occur directly in time intervals when fractions of radiation are given. It is also suggested that CSCs are less likely to die than progenitors, due to the former's resistance to the therapy. Therefore, the cell kill rate at each treatment time interval ΔT and given dose d is defined as

$$f_i(t, \mathrm{d}) = \alpha_i \frac{\mathrm{d}}{\Delta \mathrm{T}} + \beta_i \frac{\mathrm{d}^2}{\Delta \mathrm{T}}, \tag{5.4}$$

with different radiobiological parameters α_i and β_i ($i \in \{S, P\}$) for CSCs and progenitors. The hazard function $f_i(t, \mathrm{d})$ is developed based on a linear quadratic model, and cell survival after each fraction can be deduce by $\exp(-\alpha_i d - \beta_i d^2)$, ($i \in \{S, P\}$) (Hall & Giaccia, 2006). Thus, the cell death rates for CSCs and progenitors ($i \in \{S, P\}$) can be considered as the following step function

$$\Gamma(t) = \begin{cases} \alpha_i \frac{\mathrm{d}_j}{\Delta \mathrm{T}} + \beta_i \frac{\mathrm{d}_j^2}{\Delta \mathrm{T}} & t \in [t_j, t_j + \Delta T], \\ 0 & \text{otherwise}, \end{cases} \tag{5.5}$$

where t_j and d_j are the initial time and the given dose of the j^{th} fraction of radiotherapy,

respectively. The values of model 5.1 and radiosensitivity parameters are selected from (Forouzannia et al., 2018). Thus, $\rho_S = 0.1$, $\rho_{SP} = 0.7$, $\rho_P = 0.2$, $\rho_{PS} = 0.05$ and radiobiological parameters are $\alpha_S = 0.14$, $\alpha_P = 0.41$, $\beta_S = 0.048$, and $\beta_P = 0.17$. The duration of treatment at each fraction of radiation ΔT is assumed to be 15 minutes.

5.3 Results and Discussion

Radiotherapy targets cancer cells and shrinks tumors, but CSCs are apt to escape the effect due to their resistance to radiation. In general, tumors rich in CSCs are very difficult to control relative to ones with a lower CSC fraction. Consequently, studying the efficiency of radiotherapy protocols for eradicating CSCs is important. However, removing the CSC population may not be sufficient to control the disease in the presence of plasticity. Therefore, to investigate the impact of plasticity on tumor control, we evaluate the probability of CSC removal, TCP_S, and the probability of tumor eradication, TCP_{S+P}, for model 5.1 in the presence and absence of plasticty.

In this direction, TCP_S and TCP_{S+P} are compared for standard (ST), hyperfractionated (HR), and accelerated hyperfrationated (AC) radiotherapy schedules over three weeks of treatment. The conventional treatment regimen delivers a dose of 2 Gy per fraction, once each weekday. For the hyperfractionated and accelerated hyperfrationated protocols, the respective doses of 1.2 Gy and 1.5 Gy are given twice each weekday.

Figure 5.1 represents TCP_S and TCP_{S+P}, applying a standard radiotherapy regimen in both the presence and absence of plasticity in the system. The curves are relatively

close to each other in Figure 5.1a due to the high radiotherapy-induced cell kill rates. Consequently, the cell kill rates at each fraction of radiation are reduced by assuming that β_S and β_P equal zero, to better distinguish the differences between various possible cases (Figure 5.1b). The results confirm that both TCP_S and TCP_{S+P} reduce when non-CSCs are able to behave like CSCs.

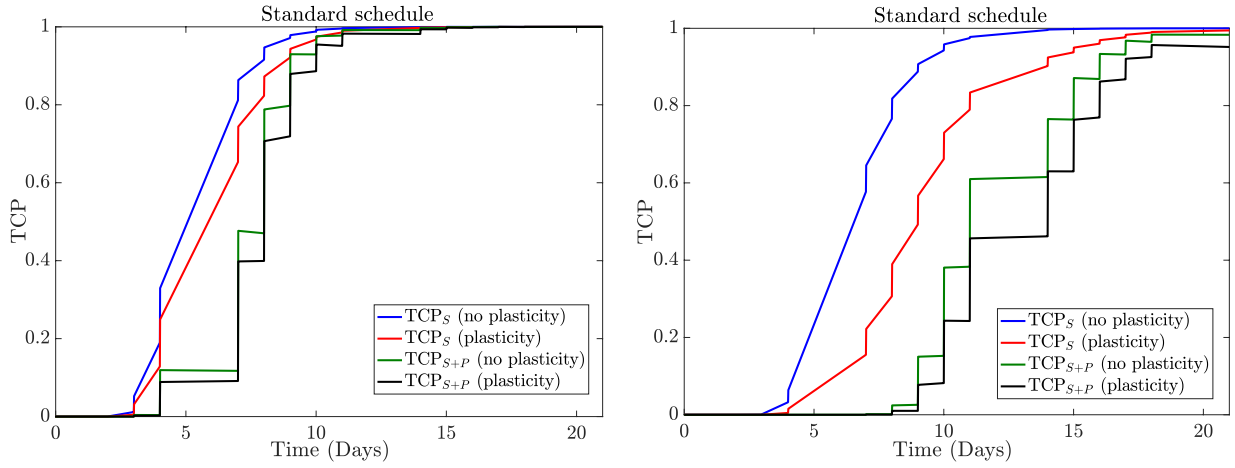

Figure 5.1: *TCP_S and TCP_{S+P} for a standard radiotherapy schedule in the absence and presence of plasticity with initial numbers of cells $n_S^0 = 100$ and $n_P^0 = 100$. (a) $\alpha_S = 0.14$, $\alpha_P = 0.41$, $\beta_S = 0.048$, and $\beta_P = 0.17$. (b) $\beta_S = 0$ and $\beta_P = 0$.*

In Figure 5.2, TCP_S and TCP_{S+P} are compared for standard, hyperfractionated, and accelerated hyperfactionated protocols. Whether or not plasticity exists, accelerated hyperfractionated and standard protocols correspond, respectively, to the largest and lowest TCP_S and TCP_{S+P}. In general, the existence of plasticity leads to a smaller probability of CSC and tumor removal for these three radiotherapy schedules. The probability of CSC removal is relatively close for these three radiotherapy schedules in the absence of plasticity,

but the calculated TCP_S is more distinct in the presence of plasticity (Figure 5.2a). Furthermore, Figure 5.2a reveals that the difference between the calculated values for TCP_S with and without plasticity are much less for the accelerated hyperfractionated schedule than for the other two, indicating that the existence of plasticity does not substantially impact the accelerated hyperfractionated schedule's effectiveness. The same trend is also observed for TCP_{S+P} (Figure 5.2b).

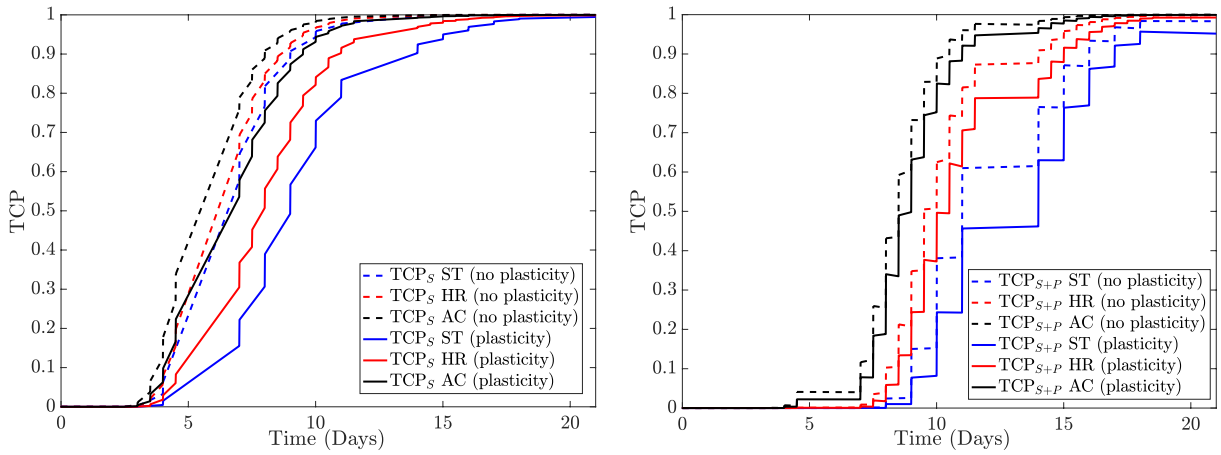

(a) (b)

Figure 5.2: *(a) TCP_S and (b) TCP_{S+P} with respect to time for standard, hyperfractionated, and accelerated hyperfractionated schedules in the absence and presence of plasticity. The initial numbers of cells are $n_S^0 = 100$ and $n_P^0 = 100$.*

Figure 5.3 is the graph of (a) the probability of CSC and (b) tumor extinction with respect to dose in the presence and absence of plasticity. The results confirm that a larger total dose is required for CSC and tumor extinction in the presence of plasticity. Furthermore, comparing 5.2 and 5.3 shows that although the accelerated hyperfractionated schedule achieves a higher probability of CSC and tumor removal than the other two

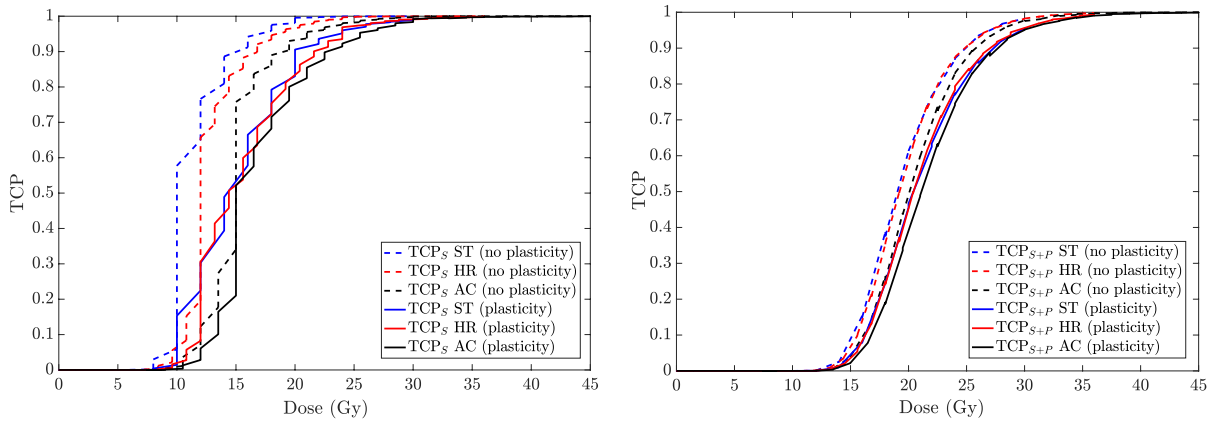

Figure 5.3: *(a) TCP$_S$ and (b) TCP$_{S+P}$ with respect to dose for standard, hyperfractionated, and accelerated hyperfractionated schedules in the absence and presence of plasticity. The initial numbers of cells are $n_S^0 = 100$ and $n_P^0 = 100$.*

schedules over time, this protocol uses a larger total dose of radiation to obtain the same TCP$_S$ and TCP$_{S+P}$.

In addition, increasing the plasticity in the tumor decreases the TCP$_S$ and TCP$_{S+P}$, implying greater challenges in controlling the disease (Figure F.1 in Appendix F). In Figures 5.4 and 5.5, TCP$_S$ and TCP$_{S+P}$ are graphed to explain the impact of a highly resistant CSC subpopulation on treatment efficiency in both the presence and absence of plasticity. The results confirm that reducing the sensitivity of CSCs to radiation yields a lower probability of control of both the CSC subpopulation and tumor. Consequently, radiotherapy protocols are much less efficient against highly resistant tumors than less-resistant ones (Figures 5.4 and 5.5). In particular, the performance of the accelerated hyperfractionated protocol drops enormously. Furthermore, the probability of CSC eradication is comparatively close for standard, hyperfractionated and accelerated hypefractionated schedules when plasticity

does not exist in a tumor (Figure 5.4a). Consequently, increasing the number of fractions does not improve the probability of CSC removal for extremely resistant tumors in the absence of plasticity.

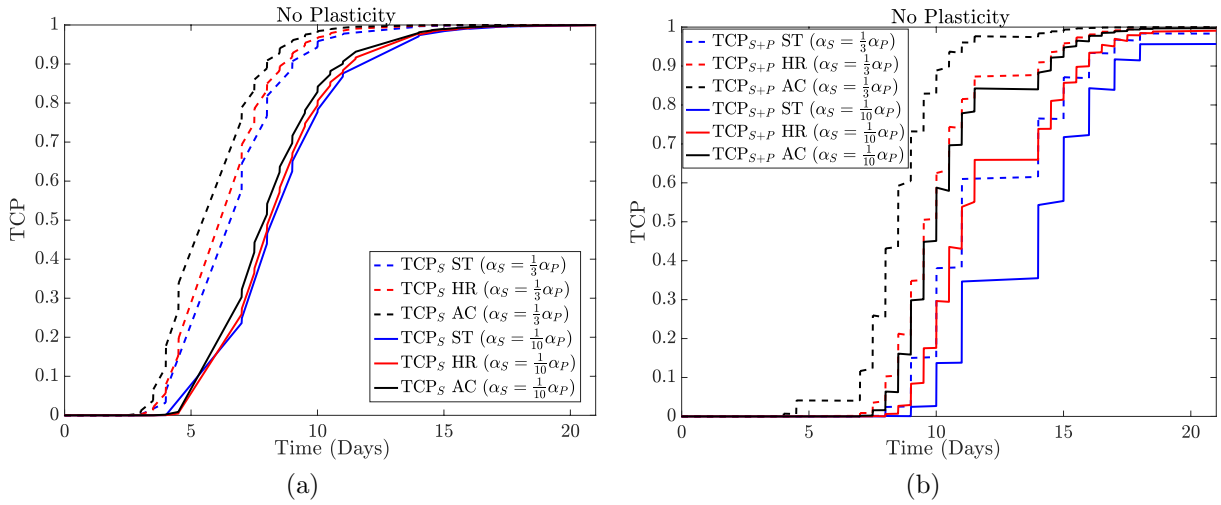

Figure 5.4: *(a) TCP_S and (b) TCP_{S+P} for standard, hyperfractionated, and accelerated hyperfractionated schedules in the absence of plasticity for different radiosensitivities among CSCs.*

It is necessary to understand that CSC removal can ultimately contribute to tumor control when there is no plasticity in the system, although expecting this absence may not be biologically realistic. CSC elimination is not enough to attain a cure when plasticity exist, but is still important in decreasing the most-resistant subpopulation of cells. Consequently, it is crucial to consider TCP_{S+P} as a measure for evaluating therapeutic regimen efficiency in the presence of plasticity, while simultaneously monitoring CSC elimination.

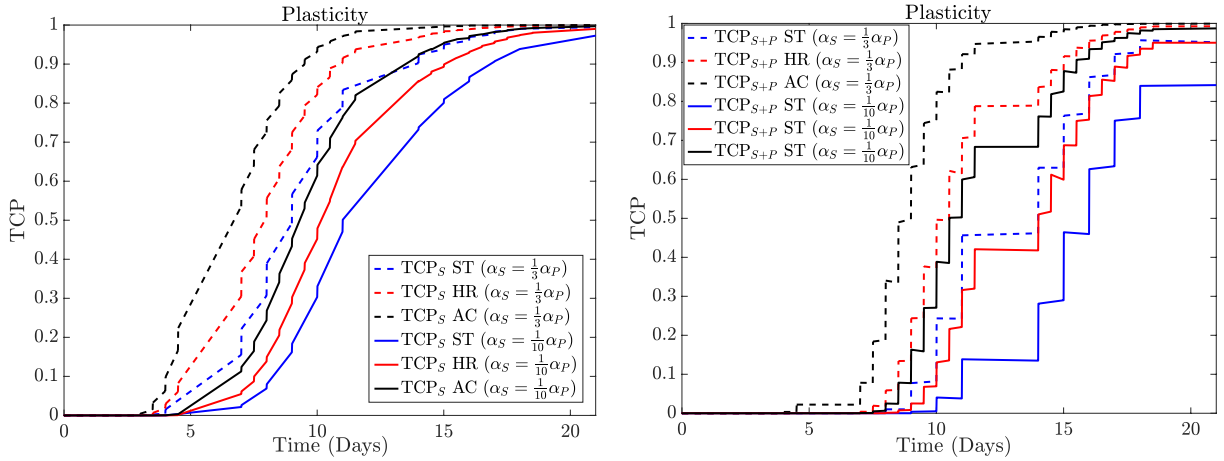

Figure 5.5: *(a) TCP_S and (b) TCP_{S+P} for the three radiotherapy protocols in the presence of plasticity for different radiosensitivities among CSCs. The initial numbers of cells are $n_S^0 = 100$ and $n_P^0 = 100$.*

Combination of treatments

Experimental results suggest that the fraction of CSCs increases following ionizing radiation, due to the resistance of this subset of cells to the therapy (Bao et al., 2006; Lagadec et al., 2010). This frequently results in relapse and treatment failure. In this direction, both in vitro and in vivo experiments have shown that certain bone morphogenetic proteins (BMPs) are capable of inducing positive biomarker cells (stem-like cancer cells) to differentiate into negative biomarker cells (non-CSCs) in brain tumors (Piccirillo et al., 2006). Consequently, applying this targeted strategy is expected to escalate the differentiation of radioresistant cells into non-CSCs that are more sensitivite to radiation and have less tumorigenic potential. Therefore, a reduction in the CSC pool can contribute to better therapeutic outcomes. However, the plastic transition from non-CSCs to CSCs can

reverse the process and diminish the impact of BMPs. Thus, it is of interest to investigate the impact on TCP increasing CSC differentiation rates in the presence and absence of plasticity, which will be discussed next.

Here, we consider three types of combination treatments over 15 days, consisting of 10 fractions of radiation (the dose of 2Gy is administered per fraction once a day) and 5 days of targeted strategy that trigger CSCs to differentiate into non-CSCs. The first protocol includes 10 days of radiation, followed by a targeted strategy of increasing the differentiation rate ρ_{SP} for 5 days (scheme 1). The second starts with 5 days of increasing CSCs differentiation, followed by 10 days of radiation (scheme 2). Finally, the third involves 5 days of radiation, followed by 5 days of targeted therapy, and last, another 5 days of radiation (scheme 3). We consider a base protocol for each of these three schedules, denoted as schemes 1-b, 2-b, and 3-b, in which the ρ_{SP} does not change.

Figure 5.6 shows TCP_S and TCP_{S+P} for schemes 1-b, 2-b, and 3-b in the absence and presence of plasticity. As explained in the previous section, both TCP_S and TCP_{S+P} decrease when plasticity exists. Comparing the results for these three schedules indicates that the minimum TCP_S and TCP_{S+P} are obtained by scheme 1-b, suggesting that a large gap between fractionations reduces the probability of CSC and tumor removal (Solid and dashed black curves) in the absence and presence of plasticity. In addition, scheme 3-b reports the highest TCP_{S+P}, but this schedule does not lead to the best control of the CSC population (solid and dashed red curves). Employing the targeted therapy in combination with the radiotherapy (schemes 1–3) shows an improvement in TCP_S and TCP_{S+P} for scheme 2 when plasticity does not exist, with the most increase occurring in the former (TCP_S). However, the impact of targeted therapy on schemes 1 and 3 is

limited, with almost no increase in TCP_{S+P} for either of the schemes (Figures 5.6a and 5.7a). On the other hand, combining the targeted therapy with radiation in the presence of plasticity enhances TCP_S and TCP_{S+P} somewhat for schemes 1–3, with almost no increase in TCP_{S+P} for scheme 1 (Figures 5.6b and 5.7b). Similar trends are also observed when ρ_{SP} increases to 2.1. In Figure 5.7*b*, TCP_S decreases over a short period of time and increases after for scheme 3. This behavior occurs because reducing ρ_{SP} after 10 days in the presence of plasticity decreases CSC elimination. Consequently, the generation of CSCs from progenitors can reduce the probability of complete CSC removal.

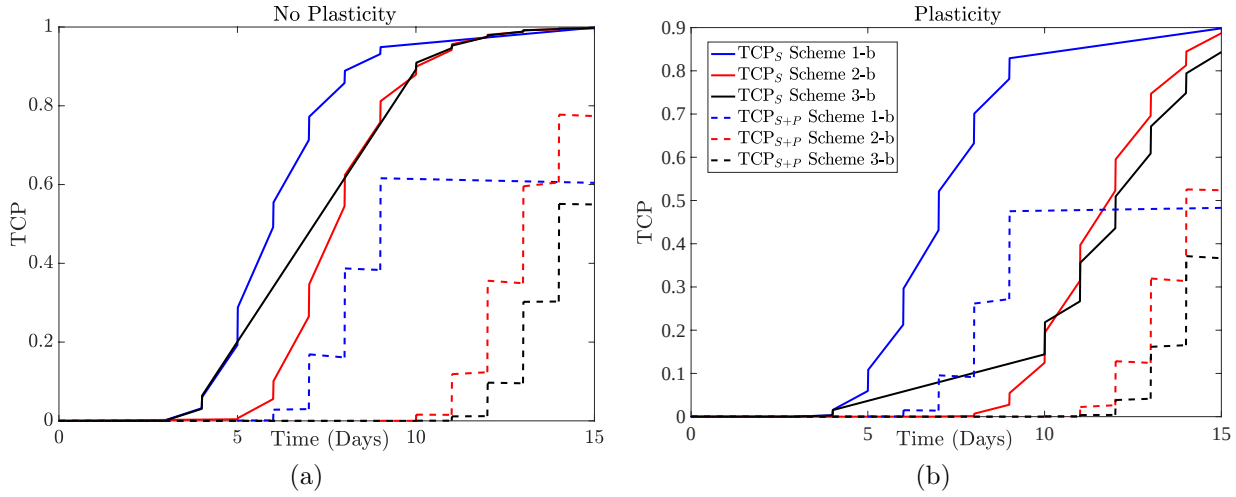

Figure 5.6: *TCP_S and TCP_{S+P} for schemes 1-b, 2-b, and 3-b in the (a) absence and (b) presence of plasticity, with initial numbers of cells $n_S^0 = 100$ and $n_P^0 = 100$.*

The above results demonstrate that increasing ρ_{SP} before radiotherapy has the most effect in improving the probability of CSC removal in the absence of plasticity. In addition, the probability of tumor control increases in this case. However, in the presence of plasticity the tumor control is complicated, and even triggering CSCs to differentiate does

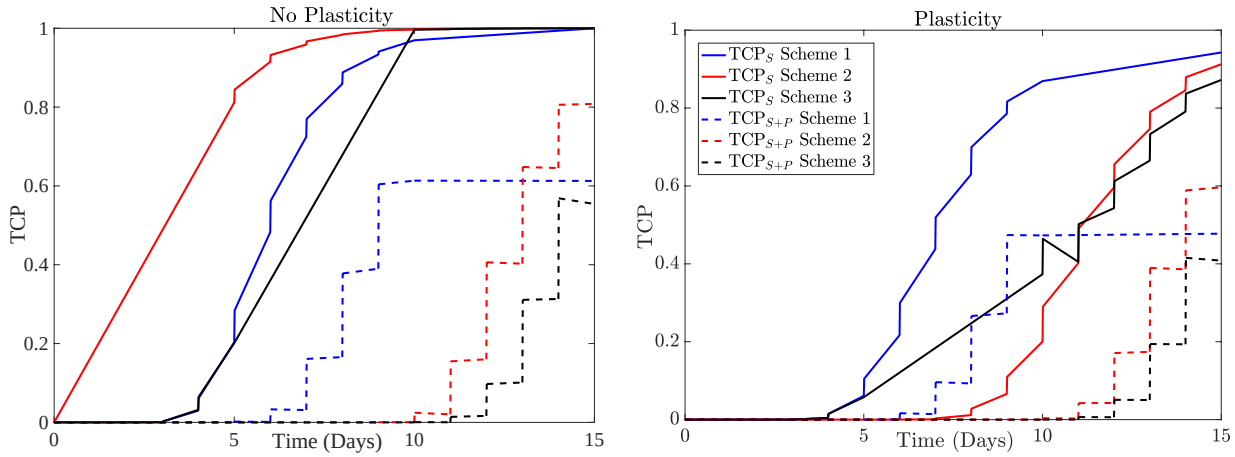

Figure 5.7: *TCP$_S$ and TCP$_{S+P}$ for schemes 1, 2, and 3 in the (a) absence and (b) presence of plasticity, with initial numbers of cells $n_S^0 = 100$ and $n_P^0 = 100$. ρ_{SP} is increased to 1.4 during targeted therapy.*

not enhance TCP$_S$ and TCP$_{S+P}$ significantly. Nevertheless, increasing CSC differentiation before radiotherapy leads to better tumor removal control. But TCP$_S$ is still less than the case when CSC differentiation increases after radiotherapy. In general, these outcomes confirm that understanding the heterogeneity of tumors is important in order to develop optimum protocols.

5.4 Conclusion

Here, we have presented a stochastic model to investigate the impact of plasticity on the tumor control probability. The radiation induced cell kill rate has been modeled using a step function in which the cancer cell kill rate is high during radiotherapy and lower otherwise. Therefore, the time evolution trajectory of a hierarchical stochastic model

consisting of CSCs and progenitors has been calculated using a modified Gillespie algorithm for rates that are changing discontinuously. Thus, $\mathrm{TCP_S}$ and $\mathrm{TC_{S+P}}$ are defined as the probability of removing CSCs and the probability of eliminating a tumor, respectively. The response of cancer cells to the radiation varies among cancer cells with, CSCs showing more resistance to the treatment. TCP_S and TCP_{S+P} have been computed for standard, hyperfractionated, and accelerated hyperfractionated protocols. The results suggest that TCP_S and TCP_{S+P} are reduced in the presence of plasticity under these three radiotherapy schedules. In the presence and absence of plasticity, the best control is achieved by the accelerated hyperfractionated regimen. The existence of plasticity between non-CSCs and CSCs does not greatly affect TCP for the accelerated hyperfractionated protocol. However, the effectiveness of the accelerated hyperfactionated regimen is also decreased significantly for highly resistant tumors. The lower sensitivity to radiation among CSCs also contributes to a lower probability of CSC and tumor removal. The results also confirm that combination therapy can improve TCP_S and TCP_{S+P} in the absence of plasticity, with the most increase in the former. However, combination therapy does not increase the probability of CSC and tumor removal appreciably when plasticity exists.

The results indicate that cellular heterogeneity and the existence of plasticity in a tumor significantly impact the efficacy of treatment. Thus, it is important to consider this cellular diversity when determining an appropriate treatment protocol.

Chapter 6

The impact of plasticity and negative feedback regulation on sphere formation ability

CSCs are at the apex of a cancer cellular hierarchy and possess high tumorigenic potential to reproduce themselves and their progeny which form the bulk of a tumor. Moreover, it has been suggested that this hierarchical structure is not unidirectional; there is degree of plasticity between CSCs and progenitor cells. The presence of tissue homeostasis is maintained through cellular mechanisms and regulatory feedback, whose inhibition may lead to tumor growth. For example, several mathematical studies have suggested that disruption of the negative feedback controlling CSC proliferation and dedifferentiation rates can lead to tumor growth in a large cellular population. In this chapter, we apply the

Gillespie algorithm to investigate the effect of negative regulatory feedback on the ability of a single CSC to form a sphere. The results suggest that both sphere formation efficiency (SFE) and average sphere size (AVSS) decrease when CSC division and the process of dedifferentiation are regulated by negative feedback.

6.1 Introduction

In healthy tissue, stem cells have the ability to undergo protracted selfrenewal, and to generate progenitors with limited proliferation potential that finally produce terminally differentiated cells. Therefore, the maintenance of tissue homeostasis is governed by the regulatory mechanisms of positive and negative feedback loops that are properly governed based on tissue requirements. For example, the regulatory feedback that prevents CSC symmetric and asymmetric division is crucial to maintaining tissue homeostasis (Biteau et al., 2011; Rodriguez-Brenes et al., 2011; Watt & Hogan., 2000).

Based on the CSC hypothesis, tumors also consist of a hierarchal structure in which CSCs are capable of reproducing themselves, progenitors, and other cell lineages, resulting in tumorigenesis. Recent evidence suggests that sometimes non-CSCs behave like CSCs, implying a degree of plasticity among tumor cells (Cabrera et al., 2015; Gupta et al., 2011; Hanahan & Weinberg, 2011; Kreso & Dick, 2014; Marjanovic et al., 2013a,b). In addition, it has been proposed that escaping from feedback loops plays an important role in the process of carcinogenesis (Vogelstein et al., 2004; Wodarz, 2018). For example, in healthy tissues, the high number of differentiated cells keeps the process of plasticity under control, and dedifferentiation can occur in cases of injury and tissue damages (Stange et al., 2013; Yanger & Stanger, 2014). Consequently, disruption of the negative feedback that controls plasticity can lead to an increased number of CSCs with high tumorigenic potential. Therefore, it is clearly of interest and importance to investigate the impact of plasticity on tissue homeostasis.

Several mathematical models have been developed based on the CSC hypothesis, to

explore and develop an understanding of multiple different important factors driving the process of tumorigenesis, therapeutic resistance, and treatment optimization (Anderson & Quaranta, 2008; Enderling & Hahnfeldt, 2011; Forouzannia & Sivaloganathan, 2017; Werner et al., 2016). In addition, the impact of plasticity on cancer progression and therapeutic outcomes has also been investigated in the literature recently (Forouzannia et al., 2018; Jilkine & Gutenkunst, 2014; Mahdipour et al., 2017; Tonekaboni et al., 2017). There is also work on the effects of negative feedback on CSC differentiation and dedifferentiation in a large population of cells in the literature (Rodriguez-Brenes et al., 2011; Wodarz, 2018). However, negative feedback has not been investigated in a stochastic context. In this chapter, we explore the impact of negative feedback regulators that progenitors secrete during CSC division and the negative feedback that CSCs trigger during in the process of plasticity for a small number of cells. For this purpose, a stochastic Gillespie algorithm is applied to study the negative feedback regulation on the ability of a single cell to generate a sphere.

6.2 Method and discussion

We consider a simple mathematical model that describes the dynamics of tumor tissues, composed of a hierarchical population of cells. The model is constructed by splitting the total cancer cell population into sub populations of cancer stem cells (CSCs) and progenitors. CSCs (S) proliferate at a rate ρ_S and undergo symmetric and asymmetric selfrenewal with probabilities r_1 and r_2, respectively. CSCs also generate two progenitor cells (symmetric commitments), with a probability of r_3, and so $r_1 + r_2 + r_3 = 1$. Furthermore, progenitors

are capable of switching phenotypically into CSCs at a rate ρ_{PS}. It is also assumed that progenitors can die at rate Γ_P, but CSCs are considered not to go through apoptosis due to their prolonged survival potential. Therefore, the dynamics of the cancer cells can be mathematically represented by the following division pathways.

$$\begin{aligned} S &\to S + S : \rho_S r_1, \\ S &\to S + P : \rho_S r_2, \\ S &\to P + P : \rho_S r_3, \\ P &\to S : \rho_{PS}, \\ P &\to 0 : \Gamma_P, \end{aligned} \tag{6.1}$$

In addition, the dynamics of stem cells and progenitors are governed by the following differential equations for large numbers of cells.

$$\begin{aligned} \frac{dS}{dt} &= \rho_S(r_1 - r_3)S + \rho_{PS}P \\ \frac{dP}{dt} &= \rho_S(r_2 + 2r_3)S - (\rho_{PS} + \Gamma_P)P. \end{aligned} \tag{6.2}$$

The model can be reduced to the one discussed in (Wodarz, 2018), by assuming $r_2 = 0$, and so $r_3 = 1 - r_1$. It has been suggested that progenitors imply a hidden negative feedback, in which increasing the number of progenitors decreases the proliferation rate of CSCs (Rodriguez-Brenes et al., 2011; Wodarz, 2018). To incorporate this effect, r_1 is replaced by $\overline{r_1} = \frac{r_1}{1+h_1 P^{k_1}}$ and ρ_S is replaced by $\overline{\rho_S} = \frac{\rho_S}{1+h_2 P^{k_2}}$ with the positive constants h_1, h_2, k_1, and k_2.

Clearly, in the absence of plasticity, $\rho_{PS} = 0$, and when there is no feedback in the sys-

tem, the solutions become extinct for $r_1 < 0.5$, undergo exponential growth for $r_1 > 0.5$, and converge to equilibrium (tissue homeostasis) for $r_1 = 0.5$. The results show that tissue homeostasis occurs when $r_1 > 0.5$ if progenitors secrete negative feedback regulators that impact the CSC division rate and the probability of CSC symmetric division. In addition, in the presence of plasticity when there is no feedback in the system, the population grows when $r_1 > (\Gamma_P - \rho_{PS})/2\Gamma_P$, which implies the presence of a population for $r_1 > 0$ if the dedifferentiation rate is greater than the death rate for progenitors ($\rho_{PS} > \Gamma_P$). The number of cells converges to equilibrium if r_1 and ρ_S are subject to negative feedback and $\rho_{PS} < \Gamma_P$. However, if $\rho_{PS} > \Gamma_P$, the population grows even in the presence of negative feedback regulators affecting CSC proliferation. On the other hand, if increasing the CSC population decreases the number of progenitors through negative feedback regulation ($\overline{\rho_{PS}} = \frac{\rho_{PS}}{1+h_3 S^{k_3}}$), tissue homeostasis is possible even when $\rho_{PS} > \Gamma_P$. In this direction the results also confirm that if $\rho_{PS} < \Gamma_P$ and $r_1 < 0.5$, negative feedbacks regulators in both CSCs division and plasticity need to be removed for the population to grow (Wodarz, 2018). It also can be observed that if only $r_1 > 0.5$, the negative feedback on CSC proliferation is necessary for tissue maintenance, but if only $\rho_{PS} > \Gamma_P$, the negative feedback on the plasticity rate is crucial for tissue homeostasis.

In the next section, employing a Gillespie algorithm we explore the impact of negative feedback regulation on a small number of such populations.

6.2.1 Negative feedback impacts on sphere forming efficiency

Sphere forming efficiency is a measurement used to evaluate the ability of stem cells or early progenitor cells to form a sphere. The related experimental protocols are usually designed based on the purpose of the study, but nearly all these protocols start with seeding cells in a well such that they are properly dispersed and then allowing them to grow. These cultured cells are considered to be a sphere when they reach a certain size. Here, we investigate the impact of negative feedback on sphere formation efficiency and on the average sphere size, both in the presence and absence of plasticity.

As discussed above, the sphere formation experiment monitors the cell proliferation capacity by harvesting single cells. Thus, because stochastic simulations are well established approaches to studying the evolution of small populations, the Gillespie algorithm is used to simulate the ability of a single CSC to form a sphere. Initially, the simulation considers cellular pathway 6.1 with no plasticity ($\rho_{PS} = 0$). The procedure is initiated by choosing the number of single CSCs that are seeded in a well, and so the initial condition is $S_0 = 1$ and $P_0 = 0$. These single CSCs are allowed to grow for 10 days, and are said to have generated a sphere if the total number of cells produced from each of these single cells hits set goal of 50 plus cells. Therefore, the sphere formation efficiency is defined as the fraction of the number of single stem cells that are able to form a sphere, and the average sphere size equals the total number of cells divided by the total number of single stem cells that reach 50 and above. The SFE and AVSS for different possible cases of negative feedback are reported in Table 6.1.

The results (Table 6.1) confirm that the ability of a single CSC to form a sphere and the

average sphere size are reduced when the division rate ρ_S is subject to negative feedback. Changing either r_1 or r_2 by $r_1 = \frac{r_1}{1+g_2 P^{n_2}}$ or $r_2 = \frac{r_2}{1+g_3 P^{n_3}}$ also results in a decrease of SFE and AVSS. However, the SFE and AVSS slightly increase if progenitors secret factors that reduce a negative feedback affecting the symmetric commitment rate r_3. The reduction in r_3, in which one CSC is replaced with two progenitors, leads to a reduction in the population of CSCs. Consequently, it can be observed that a lower r_3 rate results in less CSC death, showing the importance of CSCs in sphere formation. Furthermore, replacing both ρ_S and r_3 with $\rho_{S=\frac{\rho_S}{1+g_1 P^{n_1}}}$ and $r_3 = \frac{r_3}{1+g_4 P^{n_4}}$ reduces SFE and AVSS.

No plasticity		
conditions	SFE	AVSS
No feed back	0.11	73.17
$\rho_S = \frac{\rho_S}{1+g_1 P^{n_1}}$ ($g_1 = 0.01$, $n_1 = 1$)	0.06	63.62
$\rho_S = \frac{\rho_S}{1+g_1 P^{n_1}}$ ($g_1 = 0.02$, $n_1 = 1$)	0.034	59.9
$\rho_S = \frac{\rho_S}{1+g_1 P^{n_1}}$ ($g_1 = 0.03$, $n_1 = 1$)	0.02	57.69
$r_1 = \frac{r_1}{1+g_2 P^{n_2}}$ ($g_2 = 0.01$, $n_2 = 1$)	0.07	65.63
$r_1 = \frac{r_1}{1+g_2 P^{n_2}}$ ($g_2 = 0.02$, $n_2 = 1$)	0.05	62.32
$r_1 = \frac{r_1}{1+g_2 P^{n_2}}$ ($g_2 = 0.03$, $n_2 = 1$)	0.03	60.14
$r_2 = \frac{r_2}{1+g_3 P^{n_3}}$ ($g_3 = 0.01$, $n_3 = 1$)	0.09	69.19
$r_2 = \frac{r_2}{1+g_3 P^{n_3}}$ ($g_3 = 0.02$, $n_3 = 1$)	0.08	67.24
$r_2 = \frac{r_2}{1+g_3 P^{n_3}}$ ($g_3 = 0.03$, $n_3 = 1$)	0.07	66.13
$r_3 = \frac{r_3}{1+g_4 P^{n_4}}$ ($g_4 = 0.01$, $n_4 = 1$)	0.11	74.59
$r_3 = \frac{r_3}{1+g_4 P^{n_4}}$ ($g_4 = 0.02$, $n_4 = 1$)	0.12	75.43
$r_3 = \frac{r_3}{1+g_4 P^{n_4}}$ ($g_4 = 0.03$, $n_4 = 1$)	0.12	75.98
$\rho_S = \frac{\rho_S}{1+g_1 P^{n_1}}$ and $r_3 = \frac{r_3}{1+g_4 P^{n_4}}$ ($g_1 = g_4 = 0.01$, $n_1 = n_4 = 1$)	0.06	64.30
$\rho_S = \frac{\rho_S}{1+g_1 P^{n_1}}$ and $r_3 = \frac{r_3}{1+g_4 P^{n_4}}$ ($g_1 = g_4 = 0.02$, $n_1 = n_4 = 1$)	0.039	60.45
$\rho_S = \frac{\rho_S}{1+g_1 P^{n_1}}$ and $r_3 = \frac{r_3}{1+g_4 P^{n_4}}$ ($g_1 = g_4 = 0.03$, $n_1 = n_4 = 1$)	0.024	58.26

Table 6.1: The sphere formation efficiency and average sphere size in the absence of plasticity when $\rho_S = 0.9$, $r_1 = 0.3$, $r_2 = 0.6$, $r_3 = 0.1$, and $\Gamma_P = 0.1$

Plasticity		
conditions	SFE	AVSS
No feed back	0.22	82.59
$\rho_S = \frac{\rho_S}{1+g_1 P^{n_1}}$ ($g_1 = 0.01$, $n_1 = 1$)	0.15	68.9
$\rho_S = \frac{\rho_S}{1+g_1 P^{n_1}}$ ($g_1 = 0.02$, $n_1 = 1$)	0.1	63.6
$\rho_S = \frac{\rho_S}{1+g_1 P^{n_1}}$ ($g_1 = 0.03$, $n_1 = 1$)	0.07	60.55
$r_1 = \frac{r_1}{1+g_2 P^{n_2}}$ ($g_2 = 0.01$, $n_2 = 1$)	0.18	72.55
$r_1 = \frac{r_1}{1+g_2 P^{n_2}}$ ($g_2 = 0.02$, $n_2 = 1$)	0.14	68.09
$r_1 = \frac{r_1}{1+g_2 P^{n_2}}$ ($g_2 = 0.03$, $n_2 = 1$)	0.11	65.39
$r_2 = \frac{r_2}{1+g_3 P^{n_3}}$ ($g_3 = 0.01$, $n_3 = 1$)	0.19	76.14
$r_2 = \frac{r_2}{1+g_3 P^{n_3}}$ ($g_3 = 0.02$, $n_3 = 1$)	0.17	73.13
$r_2 = \frac{r_2}{1+g_3 P^{n_3}}$ ($g_3 = 0.03$, $n_3 = 1$)	0.15	71.41
$r_3 = \frac{r_3}{1+g_4 P^{n_4}}$ ($g_4 = 0.01$, $n_4 = 1$)	0.23	83.96
$r_3 = \frac{r_3}{1+g_4 P^{n_4}}$ ($g_4 = 0.02$, $n_4 = 1$)	0.23	84.85
$r_3 = \frac{r_3}{1+g_4 P^{n_4}}$ ($g_4 = 0.03$, $n_4 = 1$)	0.24	85.57
$\rho_S = \frac{\rho_S}{1+g_1 P^{n_1}}$ and $r_3 = \frac{r_3}{1+g_4 P^{n_4}}$ ($g_1 = g_4 = 0.01$, $n_1 = n_4 = 1$)	0.16	69.55
$\rho_S = \frac{\rho_S}{1+g_1 P^{n_1}}$ and $r_3 = \frac{r_3}{1+g_4 P^{n_4}}$ ($g_1 = g_4 = 0.02$, $n_1 = n_4 = 1$)	0.11	64.25
$\rho_S = \frac{\rho_S}{1+g_1 P^{n_1}}$ and $r_3 = \frac{r_3}{1+g_4 P^{n_4}}$ ($g_1 = g_4 = 0.03$, $n_1 = n_4 = 1$)	0.08	61.29
$\rho_{PS} = \frac{\rho_{PS}}{1+g_5 P^{n_5}}$ ($g_5 = 0.01$, $n_5 = 1$)	0.22	80.93
$\rho_{PS} = \frac{\rho_{PS}}{1+g_5 P^{n_5}}$ ($g_5 = 0.02$, $n_5 = 1$)	0.21	79.95
$\rho_{PS} = \frac{\rho_{PS}}{1+g_5 P^{n_5}}$ ($g_5 = 0.03$, $n_5 = 1$)	0.21	79.1

Table 6.2: The sphere formation efficiency and average sphere size in the presence of plasticity when $\rho_S = 0.9$, $r_1 = 0.3$, $r_2 = 0.6$, $r_3 = 0.1$, $\rho_{PS} = 0.05$ and $\Gamma_P = 0.1$

Plasticity		
conditions	SFE	AVSS
No feed back	0.34	93.62
$\rho_S = \frac{\rho_S}{1+g_1 P^{n_1}}$ ($g_1 = 0.01$, $n_1 = 1$)	0.26	74.98
$\rho_S = \frac{\rho_S}{1+g_1 P^{n_1}}$ ($g_1 = 0.02$, $n_1 = 1$)	0.2	67.89
$\rho_S = \frac{\rho_S}{1+g_1 P^{n_1}}$ ($g_1 = 0.03$, $n_1 = 1$)	0.14	64.05
$r_1 = \frac{r_1}{1+g_2 P^{n_2}}$ ($g_2 = 0.01$, $n_2 = 1$)	0.3	80.7
$r_1 = \frac{r_1}{1+g_2 P^{n_2}}$ ($g_2 = 0.02$, $n_2 = 1$)	0.26	74.72
$r_1 = \frac{r_1}{1+g_2 P^{n_2}}$ ($g_2 = 0.03$, $n_2 = 1$)	0.22	71.26
$r_2 = \frac{r_2}{1+g_3 P^{n_3}}$ ($g_3 = 0.01$, $n_3 = 1$)	0.31	84.03
$r_2 = \frac{r_2}{1+g_3 P^{n_3}}$ ($g_3 = 0.02$, $n_3 = 1$)	0.29	80.02
$r_2 = \frac{r_2}{1+g_3 P^{n_3}}$ ($g_3 = 0.03$, $n_3 = 1$)	0.26	77.33
$r_3 = \frac{r_3}{1+g_4 P^{n_4}}$ ($g_4 = 0.01$, $n_4 = 1$)	0.35	94.87
$r_3 = \frac{r_3}{1+g_4 P^{n_4}}$ ($g_4 = 0.02$, $n_4 = 1$)	0.35	95.57
$r_3 = \frac{r_3}{1+g_4 P^{n_4}}$ ($g_4 = 0.03$, $n_4 = 1$)	0.36	96.3
$\rho_S = \frac{\rho_S}{1+g_1 P^{n_1}}$ and $r_3 = \frac{r_3}{1+g_4 P^{n_4}}$ ($g_1 = g_4 = 0.01$, $n_1 = n_4 = 1$)	0.27	75.63
$\rho_S = \frac{\rho_S}{1+g_1 P^{n_1}}$ and $r_3 = \frac{r_3}{1+g_4 P^{n_4}}$ ($g_1 = g_4 = 0.02$, $n_1 = n_4 = 1$)	0.21	68.73
$\rho_S = \frac{\rho_S}{1+g_1 P^{n_1}}$ and $r_3 = \frac{r_3}{1+g_4 P^{n_4}}$ ($g_1 = g_4 = 0.03$, $n_1 = n_4 = 1$)	0.16	64.7
$\rho_{PS} = \frac{\rho_{PS}}{1+g_5 P^{n_5}}$ ($g_5 = 0.01$, $n_5 = 1$)	0.33	89.94
$\rho_{PS} = \frac{\rho_{PS}}{1+g_5 P^{n_5}}$ ($g_5 = 0.02$, $n_5 = 1$)	0.32	87.43
$\rho_{PS} = \frac{\rho_{PS}}{1+g_5 P^{n_5}}$ ($g_5 = 0.03$, $n_5 = 1$)	0.32	85.56

Table 6.3: The sphere formation efficiency and average sphere size in the presence of plasticity when $\rho_S = 0.9$, $r_1 = 0.3$, $r_2 = 0.6$, $r_3 = 0.1$, $\rho_{PS} = 0.1$ and $\Gamma_P = 0.1$

The results in Tables 6.2 and 6.3 show an increase in both the SFE and AVSS in the presence of plasticity. Here, similar to the case with no plasticity, the negative feedback on each of ρ_S, r_1, and r_2 leads to a reduction in SFE and AVSS. The SFE and AVSS are slightly increased if negative feedback is applied to the symmetric commitment rate r_3. In addition, the impact of negative feedback regulators secreted from CSCs, which reduces the dedifferentiation rate ρ_{PS}, is studied, showing minor reductions in SFE and AVSS. The error for SFE and AVSS are $\sigma_{SFE} = 0.00058$ and $\sigma_{AVSS} = 0.14$, respectively, when there is no plasticity and feedback in the system. The error corresponding to the other cases is also similar.

6.3 Conclusion

In this chapter we have investigated how negative feedback controlling CSC proliferation and plasticity affects the ability of a single cell to form a sphere. To do so, the trajectories of cell numbers undergoing different cellular proliferation pathways have been calculated using a Gillespie algorithm. Previous studies have shown that such negative feedback on CSC division and dedifferentiation has an important role in the maintenance of tissue homeostasis in large cell populations. The results in this chapter show a decrease in sphere formation capacity and average sphere size when CSC division and dedifferentiation are subject to negative feedback. The SFE and AVSS are increased if the probability of the symmetric commitment division pathway in which a single CSC generates progenitors undergoes negative feedback. Consequently, the increasing number of progenitors in the tumor reduces the rate of symmetric commitments, corresponding to lower CSC death,

underlying the importance of CSCs in SFE and AVSS. In addition, the results show that SFE and AVSS increase slightly if cells escape negative feedback through dedifferentiation.

Chapter 7

Conclusion

7.1 Concluding remarks

This thesis has introduced mathematical models developed to study the impact of tumor heterogeneity and microenvironmental changes on the performance of radiotherapy schedules. In this direction, Chapter 1 introduced the necessary background on tumor heterogeneity and tumor microenvironments as well as the underlying mechanisms explaining radiation induced cell kill. Chapter 2 reviewed the role of the CSCs in therapeutic resistance and new treatment approaches, and Chapter 3 presented a deterministic model for exploring the effect of radiotherapy on the resistant subpopulation of cells. In Chapters 4 and 5, stochastic models have been developed to study the impact of random birth and death rates, and plasticity on tumor control probability. In addition, the effect of negative regulatory feedback on sphere formation efficiency and average sphere size were explored

in Chapter 6.

In Chapter 2, we comprehensively reviewed mathematical models that probe the impact of CSCs on therapeutic approaches. CSCs benefit from the development of upregulated DNA repair mechanisms and underlying cellular pathways that support CSCs resulting in the emergence of resistance to therapeutic kill agents. Furthermore, this resistant subpopulation is potentially tumorigenic, which enables them to regrow and lead to relapse. Mathematical modeling is a useful approach for understanding these complicated biological mechanisms grounded on valid experimental observations on a par with other experimental techniques. In this direction, we also discussed mathematical models exploring various CSC properties, and their role in developing new treatment strategies targeting CSCs, and optimizing treatment outcomes. Cancer biology is extremely complex with many unknown parameters that need to be identified and understood. Mathematical and computational approaches can be applied to find the most important parameters and mechanisms using experimental results. In addition, they can suggest new experimental studies that may explain related biological questions, ultimately resulting in therapeutic improvements.

In Chapter 3, a simple mathematical model has been presented to study the impact of radiotherapy on tumor heterogeneity. According to the numerical results, fractionated radiotherapy can increase the fraction of CSCs and change the cellular diversity of tumors. Most proposed radiotherapy regimens aim to reduce tumor bulk. However, our results suggest that the impact of radiotherapy schedules on the population of CSCs needs to be well understood since the enrichment of CSCs after treatment, can lead to relapse. Thus, in addition to decreasing tumor size, optimal radiotherapy protocols should control the CSC population and inhibit the increase of this resistant subpopulation of cells. The

results suggest that the standard schedule is not the best treatment protocol, and highlights the need to improve this conventional approach. The optimum regimen for PDGF-driven glioblastoma suggested in the literature is not validated by our model, which has been parametrized using breast cancer data. This observation indicates that optimization may be affected by model design and model dependent parameters. Furthermore, due to the biological diversity among different cancer types (and even for the same cancer type in different patients), there may not exist one general optimum schedule that leads to the best outcomes for all cancers. Consequently, devising personalized therapeutic approaches would be the preferable route, but can not currently be accomplished on a large scale. Thus, further work towards reaching this goal is of critical importance.

In Chapter 4, we have investigated the impact of random microenvironmental changes on tumor control probability by applying stochastic models. In this direction, the effect of random parameter changes was described using step functions. A modified Gillespie algorithm for discontinuous changes was therefore applied to calculate TCP. Tumor control probability was calculated for demographic rates randomly altered over time. An increase in standard deviation (σ) initially leads to a corresponding increase in TCP. However, TCP diminishes overtime if it does not saturate to 1, degrading the efficiency of the radiotherapy. Furthermore, the effectiveness of radiotherapy protocols change significantly when birth and death rates are anticorrelated and modified arbitrarily.

In Chapter 5 the effect of plasticity on TCP is explored. To do so, a stochastic model consisting of a population of CSCs and progenitors was considered, in which cell kill rates due to radiation are described using a step function to account for the higher kill rate during fractionation. Using a modified Gillespie algorithm, TCP_S and TCP_{S+P}, which

are, respectively, the probability of CSC elimination and tumor removal were computed to explore the performance of standard, hyperfractionated, and accelerated hyperfractionated protocols. The results confirm a reduction in both the TCP_S and TCP_{S+P} in the presence of plasticity. In addition, an accelerated hyperfractionated schedule results in better control than the standard and hyperfractionated regimens, with or without plasticity. It was also observed that the existence of plasticity does not impact the accelerated hyperfractionated protocol's efficiency significantly. However, both TCP_S and TCP_{S+P} drop noticeably for the accelerated hyperfractionated protocol in the case of highly resistant tumors. The impact of plasticity on combination therapy that includes targeted therapy triggering CSCs differentiation and radiotherapy has also been studied. The results show that the probability of CSC and tumor removal is not enhanced greatly in the presence of plasticity.

In Chapter 6, both the sphere formation efficiency and average sphere size are studied for a system of cellular pathways, subjected to regulatory negative feedback on CSC proliferation and plasticity. A Gillespie algorithm has been used to study the trajectory of cell numbers under negative regulatory feedback. The sphere formation efficacy (SFE) and average sphere size (AVSS) decrease when CSC division and dedifferentiation are regulated through negative feedback. However, if the probability of symmetric commitment is subject to negative feedback, both the SFE and AVSS are increased, due to the reduction in CSC death. Furthermore, SFE and AVSS are decreased when the rate of plasticity is controlled through negative feedback, and so inhibition of this feedback enhances sphere formation capacity.

In summary, in this thesis, the effect of both cellular heterogeneity and microenviron-

mental fluctuations on radiotherapy protocols have been investigated. The question of how regulatory feedback on cellular division pathways affects sphere formation capacity was also explored. The results show that increasing fractionation in radiotherapy protocols modifies the heterogeneity of tumors. In addition, the existence of plasticity, which allows transition between CSC and non-CSC compartments, reduces the efficiency of radiotherapy protocols as well as of combination therapy (targeted therapy increases CSC differentiation and radiotherapy). The random fluctuations of cellular demographic factors have also been shown to influence the tumor control probability. Finally, the results confirm that avoiding the effects of the regulatory negative feedback controlling CSC division and dedifferentiation rates, increases the ability of a single CSC to form a sphere.

7.2 Future work

This section describes a future avenue for the author's research. This future work will tackle some of the prospective points of the current work as well as an ongoing project on second cancer risk estimation. Overall, the main areas for potential future work are as follows.

7.2.1 Prospective future work

The impact of radiotherapy on tumor heterogeneity, investigated in Chapter 3, assumed different radiosensitivities among cancer cells as well as dose dependent transition rates from the repair phase to the active non repairing population. The model can be extended

to consider more biological determinants, such as an increase in the selfrenewal ability of the resistant cells after exposure to radiation. It would also be useful to calibrate the model for other types of cancers so as to explore the alterations in cellular heterogeneity due to fractionated radiotherapy for various cancers with different characteristic behaviors. Furthermore, the model can be extended to study the impact of immunotherapy on radiotherapy performance.

The effects of both plasticity and random fluctuations on demographic factors and ultimately on the TCP have also been studied. These works has been described in Chapters 4 and 5. The impact of arbitrary changes on tumor control probability has been investigated for a single-cell-type population. This simple model can be extended, based on the CSC hypothesis, to a hierarchical model consisting of CSCs and progenitors. The initial results show the role of random alterations in birth and death rates for a two compartment model on the TCP_S has the same impact as that reported in Chapter 4. It would be useful and interesting to understand the impact of these changes on the TCP_{S+P}. In addition, the existence of plasticity among cancer cells results in an increase in the number of resistant cells in tumors. Thus, the effect of random changes in transition rates from non-CSCs to CSC states on the overall TCP merits further exploration. It might also be worthwhile to explore the impact of random spatial changes on the hypoxic and normoxic regions of tumors.

The impact of negative regulatory feedback on the sphere formation capacity of a single CSC was considered in Chapter 6. Extending the model to include mature cells would facilitate studying the changes that occur in SFE and AVSS due to the negative feedback secreted from mature cells and controlling CSC and progenitor division. Moreover, it is

important to investigate the sphere formation potential of a single CSC when mature cells escape from the negative feedback control that regulates the plasticity rate between either mature cells and progenitors or mature cells and CSCs.

7.2.2 Second cancers

Fractionated radiotherapy uses high doses of radiation to destroy cancer cells. It is an important part of cancer treatment and may contribute to an increase in the number of survivors; however, it is a double-edged sword and this regimen can cause complications. For instance, second cancers are among the possible late side effects of radiotherapy and can arise in organs nearby the original tumor. Developing a second cancer as a result of this treatment is an increasing concern, especially among younger survivors. Therefore, it is clearly of importance to study the risks of second cancers in patients treated with radiotherapy. A comprehensive study on atomic bomb survivors approximately correlated the cancer risk from exposure to intermediate doses of radiation; however, there is not much understanding of the effects of higher doses. The latency period between radiotherapy and the evolution of second cancers is long, so it takes significant time to monitor survivors carefully and also to provide good epidemiological data in order to explore new treatment regimens. These difficulties highlight the importance of model-based predictions.

A cascade of complicated biological mechanisms underlie the initiation and growth a second cancer in an organ. These underlying processes make it hard to introduce a practical measure for estimating the cancer risk. Therefore, applying a well defined and quantitative approach that accurately measures the cancer risk is crucial and necessary.

The year-specific excessive relative radiation risk (ERR) is a quantity that estimates by how much the risk for people who received radiotherapy exceeds the risk of non-exposed people over a specific period of time (Angell et al., 2009). The ERR is mathematically calculated for intermediate and high doses of radiation, and shows that the second cancer risk increases for patients treated for Hodgkin's lymphoma (Sachs et al., 2005). This model is implemented based on clonal evolution theory, and all the cancerous cells are assumed to be able to proliferate equally. It would be interesting to extend the model based on the CSC hypothesis and the existence of heterogeneity among cancer cells, so as to account for their differences in proliferation potentials and DNA repair mechanisms.

In addition, the dose-volume data, which shows the relation between radiation dose and tissue volume, is available experimentally and reported as a dose-volume-histogram (DVH). Hence, the organ specific ERR can also be evaluated by applying the data to the model (Hodgson, 2007; Zhang et al., 2015). However, a dose volume histogram does not provide enough information about the distribution of the dose in the tissue. Consequently, further work is needed to understand the effects of various cases of dose absorption in the tissue. Such work would assess the organ specific ERR for the same dose volume histogram data and so determine the effects of different dose distributions.

Copyright Permission

Copyright permits have been attached here.

SPRINGER NATURE LICENSE
TERMS AND CONDITIONS

Oct 24, 2018

This Agreement between University of Waterloo -- Farinaz Forouzannia ("You") and Springer Nature ("Springer Nature") consists of your license details and the terms and conditions provided by Springer Nature and Copyright Clearance Center.

License Number	4455581063445
License date	Oct 24, 2018
Licensed Content Publisher	Springer Nature
Licensed Content Publication	Current Stem Cell Reports
Licensed Content Title	Cancer Stem Cells, the Tipping Point: Minority Rules?
Licensed Content Author	Farinaz Forouzannia, Sivabal Sivaloganathan
Licensed Content Date	Jan 1, 2017
Licensed Content Volume	3
Licensed Content Issue	3
Type of Use	Thesis/Dissertation
Requestor type	academic/university or research institute
Format	print and electronic
Portion	full article/chapter
Will you be translating?	no
Circulation/distribution	>50,000
Author of this Springer Nature content	yes
Title	Studies of tumor heterogeneity, tumor microenvironment, and therapeutic regimens: A mathematical and computational approach
Institution name	University of Waterloo
Expected presentation date	Jan 2019
Requestor Location	University of Waterloo 200 university avenue west Waterloo, ON N2l3G1 Canada Attn: University of Waterloo
Billing Type	Invoice
Billing Address	University of Waterloo 200 university avenue west

SPRINGER NATURE LICENSE TERMS AND CONDITIONS

Oct 24, 2018

This Agreement between University of Waterloo -- Farinaz Forouzannia ("You") and Springer Nature ("Springer Nature") consists of your license details and the terms and conditions provided by Springer Nature and Copyright Clearance Center.

License Number	4455590271248
License date	Oct 24, 2018
Licensed Content Publisher	Springer Nature
Licensed Content Publication	Bulletin of Mathematical Biology
Licensed Content Title	Mathematical Modeling of the Effects of Tumor Heterogeneity on the Efficiency of Radiation Treatment Schedule
Licensed Content Author	Farinaz Forouzannia, Heiko Enderling, Mohammad Kohandel
Licensed Content Date	Jan 1, 2017
Licensed Content Volume	80
Licensed Content Issue	2
Type of Use	Thesis/Dissertation
Requestor type	academic/university or research institute
Format	print and electronic
Portion	full article/chapter
Will you be translating?	no
Circulation/distribution	>50,000
Author of this Springer Nature content	yes
Title	Studies of tumor heterogeneity, tumor microenvironment, and therapeutic regimens: A mathematical and computational approach
Institution name	University of Waterloo
Expected presentation date	Jan 2019
Requestor Location	University of Waterloo 200 university avenue west Waterloo, ON N2l3G1 Canada Attn: University of Waterloo
Billing Type	Invoice
Billing Address	University of Waterloo 200 university avenue west

Waterloo, ON N2l3G1
Canada
Attn: University of Waterloo

Total 0.00 CAD

Terms and Conditions

Springer Nature Terms and Conditions for RightsLink Permissions

Springer Nature Customer Service Centre GmbH (the Licensor) hereby grants you a non-exclusive, world-wide licence to reproduce the material and for the purpose and requirements specified in the attached copy of your order form, and for no other use, subject to the conditions below:

1. The Licensor warrants that it has, to the best of its knowledge, the rights to license reuse of this material. However, you should ensure that the material you are requesting is original to the Licensor and does not carry the copyright of another entity (as credited in the published version).

   If the credit line on any part of the material you have requested indicates that it was reprinted or adapted with permission from another source, then you should also seek permission from that source to reuse the material.

2. Where **print only** permission has been granted for a fee, separate permission must be obtained for any additional electronic re-use.

3. Permission granted **free of charge** for material in print is also usually granted for any electronic version of that work, provided that the material is incidental to your work as a whole and that the electronic version is essentially equivalent to, or substitutes for, the print version.

4. A licence for 'post on a website' is valid for 12 months from the licence date. This licence does not cover use of full text articles on websites.

5. Where **'reuse in a dissertation/thesis'** has been selected the following terms apply: Print rights of the final author's accepted manuscript (for clarity, NOT the published version) for up to 100 copies, electronic rights for use only on a personal website or institutional repository as defined by the Sherpa guideline (www.sherpa.ac.uk/romeo/).

6. Permission granted for books and journals is granted for the lifetime of the first edition and does not apply to second and subsequent editions (except where the first edition permission was granted free of charge or for signatories to the STM Permissions Guidelines http://www.stm-assoc.org/copyright-legal-affairs/permissions/permissions-guidelines/), and does not apply for editions in other languages unless additional translation rights have been granted separately in the licence.

7. Rights for additional components such as custom editions and derivatives require additional permission and may be subject to an additional fee. Please apply to Journalpermissions@springernature.com/bookpermissions@springernature.com for these rights.

8. The Licensor's permission must be acknowledged next to the licensed material in print. In electronic form, this acknowledgement must be visible at the same time as the figures/tables/illustrations or abstract, and must be hyperlinked to the journal/book's homepage. Our required acknowledgement format is in the Appendix below.

9. Use of the material for incidental promotional use, minor editing privileges (this does not include cropping, adapting, omitting material or any other changes that affect the meaning, intention or moral rights of the author) and copies for the disabled are permitted under this licence.

10. Minor adaptations of single figures (changes of format, colour and style) do not require the Licensor's approval. However, the adaptation should be credited as shown in Appendix below.

Appendix — Acknowledgements:

For Journal Content:
Reprinted by permission from [**the Licensor**]: [**Journal Publisher** (e.g. Nature/Springer/Palgrave)] [**JOURNAL NAME**] [**REFERENCE CITATION** (Article name, Author(s) Name), [**COPYRIGHT**] (year of publication)

For **Advance Online Publication papers:**
Reprinted by permission from [**the Licensor**]: [**Journal Publisher** (e.g. Nature/Springer/Palgrave)] [**JOURNAL NAME**] [**REFERENCE CITATION** (Article name, Author(s) Name), [**COPYRIGHT**] (year of publication), advance online publication, day month year (doi: 10.1038/sj.[JOURNAL ACRONYM].)

For Adaptations/Translations:
Adapted/Translated by permission from [**the Licensor**]: [**Journal Publisher** (e.g. Nature/Springer/Palgrave)] [**JOURNAL NAME**] [**REFERENCE CITATION** (Article name, Author(s) Name), [**COPYRIGHT**] (year of publication)

Note: For any republication from the British Journal of Cancer, the following credit line style applies:

Reprinted/adapted/translated by permission from [**the Licensor**]: on behalf of Cancer Research UK: : [**Journal Publisher** (e.g. Nature/Springer/Palgrave)] [**JOURNAL NAME**] [**REFERENCE CITATION** (Article name, Author(s) Name), [**COPYRIGHT]** (year of publication)

For **Advance Online Publication** papers:
Reprinted by permission from The [**the Licensor**]: on behalf of Cancer Research UK: [**Journal Publisher** (e.g. Nature/Springer/Palgrave)] [**JOURNAL NAME**] [**REFERENCE CITATION** (Article name, Author(s) Name), [**COPYRIGHT**] (year of publication), advance online publication, day month year (doi: 10.1038/sj.[JOURNAL ACRONYM])

For Book content:
Reprinted/adapted by permission from [**the Licensor**]: [**Book Publisher** (e.g. Palgrave Macmillan, Springer etc) [**Book Title**] by [**Book author**(s)] [**COPYRIGHT**] (year of publication)

Bibliography

Al-Hajj, Muhammad, Max S. Wicha, Adalberto Benito-Hernandez, Sean J. Morrison, and Michael F. Clarke. "Prospective identification of tumorigenic breast cancer cells." *Proceedings of the National Academy of Sciences* 100, no. 7 (2003): 3983-3988.

Altrock, Philipp M., Lin L. Liu, and Franziska Michor. "The mathematics of cancer: integrating quantitative models." *Nature Reviews Cancer* 15, no. 12 (2015): 730.

Anderson, Alexander RA, and Vito Quaranta. "Integrative mathematical oncology." *Nature Reviews Cancer* 8, no. 3 (2008): 227.

Angell, William J., H. Zeeb, and F. Shannon. "WHO handbook on indoor radon: a public health perspective." (2009).

Bachman, Jeff WN, and Thomas Hillen. "Mathematical optimization of the combination of radiation and differentiation therapies for cancer." *Frontiers in oncology* 3 (2013): 52.

Badri, Hamidreza, and Kevin Leder. "Optimal treatment and stochastic modeling of heterogeneous tumors." *Biology direct* 11, no. 1 (2016): 40.

Badri, H., K. Pitter, Eric C. Holland, F. Michor, and K. Leder. "Optimization of radiation dosing schedules for proneural glioblastoma." *Journal of mathematical biology* 72, no. 5 (2016): 1301-1336.

Bao, Shideng, Qiulian Wu, Roger E. McLendon, Yueling Hao, Qing Shi, Anita B. Hjelmeland, Mark W. Dewhirst, Darell D. Bigner, and Jeremy N. Rich. "Glioma stem cells promote radioresistance by preferential activation of the DNA damage response." *Nature* 444, no. 7120 (2006): 756.

Bayer, C., and P. Vaupel. "Acute versus chronic hypoxia in tumors." *Strahlentherapie und Onkologie* 188, no. 7 (2012): 616-627.

Biteau, Benoit, Christine E. Hochmuth, and Heinrich Jasper. "Maintaining tissue homeostasis: dynamic control of somatic stem cell activity." *Cell stem cell* 9, no. 5 (2011): 402-411.

Boman, Bruce M., and Max S. Wicha. "Cancer stem cells: a step toward the cure." *Journal of clinical oncology* 26, no. 17 (2008): 2795-2799.

Bonadonna, Gianni, Milvia Zambetti, Angela Moliterni, Luca Gianni, and Pinuccia Valagussa. "Clinical relevance of different sequencing of doxorubicin and cyclophosphamide, methotrexate, and fluorouracil in operable breast cancer." *Journal of clinical oncology* 22, no. 9 (2004): 1614-1620.

Byrne, Helen M. "Dissecting cancer through mathematics: from the cell to the animal model." *Nature Reviews Cancer* 10, no. 3 (2010): 221.

Cabrera, Marina Carla, Robert E. Hollingsworth, and Elaine M. Hurt. "Cancer stem cell plasticity and tumor hierarchy." *World journal of stem cells* 7, no. 1 (2015): 27.

Cao, Yang, Hong Li, and Linda Petzold. "Efficient formulation of the stochastic simulation algorithm for chemically reacting systems." *The journal of chemical physics* 121, no. 9 (2004): 4059-4067.

Charafe-Jauffret, Emmanuelle, Christophe Ginestier, and Daniel Birnbaum. "Breast cancer stem cells: tools and models to rely on." *BMC cancer* 9, no. 1 (2009): 202.

Chen, Wanyin, Jihu Dong, Jacques Haiech, Marie-Claude Kilhoffer, and Maria Zeniou. "Cancer stem cell quiescence and plasticity as major challenges in cancer therapy." *Stem cells international* 2016 (2016).

Citron, Marc L., Donald A. Berry, Constance Cirrincione, Clifford Hudis, Eric P. Winer, William J. Gradishar, Nancy E. Davidson et al. "Randomized trial of dose-dense versus conventionally scheduled and sequential versus concurrent combination chemotherapy as postoperative adjuvant treatment of node-positive primary breast cancer: first report of Intergroup Trial C9741/Cancer and Leukemia Group B Trial 9741." *Journal of clinical oncology* 21, no. 8 (2003): 1431-1439.

Coldman, A. J., and J. H. Goldie. "A stochastic model for the origin and treatment of tumors containing drug-resistant cells." *Bulletin of mathematical biology* 48, no. 3-4 (1986): 279-292.

Conforti, Domenico, Francesca Guerriero, and Rosita Guido. "Optimization models for radiotherapy patient scheduling." *4OR* 6, no. 3 (2008): 263-278.

Costa, M. I. S., J. L. Boldrini, and R. C. Bassanezi. "Optimal chemical control of populations developing drug resistance." *Mathematical Medicine and Biology: A Journal of the IMA* 9, no. 3 (1992): 215-226.

Cox, James D., and Kie Kian Ang. *Radiation Oncology E-Book: Rationale, Technique, Results.* Elsevier Health Sciences, 2009.

Dale, Roger G. "The application of the linear-quadratic dose-effect equation to fractionated and protracted radiotherapy." *The British journal of radiology* 58, no. 690 (1985): 515-528.

Dawson, A., and T. Hillen. "Derivation of the tumour control probability (TCP) from a cell cycle model." *Computational and Mathematical Methods in Medicine* 7, no. 2-3 (2006): 121-141.

Dean, Michael, Tito Fojo, and Susan Bates. "Tumour stem cells and drug resistance." *Nature Reviews Cancer* 5, no. 4 (2005): 275.

Dhawan, Andrew, Mohammad Kohandel, Richard Hill, and Sivabal Sivaloganathan. "Tumour control probability in cancer stem cells hypothesis." *PloS one* 9, no. 5 (2014): e96093.

Dingli, David, and Franziska Michor. "Successful therapy must eradicate cancer stem cells." *Stem cells* 24, no. 12 (2006): 2603-2610.

Dionysiou, Dimitra D., Georgios S. Stamatakos, Nikolaos K. Uzunoglu, Konstantina S. Nikita, and Antigoni Marioli. "A four-dimensional simulation model of tumour response

to radiotherapy in vivo: parametric validation considering radiosensitivity, genetic profile and fractionation." *Journal of theoretical biology* 230, no. 1 (2004): 1-20.

Enderling, Heiko. "Cancer stem cells: small subpopulation or evolving fraction?." *Integrative Biology* 7, no. 1 (2015): 14-23.

Enderling, Heiko, Alexander RA Anderson, Mark AJ Chaplain, Afshin Beheshti, Lynn Hlatky, and Philip Hahnfeldt. "Paradoxical dependencies of tumor dormancy and progression on basic cell kinetics." *Cancer research* (2009): 0008-5472.

Enderling, Heiko, and Philip Hahnfeldt. "Cancer stem cells in solid tumors: Is 'evading apoptosis'a hallmark of cancer?." *Progress in biophysics and molecular biology* 106, no. 2 (2011): 391-399.

Enderling, Heiko, Derek Park, Lynn Hlatky, and Philip Hahnfeldt. "The importance of spatial distribution of stemness and proliferation state in determining tumor radioresponse." *Mathematical Modelling of Natural Phenomena* 4, no. 3 (2009): 117-133.

Erban, Radek, Jonathan Chapman, and Philip Maini. "A practical guide to stochastic simulations of reaction-diffusion processes." *arXiv preprint arXiv:0704.*1908 (2007).

Eyler, Christine E., and Jeremy N. Rich. "Survival of the fittest: cancer stem cells in therapeutic resistance and angiogenesis." *Journal of clinical oncology: official journal of the American Society of Clinical Oncology* 26, no. 17 (2008): 2839.

Fillmore, Christine M., and Charlotte Kuperwasser. "Human breast cancer cell lines contain stem-like cells that self-renew, give rise to phenotypically diverse progeny and survive chemotherapy." *Breast cancer research* 10, no. 2 (2008): R25.

Forouzannia, Farinaz, Heiko Enderling, and Mohammad Kohandel. "Mathematical Modeling of the Effects of Tumor Heterogeneity on the Efficiency of Radiation Treatment Schedule." *Bulletin of mathematical biology* 80, no. 2 (2018): 283-293.

Forouzannia, Farinaz, and Sivabal Sivaloganathan. "Cancer Stem Cells, the Tipping Point: Minority Rules?." *Current Stem Cell Reports* 3, no. 3 (2017): 240-247.

Foo, Jasmine, and Franziska Michor. "Evolution of resistance to targeted anti-cancer therapies during continuous and pulsed administration strategies." *PLoS computational biology* 5, no. 11 (2009): e1000557.

Fowler, John F. "The linear-quadratic formula and progress in fractionated radiotherapy." *The British journal of radiology* 62, no. 740 (1989): 679-694.

Fukumura, Dai, and Rakesh K. Jain. "Tumor microenvironment abnormalities: causes, consequences, and strategies to normalize." *Journal of cellular biochemistry* 101, no. 4 (2007): 937-949.

Gao, Xuefeng, J. Tyson McDonald, Lynn Hlatky, and Heiko Enderling. "Acute and fractionated irradiation differentially modulate glioma stem cell division kinetics." *Cancer research* 73, no. 5 (2013): 1481-1490.

Gillespie, Daniel T. "Stochastic simulation of chemical kinetics." Annu. *Rev. Phys. Chem.* 58 (2007): 35-55.

Goldie, J. H., and A. J. Coldman. "Quantitative model for multiple levels of drug resistance in clinical tumors." *Cancer treatment reports* 67, no. 10 (1983): 923-931.

Goldman, Aaron, Biswanath Majumder, Andrew Dhawan, Sudharshan Ravi, David Goldman, Mohammad Kohandel, Pradip K. Majumder, and Shiladitya Sengupta. "Temporally sequenced anticancer drugs overcome adaptive resistance by targeting a vulnerable chemotherapy-induced phenotypic transition." *Nature communications* 6 (2015): 6139.

Gong, Jiafen, Mairon M. Dos Santos, Chris Finlay, and Thomas Hillen. "Are more complicated tumour control probability models better?." *Mathematical medicine and biology: a journal of the IMA* 30, no. 1 (2011): 1-19.

Gupta, Piyush B., Christine M. Fillmore, Guozhi Jiang, Sagi D. Shapira, Kai Tao, Charlotte Kuperwasser, and Eric S. Lander. "Stochastic state transitions give rise to phenotypic equilibrium in populations of cancer cells." *Cell* 146, no. 4 (2011): 633-644.

Hall, Eric J., and Amato J. Giaccia. *Radiobiology for the Radiologist.* Vol. 6. Philadelphia: Lippincott Williams Wilkins, 2006.

Hanahan, Douglas, and Robert A. Weinberg. "Hallmarks of cancer: the next generation." *Cell* 144, no. 5 (2011): 646-674.

Haviland, Joanne S., J. Roger Owen, John A. Dewar, Rajiv K. Agrawal, Jane Barrett, Peter J. Barrett-Lee, H. Jane Dobbs et al. "The UK Standardisation of Breast Radiotherapy (START) trials of radiotherapy hypofractionation for treatment of early breast cancer: 10-year follow-up results of two randomised controlled trials." *The lancet oncology* 14, no. 11 (2013): 1086-1094.

Heppner, Gloria H. "Tumor heterogeneity." *Cancer research* 44 (1984): 2259-2265.

Hodgson, David C., Eng-Siew Koh, Tu Huan Tran, Mostafa Heydarian, Richard Tsang, Melania Pintilie, Tony Xu, Lei Huang, Rainer K. Sachs, and David J. Brenner. "Individualized estimates of second cancer risks after contemporary radiation therapy for Hodgkin lymphoma." *Cancer: Interdisciplinary International Journal of the American Cancer Society* 110, no. 11 (2007): 2576-2586.

Iwasa, Yoh, Martin A. Nowak, and Franziska Michor. "Evolution of resistance during clonal expansion." *Genetics* 172, no. 4 (2006): 2557-2566.

Jilkine, Alexandra, and Ryan N. Gutenkunst. "Effect of dedifferentiation on time to mutation acquisition in stem cell-driven cancers." *PLoS computational biology* 10, no. 3 (2014): e1003481.

Johnson, Sara, Hexin Chen, and Pang-Kuo Lo. "In vitro tumorsphere formation assays." *Bio-protocol* 3, no. 3 (2013).

Kendal, W. S. "Technical Report A closed-form description of tumour control with fractionated radiotherapy and repopulation." *International journal of radiation biology* 73, no. 2 (1998): 207-210.

Klement, Giannoula, Sylvain Baruchel, Janusz Rak, Shan Man, Katherine Clark, Daniel J. Hicklin, Peter Bohlen, and Robert S. Kerbel. "Continuous low-dose therapy with vinblastine and VEGF receptor-2 antibody induces sustained tumor regression without overt toxicity." *The Journal of clinical investigation* 105, no. 8 (2000): R15-R24.

Kohandel, M., S. Sivaloganathan, and A. Oza. "Mathematical modeling of ovarian cancer

treatments: sequencing of surgery and chemotherapy." *Journal of theoretical biology* 242, no. 1 (2006): 62-68.

Komarova, Natalia L., and Dominik Wodarz. "Effect of cellular quiescence on the success of targeted CML therapy." *PLoS One* 2, no. 10 (2007): e990.

Koury, Jeffrey, Li Zhong, and Jijun Hao. "Targeting signaling pathways in cancer stem cells for cancer treatment." *Stem cells international* 2017 (2017).

Kreso, Antonija, and John E. Dick. "Evolution of the cancer stem cell model." *Cell stem cell* 14, no. 3 (2014): 275-291.

Lagadec, Chann, Erina Vlashi, Lorenza Della Donna, YongHong Meng, Carmen Dekmezian, Kwanghee Kim, and Frank Pajonk. "Survival and self-renewing capacity of breast cancer initiating cells during fractionated radiation treatment." *Breast cancer research* 12, no. 1 (2010): R13.

Leder, Kevin, Ken Pitter, Quincey LaPlant, Dolores Hambardzumyan, Brian D. Ross, Timothy A. Chan, Eric C. Holland, and Franziska Michor. "Mathematical modeling of PDGF-driven glioblastoma reveals optimized radiation dosing schedules." *Cell* 156, no. 3 (2014): 603-616.

Lonardo, Enza, Michele Cioffi, Patricia Sancho, Yolanda Sanchez-Ripoll, Sara Maria Trabulo, Jorge Dorado, Anamaria Balic, Manuel Hidalgo, and Christopher Heeschen. "Metformin targets the metabolic achilles heel of human pancreatic cancer stem cells." *PloS one* 8, no. 10 (2013): e76518.

Lu, Ting, Dmitri Volfson, Lev Tsimring, and Jeff Hasty. "Cellular growth and division in the Gillespie algorithm." *Systems biology* 1, no. 1 (2004): 121-128.

Mahdipour-Shirayeh, Ali, Kamran Kaveh, Mohammad Kohandel, and Sivabal Sivaloganathan. "Phenotypic heterogeneity in modeling cancer evolution." *PloS one* 12, no. 10 (2017): e0187000.

Marjanovic, Nemanja D., Robert A. Weinberg, and Christine L. Chaffer. "Poised with purpose: cell plasticity enhances tumorigenicity." (2013): 2713-2714.

Marjanovic, Nemanja D., Robert A. Weinberg, and Christine L. Chaffer. "Cell plasticity and heterogeneity in cancer." *Clinical chemistry* 59, no. 1 (2013): 168-179.

Martin, Rory, and K. L. Teo. *Optimal control of drug administration in cancer chemotherapy*. World Scientific, 1994.

Mathews, Lesley A., Stephanie M. Cabarcas, and Elaine M. Hurt, eds. *DNA repair of cancer stem cells.* Berlin: Springer, 2013.

Maugeri-Sacc, Marcello, Paolo G. Vigneri, and Ruggero De Maria. "Cancer stem cells and chemosensitivity." *Clinical Cancer Research* (2011): clincanres-2538.

Meacham, Corbin E., and Sean J. Morrison. "Tumour heterogeneity and cancer cell plasticity." *Nature* 501, no. 7467 (2013): 328.

Mitchell, Gary. "The rationale for fractionation in radiotherapy." *Clinical journal of oncology nursing* 17, no. 4 (2013).

Michor, Franziska, Timothy P. Hughes, Yoh Iwasa, Susan Branford, Neil P. Shah, Charles L. Sawyers, and Martin A. Nowak. "Dynamics of chronic myeloid leukaemia." *Nature* 435, no. 7046 (2005): 1267.

Munro, T. R., and C. W. Gilbert. "The relation between tumour lethal doses and the radiosensitivity of tumour cells." *The British journal of radiology* 34, no. 400 (1961): 246-251.

Norton, Larry, and Richard Simon. "Tumor size, sensitivity to therapy, and design of treatment schedules." *Cancer treatment reports* 61, no. 7 (1977): 1307-1317.

Norton, Larry, and Richard Simon. "The norton-simon hypothesis revisited." *Cancer treatment reports* 70, no. 1 (1986): 163.

Nowak, Martin A., Franziska Michor, and Yoh Iwasa. "The linear process of somatic evolution." *Proceedings of the national academy of sciences* 100, no. 25 (2003): 14966-14969.

Nowell, Peter C. "The clonal evolution of tumor cell populations." *Science* 194, no. 4260 (1976): 23-28.

Ogawa, Kazuhiko, Yasuo Yoshioka, Fumiaki Isohashi, Yuji Seo, Ken Yoshida, and Hideya Yamazaki. "Radiotherapy targeting cancer stem cells: current views and future perspectives." *Anticancer research* 33, no. 3 (2013): 747-754.

Oliver, R. "A comparison of the effects of acute and protracted gamma-radiation on the growth of seedlings of Vicia faba: part II. Theoretical calculations." *International Journal of Radiation Biology and Related Studies in Physics, Chemistry and Medicine* 8, no. 5 (1964): 475-488.

Otani, Keisuke, Yoko Naito, Yukako Sakaguchi, Yuji Seo, Yutaka Takahashi, Junichi Kikuta, Kazuhiko Ogawa, and Masaru Ishii. "Cell-cycle-controlled radiation therapy was effective for treating a murine malignant melanoma cell line in vitro and in vivo." *Scientific reports* 6 (2016): 30689.

Pajonk, Frank, Erina Vlashi, and William H. McBride. "Radiation resistance of cancer stem cells: the 4 R's of radiobiology revisited." *Stem cells* 28, no. 4 (2010): 639-648.

Pastrana, Erika, Violeta Silva-Vargas, and Fiona Doetsch. "Eyes wide open: a critical review of sphere-formation as an assay for stem cells." *Cell stem cell* 8, no. 5 (2011): 486-498.

Panetta, John Carl. "A mathematical model of periodically pulsed chemotherapy: tumor recurrence and metastasis in a competitive environment." *Bulletin of mathematical Biology* 58, no. 3 (1996): 425-447.

Piccirillo, S. G. M., Brent A. Reynolds, Nadia Zanetti, Giuseppe Lamorte, Elena Binda, Giovanni Broggi, Henry Brem, Alessandro Olivi, Francesco Dimeco, and Angelo L. Vescovi. "Bone morphogenetic proteins inhibit the tumorigenic potential of human brain tumour-initiating cells." *Nature* 444, no. 7120 (2006): 761.

Pilpel, Yitzhak. "Noise in biological systems: pros, cons, and mechanisms of control." *In Yeast Systems Biology,* pp. 407-425. Humana Press, 2011.

Poleszczuk, Jan, and Heiko Enderling. "Cancer stem cell plasticity as tumor growth promoter and catalyst of population collapse." *Stem cells international* 2016 (2016).

Powathil, G., M. Kohandel, S. Sivaloganathan, A. Oza, and M. Milosevic. "Mathematical modeling of brain tumors: effects of radiotherapy and chemotherapy." *Physics in Medicine & Biology* 52, no. 11 (2007): 3291.

Reya, Tannishtha, Sean J. Morrison, Michael F. Clarke, and Irving L. Weissman. "Stem cells, cancer, and cancer stem cells." *nature* 414, no. 6859 (2001): 105.

Rich, Jeremy N. "Cancer stem cells: understanding tumor hierarchy and heterogeneity." *Medicine* 95, no. Suppl 1 (2016).

Rodriguez-Brenes, Ignacio A., Natalia L. Komarova, and Dominik Wodarz. "Evolutionary dynamics of feedback escape and the development of stem-cell-driven cancers." *Proceedings of the National Academy of Sciences* 108, no. 47 (2011): 18983-18988.

Roesch, W. C. "Third symposium on neutron dosimetry in biology and medicine." *Google Scholar* (1978).

Sachs, Rainer K., and David J. Brenner. "Solid tumor risks after high doses of ionizing radiation." *Proceedings of the National Academy of Sciences* 102, no. 37 (2005): 13040-13045.

Schatton, Tobias, Natasha Y. Frank, and Markus H. Frank. "Identification and targeting of cancer stem cells." *Bioessays* 31, no. 10 (2009): 1038-1049.

Sarcar, Bhaswati, Soumen Kahali, Antony H. Prabhu, Stuart D. Shumway, Yang Xu, Tim Demuth, and Prakash Chinnaiyan. "Targeting radiation-induced G2/M checkpoint activation with the Wee-1 inhibitor MK-1775 in glioblastoma cell lines." *Molecular cancer therapeutics* (2011): molcanther-0469.

Schmidt, Mischa, Martin Creutziger, and Peter Lenz. "Influence of molecular noise on the growth of single cells and bacterial populations." *PloS one* 7, no. 1 (2012): e29932.

Shackleton, Mark, Elsa Quintana, Eric R. Fearon, and Sean J. Morrison. "Heterogeneity in cancer: cancer stem cells versus clonal evolution." *Cell* 138, no. 5 (2009): 822-829.

Shahrezaei, Vahid, Julien F. Ollivier, and Peter S. Swain. "Colored extrinsic fluctuations and stochastic gene expression." *Molecular systems biology* 4, no. 1 (2008): 196.

Singh, Sheila K., Cynthia Hawkins, Ian D. Clarke, Jeremy A. Squire, Jane Bayani, Takuichiro Hide, R. Mark Henkelman, Michael D. Cusimano, and Peter B. Dirks. "Identification of human brain tumour initiating cells." *nature* 432, no. 7015 (2004): 396.

Sjöblom, Tobias, Sin Jones, Laura D. Wood, D. Williams Parsons, Jimmy Lin, Thomas D. Barber, Diana Mandelker et al. "The consensus coding sequences of human breast and colorectal cancers." *science* 314, no. 5797 (2006): 268-274.

Stamatakos, G. S., V. P. Antipas, N. K. Uzunoglu, and R. G. Dale. "A four-dimensional computer simulation model of the in vivo response to radiotherapy of glioblastoma multiforme: studies on the effect of clonogenic cell density." *The British journal of radiology* 79, no. 941 (2006): 389-400.

Stange, Daniel E., Bon-Kyoung Koo, Meritxell Huch, Greg Sibbel, Onur Basak, Anna Lyubimova, Pekka Kujala et al. "Differentiated Troy+ chief cells act as reserve stem cells to generate all lineages of the stomach epithelium." *Cell* 155, no. 2 (2013): 357-368.

Swan, George W. *Optimization of human cancer radiotherapy.* Vol. 42. Springer Science Business Media, 2013.

Thames Jr, H. D., H. R. Withers, and L. J. Peters. "Tissue repair capacity and repair kinetics deduced from multifractionated or continuous irradiation regimens with incomplete repair." *The British journal of cancer. Supplement* 6 (1984): 263.

Thames, Howard D. "An 'incomplete-repair'model for survival after fractionated and continuous irradiations." *International Journal of Radiation Biology and Related Studies in Physics, Chemistry and Medicine* 47, no. 3 (1985): 319-339.

The START Trialists' Group. "The UK Standardisation of Breast Radiotherapy (START) Trial B of radiotherapy hypofractionation for treatment of early breast cancer: a randomised trial." *Lancet (London, England)* 371, no. 9618 (2008): 1098-1107.

Tonekaboni, Seyed Ali Madani, Andrew Dhawan, and Mohammad Kohandel. "Mathematical modelling of plasticity and phenotype switching in cancer cell populations." *Mathematical biosciences* 283 (2017): 30-37.

Trédan, Olivier, Carlos M. Galmarini, Krupa Patel, and Ian F. Tannock. "Drug resistance and the solid tumor microenvironment." *Journal of the National Cancer Institute* 99, no. 19 (2007): 1441-1454.

Tsimring, Lev S. "Noise in biology." *Reports on Progress in Physics* 77, no. 2 (2014): 026601.

Tucker, Susan L., Howard D. Thames, and Jeremy MG Taylor. "How well is the probability of tumor cure after fractionated irradiation described by Poisson statistics?." *Radiation Research* 124, no. 3 (1990): 273-282.

Turner, Colin. "Mathematical Modelling of Cancer Stem Cells." Master's thesis, University of Waterloo, 2009.

Turner, C., and M. Kohandel. "Investigating the link between epithelial-mesenchymal transition and the cancer stem cell phenotype: a mathematical approach." *Journal of theoretical biology* 265, no. 3 (2010): 329-335.

Turner, C., A. R. Stinchcombe, M. Kohandel, S. Singh, and S. Sivaloganathan. "Characterization of brain cancer stem cells: a mathematical approach." *Cell proliferation* 42, no. 4 (2009): 529-540.

Vlashi, Erina, Kwanghee Kim, Chann Lagadec, Lorenza Della Donna, John Tyson McDonald, Mansoureh Eghbali, James W. Sayre, Encrico Stefani, William McBride, and Frank Pajonk. "In vivo imaging, tracking, and targeting of cancer stem cells." *Journal of the National Cancer Institute* 101, no. 5 (2009): 350-359.

Vogelstein, Bert, and Kenneth W. Kinzler. "Cancer genes and the pathways they control." *Nature medicine* 10, no. 8 (2004): 789.

Wang, Qi-En. "DNA damage responses in cancer stem cells: implications for cancer therapeutic strategies." *World journal of biological chemistry* 6, no. 3 (2015): 57.

Wang, Maonan, Jingzhou Zhao, Lishen Zhang, Fang Wei, Yu Lian, Yingfeng Wu, Zhaojian Gong et al. "Role of tumor microenvironment in tumorigenesis." *Journal of Cancer* 8, no. 5 (2017): 761.

Watt, Fiona M., and Brigid LM Hogan. "Out of Eden: stem cells and their niches." *science* 287, no. 5457 (2000): 1427-1430.

Wein, Lawrence M., Jonathan E. Cohen, and Joseph T. Wu. "Dynamic optimization of a linear-quadratic model with incomplete repair and volume-dependent sensitivity and repopulation." *International Journal of Radiation Oncology* Biology* Physics* 47, no. 4 (2000): 1073-1083.

Werner, Benjamin, Jacob G. Scott, Andrea Sottoriva, Alexander RA Anderson, Arne Traulsen, and Philipp M. Altrock. "The cancer stem cell fraction in hierarchically organized tumors can be estimated using mathematical modeling and patient-specific treatment trajectories." *Cancer research* (2016): canres-2069.

Withers, H. Rodney. "Biological basis of radiation therapy for cancer." *Lancet* 339, no. 8786 (1992): 156-159.

Wodarz, Dominik. "Effect of cellular de-differentiation on the dynamics and evolution of tissue and tumor cells in mathematical models with feedback regulation." *Journal of theoretical biology* 448 (2018): 86-93.

Yakovlev, Andrej Yu. "Comments on the distribution of clonogens in irradiated tumors." *Radiation research* 134, no. 1 (1993): 117-120.

Yanger, Kilangsungla, and Ben Z. Stanger. "Liver cell reprogramming: parallels with iPSC biology." *Cell Cycle* 13, no. 8 (2014): 1211-1212.

Youssefpour, H., X. Li, A. D. Lander, and J. S. Lowengrub. "Multispecies model of cell lineages and feedback control in solid tumors." *Journal of theoretical biology* 304 (2012): 39-59.

Zaider, Marco, and Leonid Hanin. "Tumor control probability in radiation treatment." *Medical physics* 38, no. 2 (2011): 574-583.

Zaider, M., and G. N. Minerbo. "Tumour control probability: a formulation applicable to any temporal protocol of dose delivery." *Physics in Medicine & Biology* 45, no. 2 (2000): 279.

Zapperi, Stefano, and Caterina AM La Porta. "Do cancer cells undergo phenotypic switching? The case for imperfect cancer stem cell markers." *Scientific reports* 2 (2012): 441.

Zhang, Rui, Dragan Mirkovic, and Wayne D. Newhauser. "Visualization of risk of radiogenic second cancer in the organs and tissues of the human body." *Radiation Oncology* 10, no. 1 (2015): 107.

APPENDICES

Appendix A

Supplementary Figures

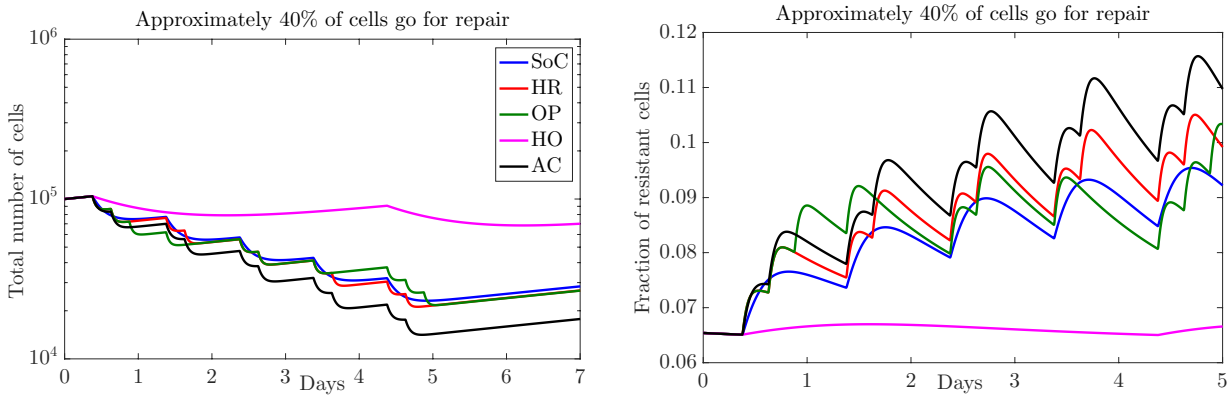

Figure A.1: *The number of cancer cells N_S+N_P and the fraction of resistant cells $N_S/(N_S+N_P)$ for the radiotherapy schedules reported in Table 3.5 when approximately 40% of cells undergo repair mechanisms.*

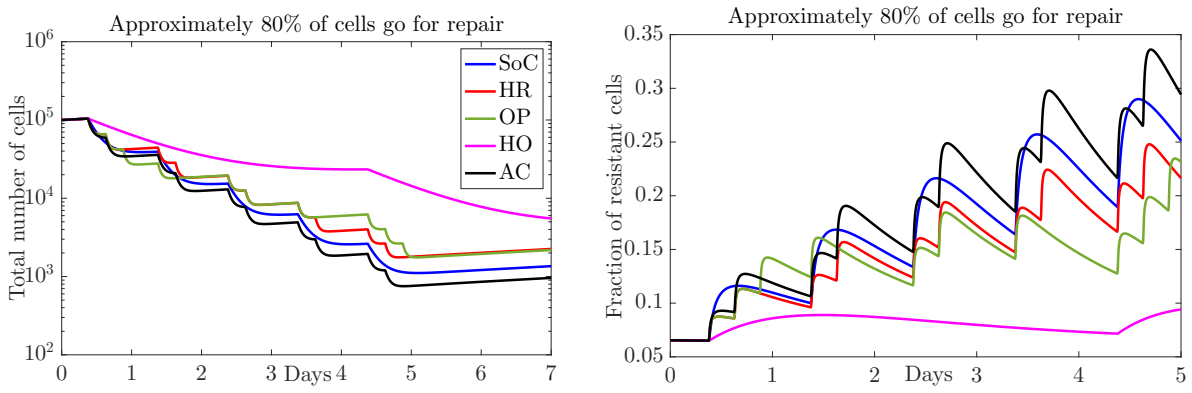

Figure A.2: *The number of cancer cells N_S+N_P and the fraction of resistant cells $N_S/(N_S+N_P)$ for the radiotherapy schedules reported in Table 3.5 when approximately 80% of cells undergo repair mechanisms.*

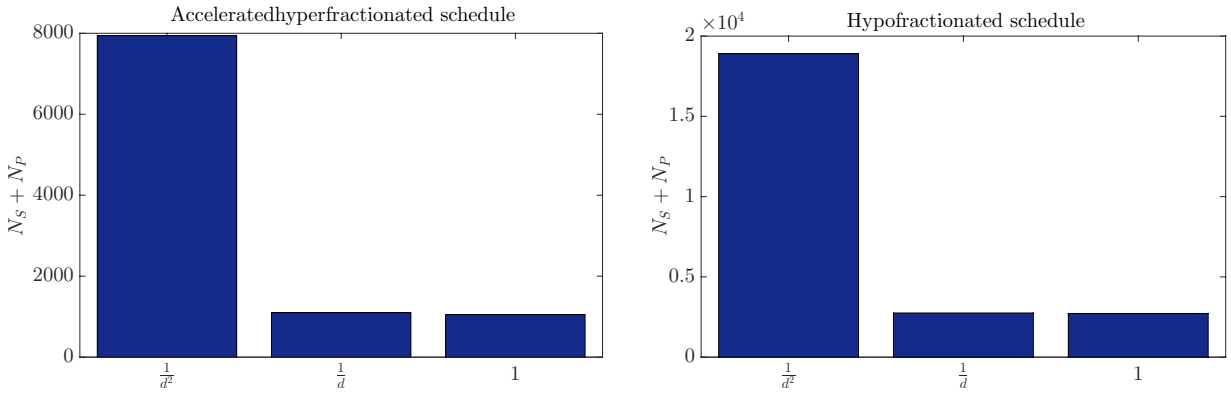

Figure A.3: *The number of cancer cells $N_S + N_P$ for the Accelerated hyperfractionated and the Hypofractionated protocols when the function $g(d)$ is assumed to be proportional to the inverse square of dose, inverse of dose, and a constant value* 1.

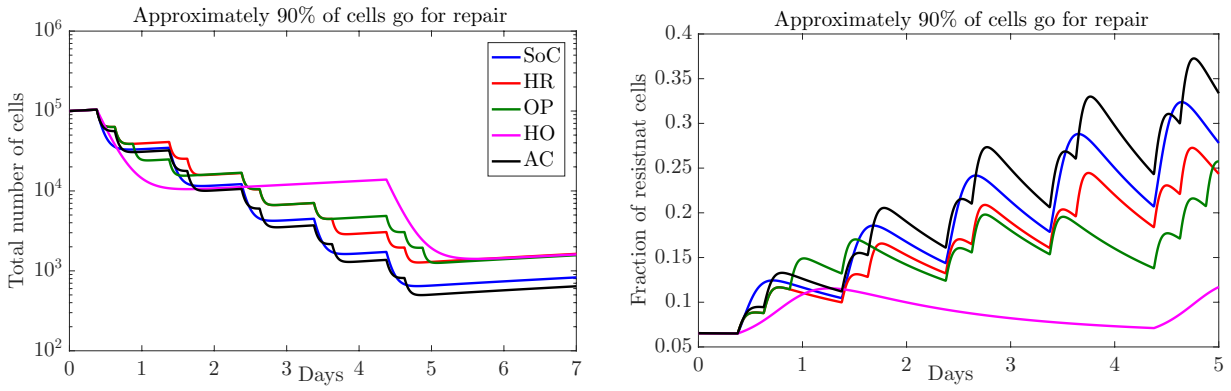

Figure A.4: *The number of cancer cells N_S+N_P and the fraction of resistant cells $N_S/(N_S+N_P)$ for the radiotherapy schedules reported in Table 3.5 when function $g(d)$ is assumed to be proportional to the inverse of dose.*

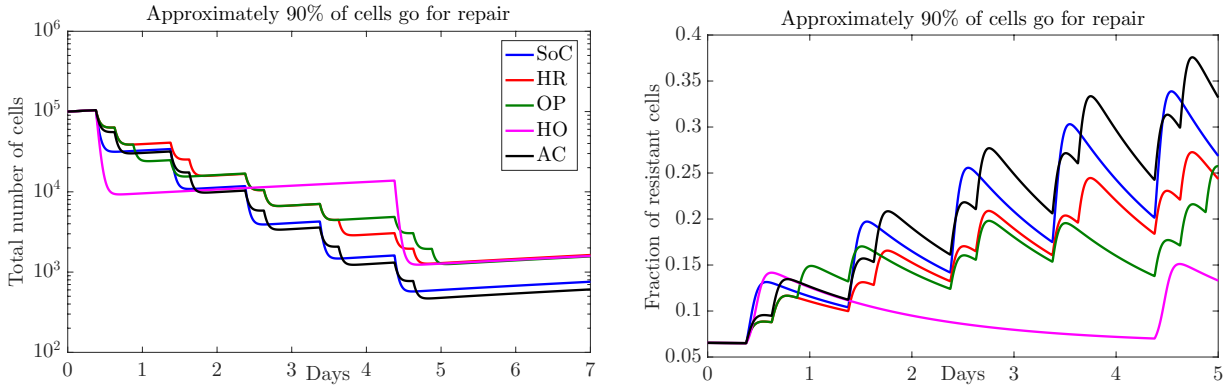

Figure A.5: *The number of cancer cells N_S+N_P and the fraction of resistant cells $N_S/(N_S+N_P)$ for the radiotherapy schedules reported in Table 3.5 when function $g(d)$ is assumed to be proportional to a constant value* 1.

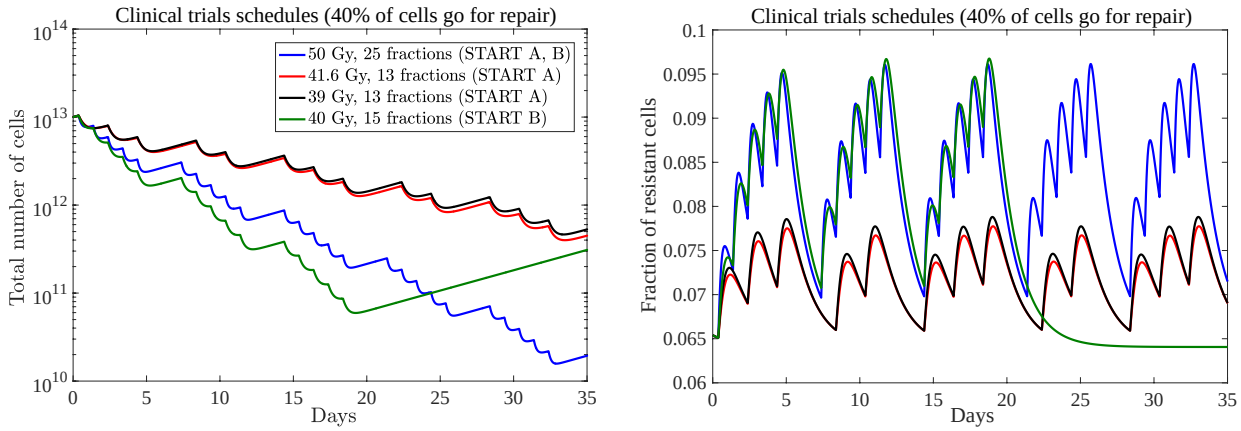

Figure A.6: *The number of cancer cells N_S+N_P and the fraction of resistant cells $N_S/(N_S+N_P)$ for the radiotherapy schedules reported in START trials when approximately 40% of cells undergo repair mechanisms.*

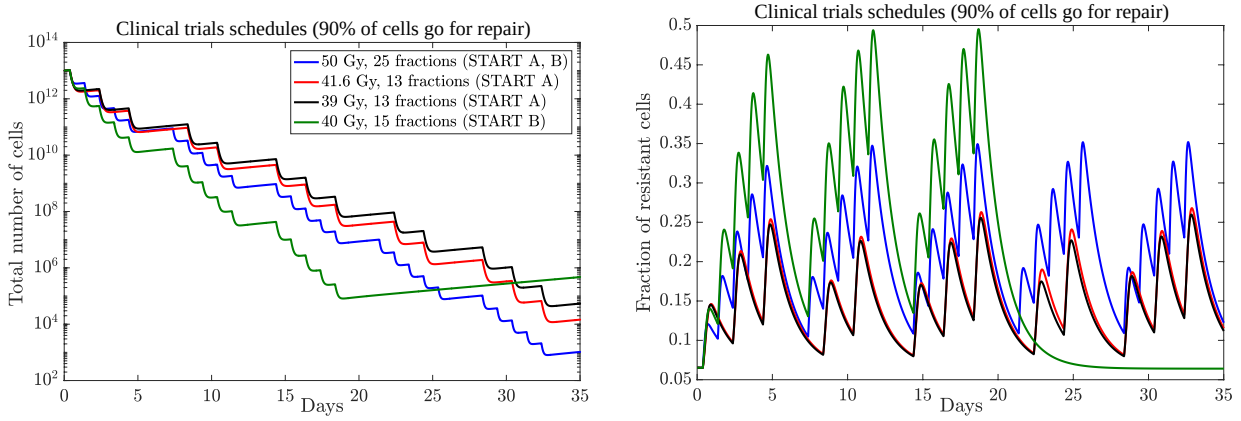

Figure A.7: *The number of cancer cells N_S+N_P and the fraction of resistant cells $N_S/(N_S+N_P)$ for the radiotherapy schedules reported in START trials when function $g(d)$ is assumed to be proportional to the inverse of dose.*

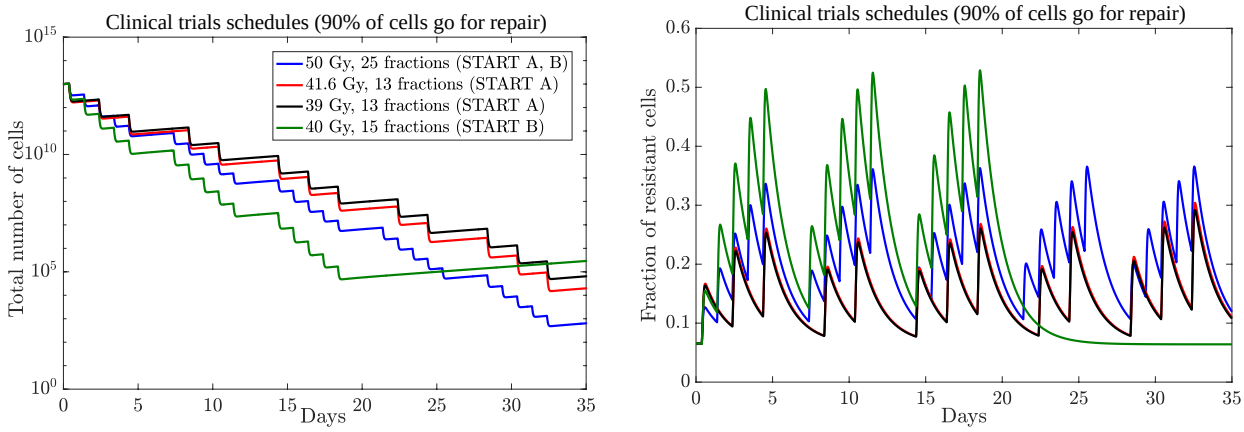

Figure A.8: *The number of cancer cells N_S+N_P and the fraction of resistant cells $N_S/(N_S+N_P)$ for the radiotherapy schedules reported in START trials when function $g(d)$ is assumed to be proportional to a constant value 1.*

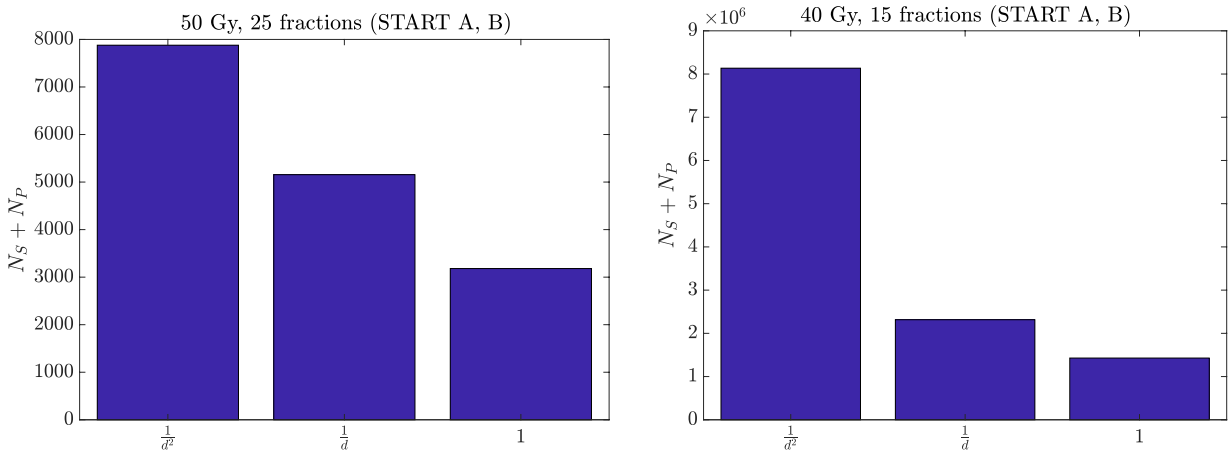

Figure A.9: *The number of cancer cells $N_S + N_P$ for the 50 Gy, 25 fractions (START A, B) and the 40 Gy, 15 fractions (START B) protocols when the function $g(d)$ is assumed to be proportional to the inverse square of dose, inverse of dose, and a constant value 1.*

Appendix B

Supplementary information

The extinction probability at time t, can be defined as $\mathrm{TCP}(t) = U(0,t)$. Assuming $U(z(\tau),t(\tau))$ is constant along the characteristic curve $C : [z(\tau),t(\tau)]$, we obtain the following ordinary differential equation

$$\frac{dz}{dt} = -(z-1)((z-1)\rho(t) + \beta(t)) = 0. \tag{B.1}$$

Considering the initial condition $t(0) = 0$, $U(z(\tau),t(\tau)) = U(z(0),0)$ along the characteristic curve. The final purpose of radiotherapy is to achieve zero cells remaining in the system at some time $t = t^*$. As a result, to compute TCP at time $t = t^*$, the characteristic curve $z(t^*) = 0$ should be considered. Thus, $\mathrm{TCP}(t^*) = U(z(0),0)$ in which $z(0)$ is determined solving differential equation B.1 with the final value condition $z(t^*) = 0$. Taking $t \to t^* - t$ changes the final value problem into an initial value problem. Finally, $\mathrm{TCP}(t)$ is obtained by solving the ordinary differential equation B.1 and substituting the solution

into the initial condition of PDE 4.2 ($U(z,0) = z^{n_0}$).

Appendix C

Gillespie algorithm

The time evolution of chemical systems can be studied using both deterministic and stochastic approaches. Deterministic models describe the behavior of the system using differential equations, but for small populations or in the presence of randomness, stochastic models can provide a better description of the evolution of species using a master equation (Erban et al., 2007). Although solving master equations is often challenging, stochastic formulations can be solved numerically using the Gillespie algorithm.

The Gillespie algorithm is a Monte Carlo type method that samples from a probability distribution that captures the underlying mechanisms governed by the master equation. Consider a system of N molecular species $\{S_1, ..., S_N\}$ in a well-mixed population that undergoes M reactions $\{R_1, ..., R_N\}$. The purpose of the algorithm is to find the state vector $X(t) = [\ X_1(t), ..., X_N(t)]$ given the initial condition $X(t_0) = x_0$, where $X_i(t)$ denotes the population size of species i at time t. The number of any particular species

varies when they go through any of the reactions R_j, $j = 1, ..., M$, which are defined by a state change vector $v_j = (v_{ij}, ..., v_{Nj})$ (v_{ij} is the change in the number of molecular type S_i induced by an event R_j) and the propensity function $a_j(x)$. Morover, $a_j(x)dt$ represents the probability of the reaction R_j being initiated in the time interval $[\ t, t + dt)$, given $X(t) = x$.

Assuming that all the reactions are separated events, the main strategy in this simulation method is to generate the trajectory of $X(t)$ starting from an initial state $X(t_0) = x_0$ by repeatedly finding the next time step τ and the next reaction μ (Cao et al., 2004; Gillespie, 2007). These two quantities are randomly determined following the distributions of the next time step τ and the next reaction μ.

Let $p(\tau = s)$ denote the probability density that one of the reactions R_j, $j = 1, ..., M$ occurs in an interval $(t + s, t + s + ds)$. Thus, $p(\tau = s) = p_0(s)a_0(x)$, where $p_0(s)$ is the probability of having no reaction during $(t, t + s)$, and $a_0(x)$ displays the probability that one of the possible M reactions fires at $(t + s, t + s + ds)$ with $a_0(x) = \sum_{j=1}^{M} a_j(x)$. It can be shown that $p_0(s) = \exp(-a_0(x)s)$, which indicates that the next time step τ given $X(t) = x$ is chosen from the exponential distribution $p(\tau = s) = a_0(x)\exp(-a_0(x)s)$ with mean $\frac{1}{a_0(x)}$ (Cao et al., 2004; Gillespie, 2007). The next reaction μ is also selected randomly with probability $p(\mu = j) = \frac{a_j(x)}{a_0(x)}$.

One basic formulation of the Gillespie algorithm is the direct method, which generates two random numbers r_1 and r_2 from the uniform distribution $U(0, 1)$. In this framework, the next time $t + \tau$ is estimated according to

$$\tau = \frac{1}{a_0(x)} \ln(\frac{1}{r_1}). \tag{C.1}$$

Moreover, the next reaction μ is represented by the smallest integers satisfying the inequality:

$$\sum_{j=1}^{\mu} a_j(t) > r_2 a_0(t). \tag{C.2}$$

Thus, the number of species at each time step $X(t)$ is calculated by applying the following stochastic algorithm.

- Let $t = 0$ and $X(0) = x_0$ (initialization)
- Evaluate propensity functions $a_j(x)$ and $a_0(x)$ at state $X(t)$.
- Calculate τ and μ by generating random numbers r_1 and r_2 from the unit interval uniform distribution and employing equations *C.1* and *C.2*.
- Update time $t \leftarrow t + \tau$ and the status of species $X \leftarrow X + \nu_\mu$.
- Go to the second step or end the simulation.

The direct method has been improved and modified into other formulations (Cao et al., 2004; Gillespie, 2007; Lu et al., 2004). One alternative to the direct method is the first reaction method, which generates values of τ and μ differently. In this approach, a τ_j is computed for each reaction R_j following

$$\tau_j = \frac{1}{a_j(x)} \ln(\frac{1}{r_j}) \qquad (j = 1, ..., M), \tag{C.3}$$

where r_1,...,r_M are M arbitrary numbers produced from the uniform distribution $U(0, 1)$. Consequently, the next time step is given as

$$\tau = \min\{\tau_1, ..., \tau_M\}, \tag{C.4}$$

and the next reaction μ corresponds to the index of the selected τ_j, $j = 1, ..., M$. Thus,

$$\mu = \text{the index related to the} \min\{\tau_1, ..., \tau_M\}. \tag{C.5}$$

Accordingly, the first reaction method algorithm is designed by changing the second and third steps in the direct method approach as below

- Calculate propensity functions $a_j(x)$ at state $X(t)$.
- Evaluate τ_j for each reaction using equation C.3 by generating $r_1, ..., r_M$ random number from the uniform distribution $U(0, 1)$.
- Compute τ and μ applying derivations C.4 and C.5.

The two procedures discussed above are valid for time independent propensity functions $a_j(x)$, $j = 1, ..., M$. However, the propensity functions can change continuously and discontinuously over time to account for extrinsic and intrinsic fluctuations in the system.

In this direction, Shahrezaei et al. (2008) developed a modified version of the Gillespie algorithm to take into account time varying discontinuous propensity functions. Therefore, assuming a discontinuous propensity function $a(t)$ as below

$$a(t) = \begin{cases} a < (t) & \text{for} \quad t < t_0, \\ a > (t) & \text{for} \quad t > t_0, \end{cases}$$

the simulation time t is set to t_0 if the next reaction time τ or the current time is larger than t_0 and $a(t)$ is changed respectively. Hence, the algorithm is given by:

- Let $t = 0$ and $X(0) = x_0$ (initialization)
- Calculate propensity functions $a_j(x)$ at state $X(t)$.
- Evaluate τ_j for each reaction using equation C.3 by generating $r_1, ..., r_M$ random number from the uniform distribution $U(0, 1)$.
- Compute μ applying equation C.5.
- If $t + \tau_\mu < t_0$, update time $t \leftarrow t + \tau_\mu$ and the status of species $X \leftarrow X + \nu_\mu$. If $t + \tau_\mu > t_0$, change the propensity function $a(t)$ and set $t = t_0$.
- Go to the second step or end the simulation.

The direct method and the extended Gillespie algorithm for discontinuous reaction rates are applied in Chapters 3 and 4 respectively.

Appendix D

Supplementary Figures

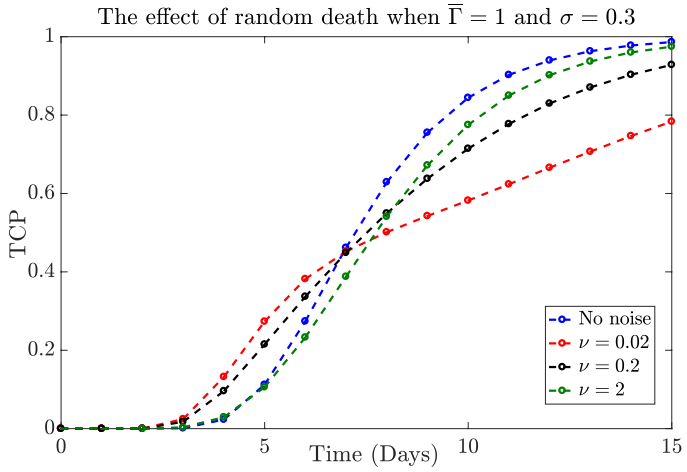

Figure D.1: The tumor control probability when death rate is switching randomly, with $\overline{\Gamma} = 1$, $\rho = 0.5$, $n_0 = 50$, and standard deviation $\sigma = 0.3$ for different switching rates.

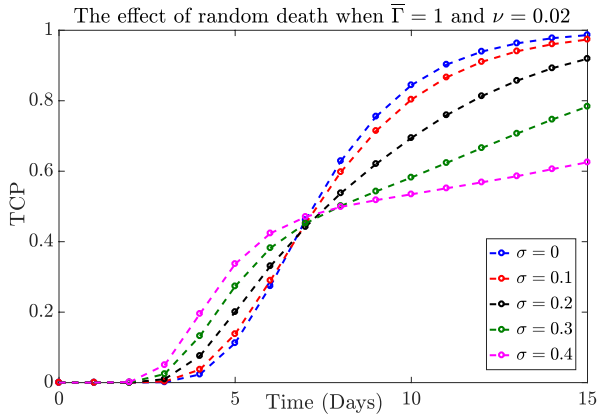

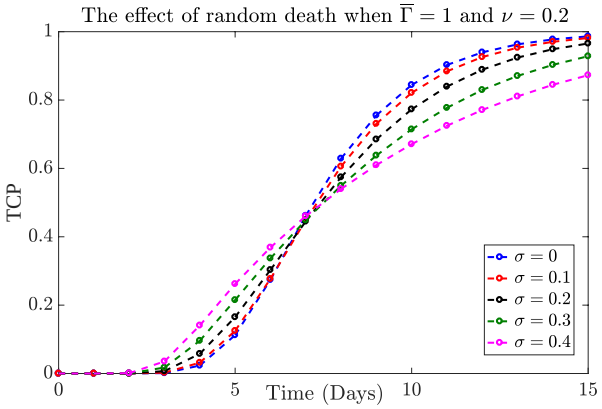

Figure D.2: Tumor control probability when death rate is switching randomly, with average $\overline{\Gamma} = 1$, $\rho = 0.5$, $n_0 = 50$, and different standard deviations for switching rates $\nu = 0.02$ and $\nu = 0.2$.

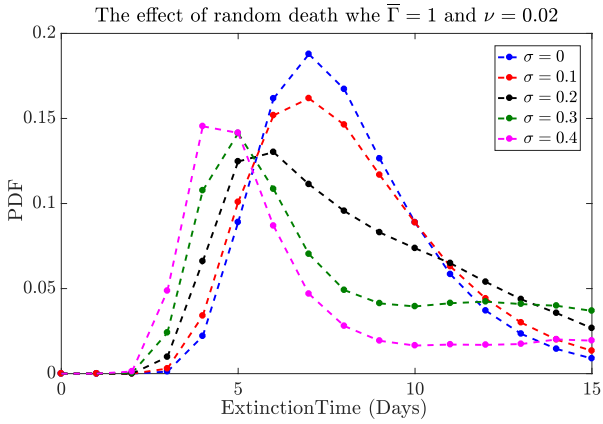

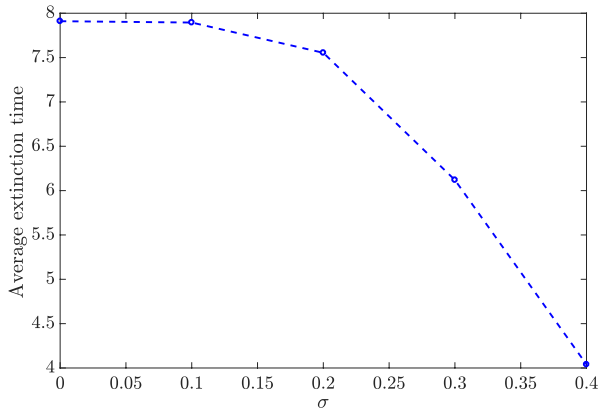

Figure D.3: The average extinction tome and extinction time distribution when $\overline{\Gamma} = 1$, $n_0 = 50$, $\rho = 1$, and different standard deviations for switching rates $\nu = 0.02$.

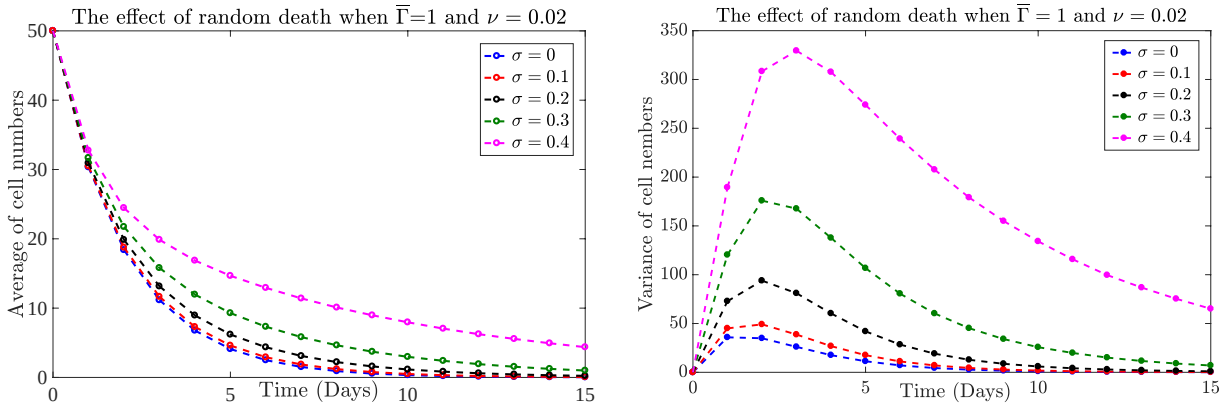

Figure D.4: The average and variance of cell numbers with $n_0 = 50$, $\overline{\Gamma} = 1$, $\rho = 0.5$, and different standard deviations for switching rate $\nu = 0.02$.

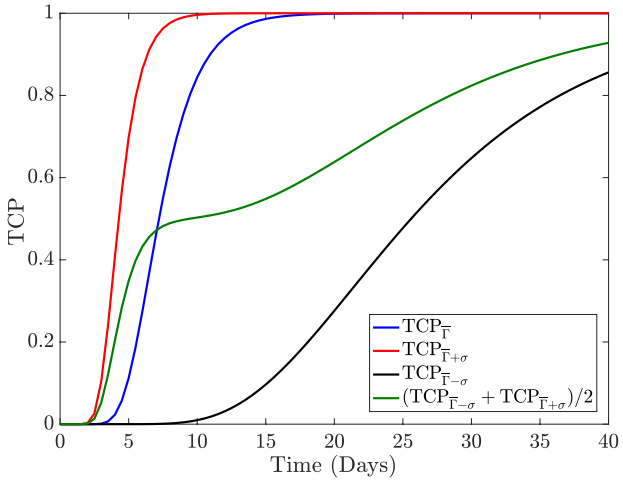

Figure D.5: Tumor control probability obtained from analytical solution with $\overline{\Gamma} = 1$, $\rho = 0.5$, $\sigma = 0.4$, and $n_0 = 50$.

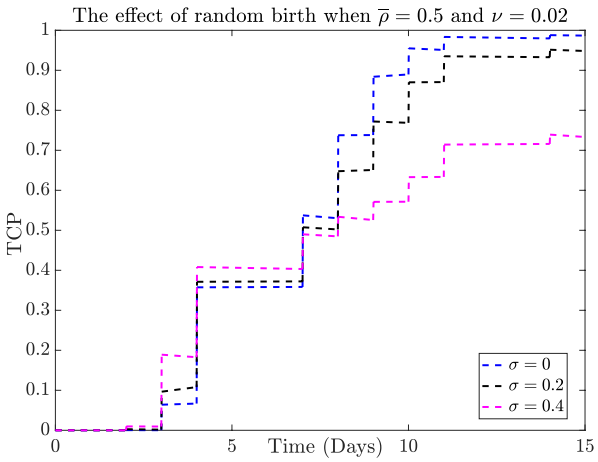

Figure D.6: The average and variance of cell numbers with $n_0 = 50$, $\overline{\rho} = 0.5$, $\Gamma = 1$, and different standard deviations for switching rate $\nu = 0.02$.

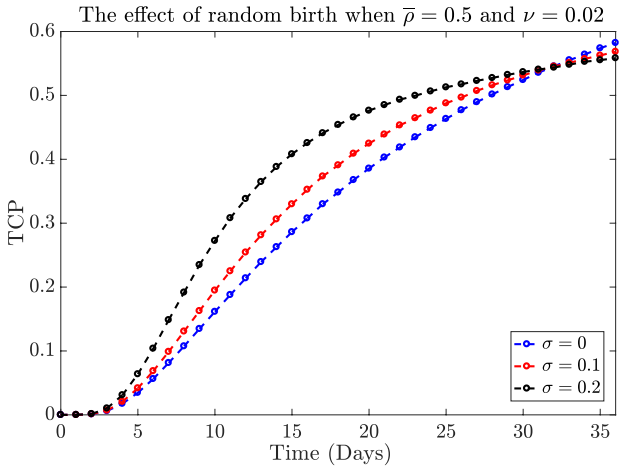

Figure D.7: The average and variance of cell numbers with $n_0 = 10$, $\Gamma = 0.5$, $\overline{\rho} = 0.5$, and different standard deviations for switching rate $\nu = 0.02$.

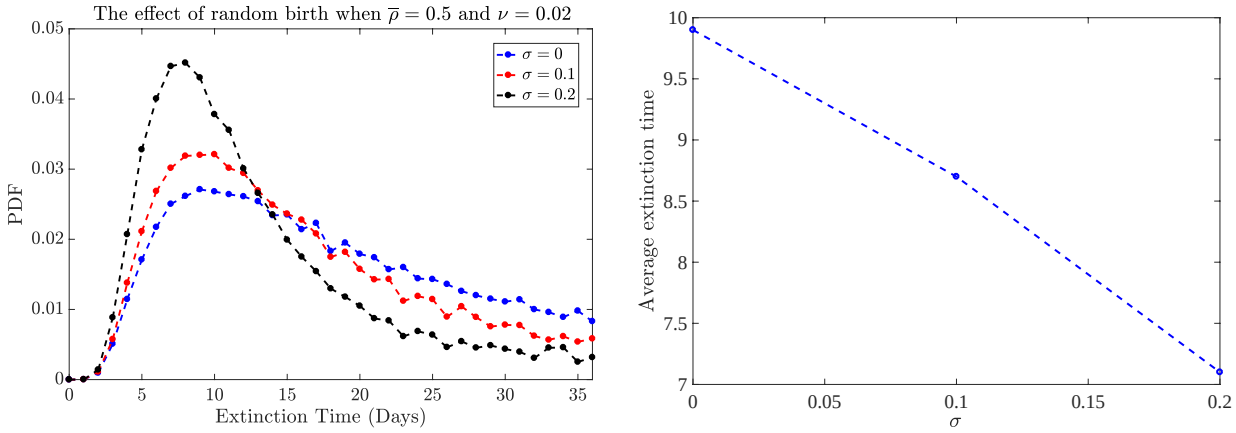

Figure D.8: The average and variance of cell numbers with $n_0 = 10$, $\Gamma = 0.5$, $\overline{\rho} = 0.5$, and different standard deviations for switching rate $\nu = 0.02$.

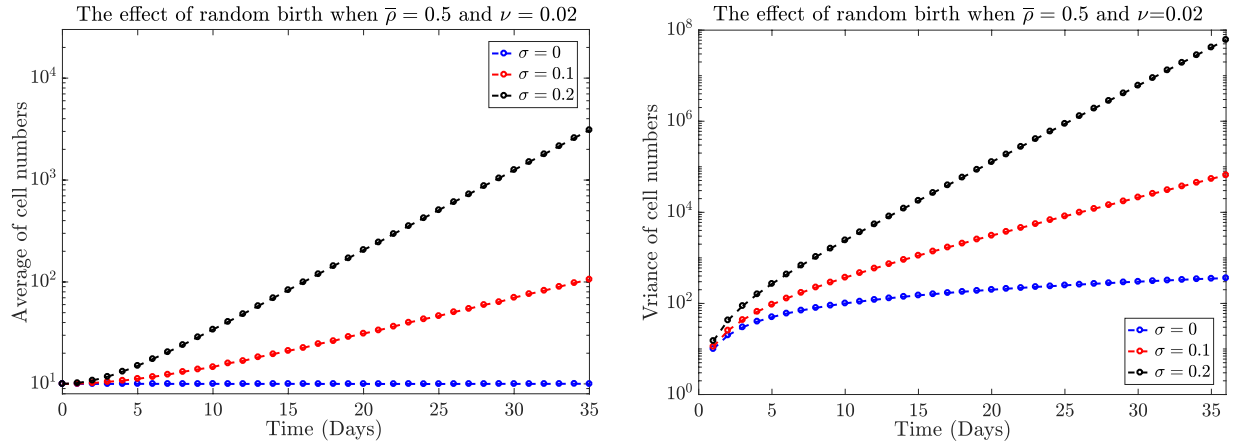

Figure D.9: The average and variance of cell numbers with $n_0 = 10$, $\Gamma = 0.5$, $\overline{\rho} = 0.5$, and different standard deviations for switching rate $\nu = 0.02$.

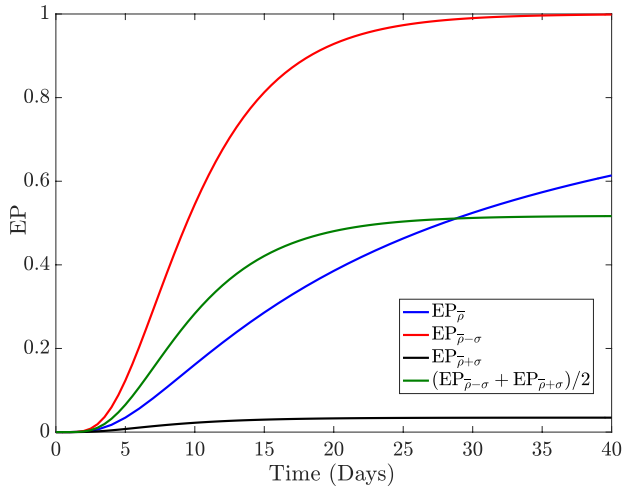

Figure D.10: Extinction probability obtained from analytical solution with $\overline{\rho} = 0.5$, $\Gamma = 0.5$, $\sigma = 0.2$, and $n_0 = 10$.

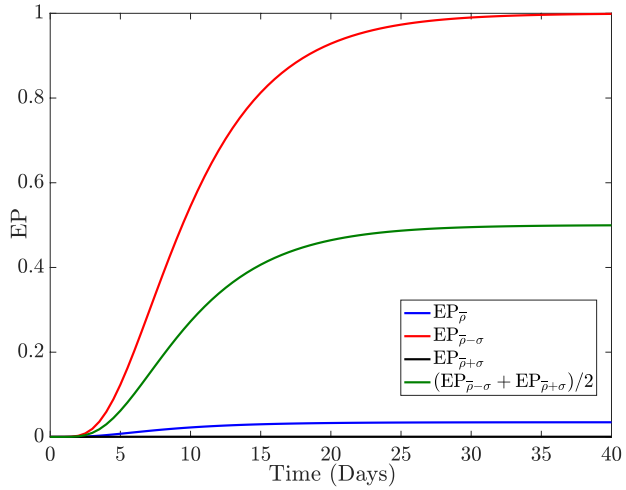

Figure D.11: Extinction probability obtained from analytical solution with $\overline{\rho} = 0.7$, $\Gamma = 0.5$, $\sigma = 0.4$, and $n_0 = 10$.

Appendix E

Supplementary information

The stochastic dynamic of model 5.1 in the absence of plasticity (i.e. $\rho_{PS} = 0$) can be explained using the following master equation showing the probability of having a population of n_S stem cells and n_P progenitors with the initial number of cells n_{S0} and n_{P0} at time t_0.

$$\begin{aligned}\frac{dp_{n_S,n_P}(t)}{dt} &= \rho_S(n_S-1)p_{n_S-1,n_P}(t) - \rho_S n_S p_{n_S,n_P}(t) + \rho_{SP}(n_S+1)p_{n_S+1,n_P-1}(t) \\ &- \rho_{SP} n_S p_{n_S,n_P}(t) + \rho_P(n_P-1)p_{n_S,n_P-1}(t) - \rho_P n_P p_{n_S,n_P}(t) + \Gamma_S(t)(n_S+1)p_{n_S+1,n_P}(t) \\ &- \Gamma_S(t) n_S p_{n_S,n_P}(t) + \Gamma_P(t)(n_P+1)p_{n_S,n_P}(t) - \Gamma_P(t) n_P p_{n_S,n_P}(t).\end{aligned} \tag{E.1}$$

The initial condition is given next with $\delta_{i,j}$ representing the Kronecker delta function:

$$p_{n_S,n_P}(t_0) = \delta_{n_S n_{S0}} \delta_{n_P n_{P0}}. \tag{E.2}$$

Using the probability distribution function introduced above, we can define the marginal probability distribution of the number of CSCs as

$$u_{n_S}(t) = \sum_{n_P} p_{n_S,n_P}(t),$$

with the following master equation

$$\frac{du_{n_S}(t)}{dt} = u_{n_S-1}\rho_S(n_S-1) - (\rho_S + \rho_{SP} + \Gamma_S(t))n_S u_{n_S} + u_{n_S+1}(\rho_{SP} + \Gamma_S(t))(n_S+1). \tag{E.3}$$

Appendix F

Supplementary Figures

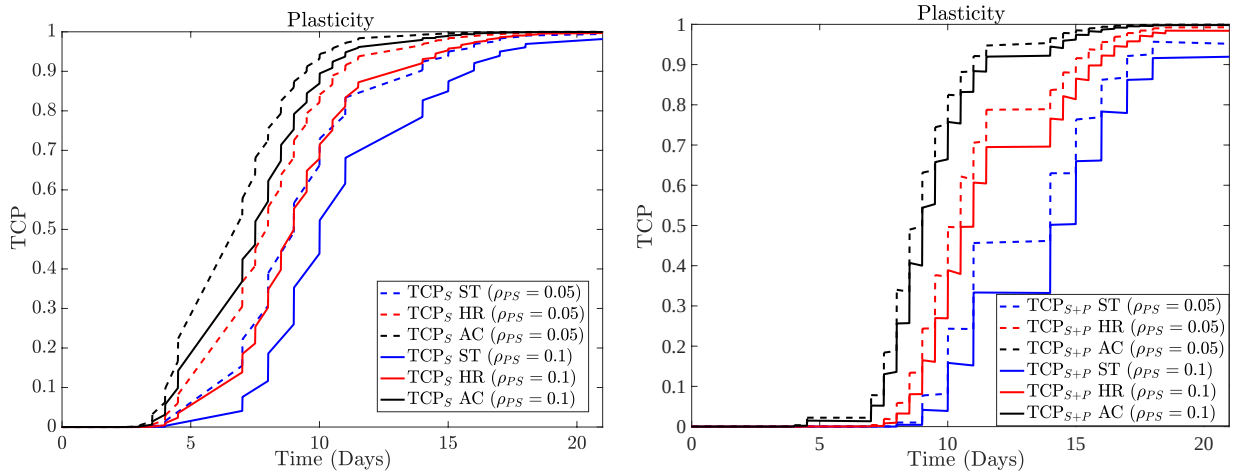

(a) (b)

Figure F.1: *(a) TCP_S and (b) TCP_{S+P} for standard, hyperfractionated, and accelerated hyperfractionated schedules with different dedifferentiation rates ρ_{PS}, between non-CSCs and CSCs. The initial numbers of cells are $n_S^0 = 100$ and $n_P^0 = 100$.*